Dissertation

Physicochemical Properties of a Pocket Existing in an Ionic Liquid

2020

Soka University
Graduate School of Engineering

KAZUYOSHI KANEKO

SOKA UNIVERSITY

Author: Kazuyoshi Kaneko

Title: Physicochemical Properties of a Pocket Existing in an Ionic Liquid

Department: Environmental Engineering for Symbiosis

Faculty: Engineering

Degree: Ph.D.

Convocation: March 2020

Permission is herewith granted to Soka University to circulate and copy for non-commercial purposes, at its discretion, the above title request of individual or institutions.

We certify that we have read this dissertation and that, in our opinion, it is satisfactory in scope and quality as a dissertation for the degree of Doctor of Philosophy in Engineering.

March 2020

DISSERTATION COMMITTEE

Dr. Akio Shimizu

Dr. Yukihiro Yoshimura

Dr. Junichi Ida

Contents

Page

Acknowledgements i

Abstract ii

Chapter 1 General introduction

1.1 Ionic liquid 1

1.2 Solution structure of ionic liquid 3

1.3 Property of ionic liquid/water mixture 4

1.4 Research Objectives 6

Figures 7

Chapter 2 Macroscopic properties of ionic liquid/water systems

2.1 Introduction 8

2.2 Material and Method

2.2.1 Samples 9

2.2.2 Refractive index measurement 10

2.3 Result and Discussion 11

Figures 14

Tables 27

Chapter 3 Physicochemical properties of water confined in the pocket formed in a typical ionic liquid $[C_4MIm]BF_4$ and the size of the pocket.

3.1 Introduction 39

3.2 Material and Method

3.2.1 Samples 40

3.2.2 NMR measurement 41

3.2.3 Viscosity measurement 42

3.2.4 Density measurement 42

3.3 Result and Discussion

3.3.1 Solubility of alcohol in $[C_4MIm]BF_4$ 43

3.3.2 Concentration dependence of density in $[C_4MIm]BF_4$/water and $[C_4MIm]BF_4$/alcohol system 44

3.3.3 Concentration dependence of chemical shift in $[C_4MIm]BF_4$/water and $[C_4MIM]BF_4$/alcohol system 46

3.3.4 About limiting effect and NMR self-diffusion coefficient measurement 49

3.3.5 Concentration dependence of self-diffusion coefficient in $[C_4MIm]BF_4$/water and $[C_4MIm]BF_4$/alcohol system 50

3.3.6 Relationship between self-diffusion coefficient and viscosity in $[C_4MIm]BF_4$/water and $[C_4MIm]BF_4$/alcohol system 54

Figures 56

Tables 78

Chapter 4 The influence of the alkyl chain length of ionic liquid $[C_nMIm]BF_4$ to physicochemical properties of the pocket formed in the IL and water confined in the pocket.

4.1 Introduction 92

4.2 Material and Method

4.2.1 Samples 93

4.3 Result and Discussion

4.3.1 Solubility of water in $[C_nMIm]BF_4$ 94

4.3.2 Concentration dependence of density in $[C_nMIm]BF_4$/water 95

4.3.3 Concentration dependence of chemical shift in $[C_nMIm]BF_4$/water 96

4.3.4 Concentration dependence of self-diffusion coefficient in $[C_nMIm]BF_4$/water 100

4.3.5 Relationship between self-diffusion coefficient and viscosity in $[C_nMIm]BF_4$/water 103

Figures 105

Tables 120

Chapter 5 General conclusion 130

References 133

Acknowledgements

I am grateful to my supervisor, Prof. Akio Shimizu, for his guidance and valuable suggestions regarding the present study and for help rendered in the completion of this dissertation. I am also thankful to the encouragement of him and his helpful support to my student life. Besides, I would like to thank the rest of my thesis committee: Prof. Yukihiro Yoshimura (National Defense academy) and Prof. Junichi Ida for their insightful comments to improve Ph.D. thesis.

I would like to thank Prof. Yuichi Masuda (Ochanomizu University) for their helpful suggestions, ideas and tremendous support. I am sincerely grateful to my family and friends for supporting my life.

Finally, I am greatly indebted to the founder of Soka University, Dr. Daisaku Ikeda and Mrs. Kaneko Ikeda for their tremendous encouragement and high expectations.

Abstract

The purpose of this study is to clarify the pockets (cavity) that have been suggested to exist in an ionic liquid from the macroscopic and microscopic views. As a macroscopic viewpoint, the differences between the refractive index calculated from the ideal mixing rule and the measured refractive index were normalized in order to investigate the properties of the various ionic liquid water system. As a result, the individuality of the ionic liquid hardly appears from a macroscopic viewpoint regardless of the type of the ionic liquid.

Subsequently, 1-butyl-3-methylimidazolium tetrafluoroborate reported on pockets was mixed with water and alcohol having various alkyl chain length in order to investigate the size and microscopic properties of the pockets. As a result, the structure of the pure ionic liquid hardly change from dynamic and static viewpoints, even though water or alcohols was added up to 20 mol%. The size of the pocket formed in the structure is at least about 100 $Å^3$ from a dynamic view. Furthermore, it suggests the movement of water and small alcohols in the ionic liquid isn't restricted in the pocket and move between the pockets whereas that of large alcohols are restricted in the pocket compared water and small alcohols.

On the other hand, there is a possibility that the properties of the pocket may be changed by changing the alkyl chain length of ionic liquids. Therefore, how the alkyl chain length of the ionic liquid affects the properties of pockets and the water in it was investigated by using systems in which water is mixed with an ionic liquid having various alkyl chain length (1-alkyl-3-methylimidazolium

tetrafluoroborate). As a result, it suggests the structure of the pure ionic liquid hardly change from the view of the dynamic and static properties, even though water was added up to 75 mol% regardless of alkyl chain length of the ionic liquid. The movement of water in the structure isn't also restricted in the pocket. Furthermore the movement of cation, anion and water decreased with increasing alkyl chain length of the ionic liquid whereas the relative movement of water within the ionic liquid tended to increase as the alkyl chains of the ionic liquid were lengthened. It suggests that the electrostatic interactions between the surface of the pocket and the water molecules decrease and the water molecules in the pocket move more independent of the ionic liquid.

Chapter 1

General introduction

1.1 Ionic liquid

A salt is composed only of an anion and a cation, and typically has a very high melting point due to the very strong coulomb interaction between the anion and cation, and exists in a solid state around room temperature. For an example, NaCl has a melting point of about 800 ° C and needs to be heated considerably or dissolved in a solvent such as water in order to be in a liquid state. On the other hand, there is a salt that exist as a liquid state around room temperature, and it is called "*Ionic Liquid*" (IL) [Wilkes 2002]. The melting point of an IL is lowered by combining one or both of cation and anion with a large organic ion having low isotropic property. This liquid is easy to replace anions or cations, and that of physical properties can be adjusted according to the purpose. For this reason, ILs are also called designer solvents and are attracting attention both academically and industrially.

Research on ILs have been conducted since the late 19th century. Researchers at that time thought that many applications would be expected if the liquid state could be maintained while maintaining the functionality of the salt, and attempts were made to lower the melting point of the salt. As a successful example, it was reported that the melting point of a salt having an aluminate ($(AlCl_3)_nCl^-$) as an anion was lowered to around room temperature. However, since these aluminates are unstable to water and air, they have no practical utility as a solvent. In 1992, Wilkes et al. 1992 synthesized 1-ethyl-3-methylimidazolium tetrafluoroborate ($[C_2MIm]BF_4$), a stable IL against water

and air. This has led to intense research, and more than 40,000 papers related to ILs have been published, as shown in Figure 1.1.

Basic research so far has reported that ILs have very unique properties such as non-volatility, flame retardancy, high thermal stability, high ionic conductivity, and melting of persistent materials [Welton 1999]. Therefore, many researches has been conducted in a wide range of fields. For example, it has been reported that cellulose, which is a hardly degradable substance, is soluble in an IL and can be used as a solvent for pretreatment to obtain bioethanol [Swatloski et al. 2002]. In addition, it has been reported that the volume of ILs does not change significantly even when CO_2 is adsorbed, while the volume of organic solvents increases greatly when CO_2 is adsorbed [Chiehming. Et al. 1998, Aki, et al. 2004, Blanchard et al. 2001, Kordikowski et al. 1995, Makino et al. 2012]. Such volume behavior is interpreted to indicate that the solution structure of the ILs is maintained even when CO_2 is added and the IL has a large pocket where CO_2 can exist compared to the molecular solvent, and that CO_2 occupies the pocket [Hung et al. 2005, Cadena et al. 2004, Anthony et al. 2005]. In the case that water is mixed with ILs, water is also confined in the pocket in ILs, and the pocket is called "water pocket". Furthermore, since ILs is non-volatile, it can be reused by vacuum treatment after mixing with another solvent or gas, so it can be reduced in cost by repeated use. On the other hand, since ILs hardly volatilize even under vacuum, some researches is being conducted to observe while maintaining a moist state by substituting water for IL instead of drying the sample during Scanning Electron Microscope observation [Arimoto et al. 2008] .

1.2 Solution structure of ionic liquid

The solution structure of imidazolium-based IL (1-alkyl-3-methylimidazolium Hexafluorophosphates: $[C_nMIm]PF_6$) obtained from the molecular dynamics (MD) simulation reported by Lopes et al. 2006 is showed in Figure 1.2. Pure liquids and solutions are typically treated as spatially homogeneous systems in the case of a single phase. However, in some IL, when viewed from a polarity, polar anions and imidazolium rings gather to form a polar domain, and nonpolar alkyl chains gather to form a nonpolar domain. Therefore, it has been reported that a heterogeneous structure is formed on the nanoscale. This structure depends on the number of carbon atoms in the alkyl chain of the IL. Further, it has been reported that the number of carbon atoms increases and the nonpolar domain becomes thicker [Lopes et al. 2006]. Sugimori et al. Have also attempted to directly observe the nanodomain structure using an annular dark-field method with a scanning transmission electron microscope [Sugimori et al. 2019]. Dark-field images of solutions of IL and barium stearate showed 10 nm scale heterogeneity in image intensity, suggesting that the distribution of heterogeneous ions in the solution was reflected.

1.3 Property of ionic liquid/water mixture

As described above, since ILs have properties different from those of typical solutions, ILs have been attracted the interest of researchers in a wide range of fields. Especially, the physicochemical property of "pocket" or "water pocket" is a hot topic in solution chemistry. Some of these studies provided experimental and theoretical evidence for the existence of water pockets in the ILs. In one recent report, Sieffert et al. 2006 suggested the presence of a water pocket where water molecules diffuse and rotate in the nano-heterogeneous structure of 1-butyl-3-methylimidazolium bis (trifluoromethylsulfonyl) imide/water mixture based on molecular dynamics simulation. Studying the same IL, Rollet et al. 2007 obtained data for the self-diffusion coefficient at 0.3–30 water mol% by using pulsed field gradient spin-echo NMR, and suggested that the water pocket are connected at the local scale. Subsequently, using small-angle neutron scattering (SANS) measurements, Gao et al. 2016 investigated the microstructure of mixtures of 1-butyl-3-methylimidazolium tetrafluoroborate ([C_4MIM][BF_4]) and water at 70–84 water mol% and the water cluster size has a radius of 0.55 nm at 74 water mol% as determined by SANS. Remarkably, Kashin et al. 2016 succeeded in obtaining the morphology and formation dynamics of water-containing compartments in [C_4MIm]BF_4 at ~20 water wt% directly by field-emission scanning electron microscopy, and the radius of a water-containing particle was determined to be 33 nm at 10 water vol% by dynamic light scattering measurements. A variety of morphologies were detected and depended on the water concentration. In addition, Abe et al. 2015 reported that the radius of the water pocket was about 0.8

nm at 69.9 water mol% in 1-butyl-3-methylimidazolium nitrate, as determined by SANS. As described above, the size of the water pocket depends on viewpoints. Furthermore, the physicochemical properties of the water confined in the water pocket and the size of the pocket are not elucidated well. The physicochemical properties of the water confined in ionic liquid having various alkyl chain length is also not clarified.

1.4 Research Objectives

In order to clarify the properties of the pocket and the water in an IL/water system, the research objectives for this doctoral thesis were set following:

(1) Revealing the macroscopic properties of IL/water systems based on the refractive index.

(2) Estimating the size of a pocket formed in a typical IL and elucidating the physicochemical properties of water confined in a pocket formed in an IL from static, dynamic and volumetric viewpoints.

(3) Elucidating how the physicochemical properties of a pocket and water confined in the pocket change depending on the alkyl chain length of the ILs from static, dynamic and volumetric viewpoints.

In Chapter 2, how the macroscopic physicochemical property of IL/water systems depend on the type of IL [Kaneko et al. 2018a] was investigated and described. In Chapter 3, the pocket size was estimated by mixing water or alcohol with various alkyl chain length into an IL, respectively. The physicochemical properties of IL/water and IL/alcohol systems [Kaneko et al. 2019] were also investigated and described based on chemical shift, self-diffusion coefficient, density and viscosity. In Chapter 4, the influence of the alkyl chain length of the IL to the properties of pockets and the water in it [Kaneko et al. 2018b] were investigated and described based on chemical shift, self-diffusion coefficient, density and viscosity. In Chapter 5, over all discussion and conclusions of this doctoral thesis are presented.

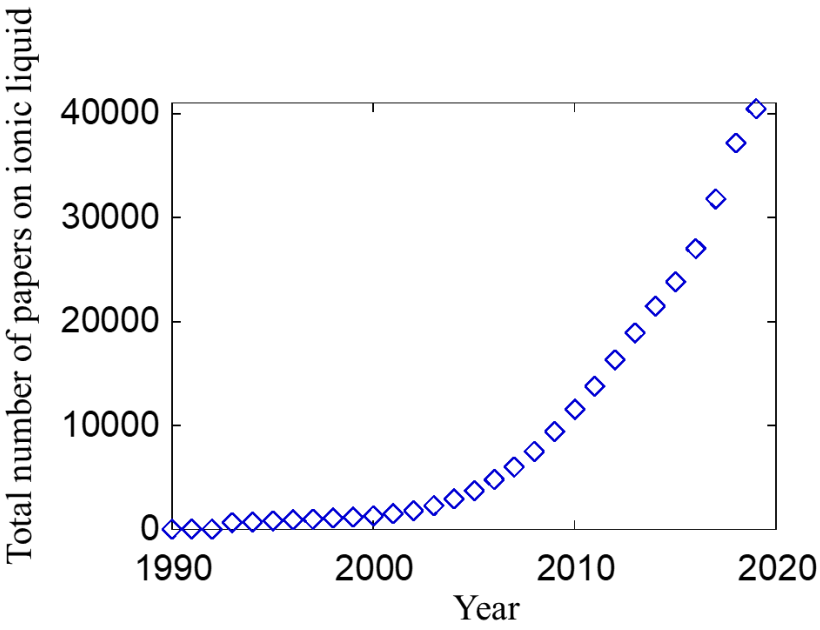

Figure 1.1 Total number of papers on ionic liquid [J dream III].

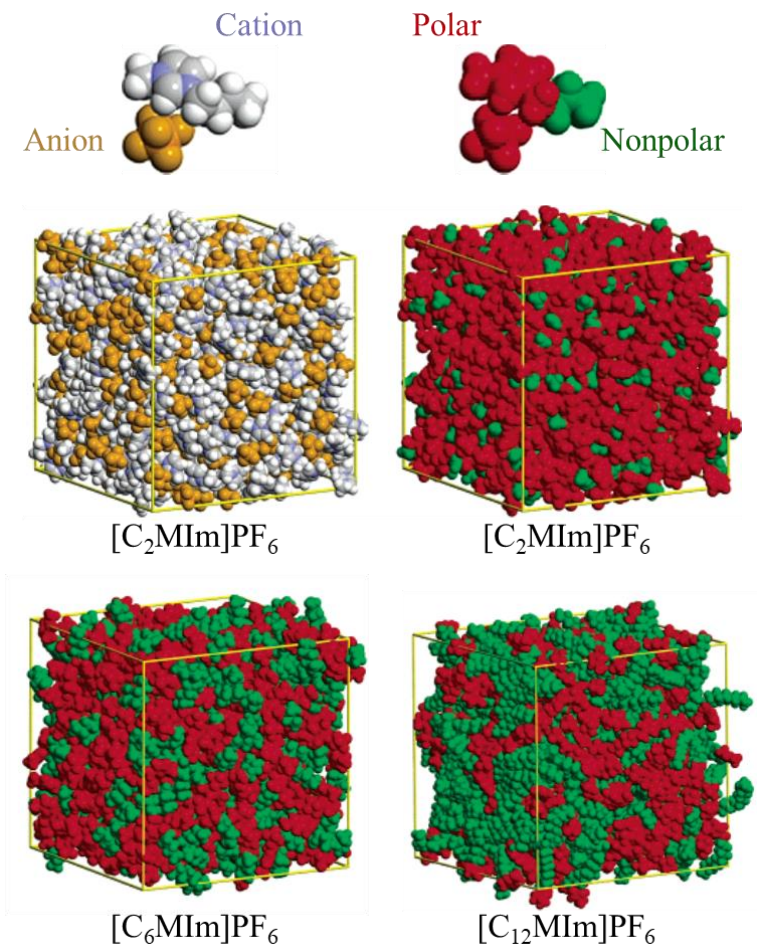

Figure 1.2 Nano-heterogeneous structure of $[C_nMIm]PF_6$ [Lopes et al. 2006].

Chapter 2

Macroscopic properties of ionic liquid/water system

2.1 Introduction

In preceding studies, the microscopic properties of IL/water system has been investigated by molecular dynamic simulation and NMR and small angle X-ray diffraction etc. [Jiang et al. 2007, Saha et al. 2006, Rollet et al. 2007] However, there are few studies about macroscopic properties of IL/water system.

The refractive index is a fundamental physical quantity that can be used to easily determine the identity and concentration of a substance, also used to investigate a change of macroscopic property of a substance. The temperature dependence of the refractive index has been reported recently for pure ILs [Seki et al. 2012, Tariq et al. 2009, Soriano et al. 2009] and IL-alcohol systems [Mokhtarani et al. 2008, Iglesias-Otero et al. 2008, Anouti et al. 2010]. However, there have been few studies that examined the water concentration dependence of the refractive index for various IL-water system.

In the present study, I investigate the refractive index of various IL-water systems across the entire composition ranging from pure IL to pure water. Based on the results, I investigate the macroscopic properties of ILs/water systems based on the refractive index.

2.2 Material and Method

2.2.1 Samples

The following nine ILs were purchased from the Kanto Chemical Co., Inc. or Sigma Aldrich Co. : 1-ethyl-3-methylimidazolium tetrafluoroborate ([C_2MIm]BF_4), 1-ethyl-3-methylimidazolium diethylphosphate ([C_2MIm][DEP]), 1-butyl-3-methylimidazolium tetrafluoroborate, ([C_4MIm]BF_4), 1-butyl-3-methylimidazolium acetate, ([C_4MIm][OAc]), 1-butyl-3-methylimidazolium iodide, ([C_4MIm]I), 1-methyl-3-octylimidazolium bromide, ([C_8MIm]Br), *N*,*N*-diethyl-*N*-methyl-*N*-(2-methoxyethyl)ammonium tetrafluoroborate ([DEME]BF_4), ethylammonium nitrate (EAN), and propylammonium nitrate (PAN) which are summarized in Table 2.1. These ILs were vacuumed (less than 4 Pa) to remove impurities at room temperature for more than 72h. After vacuumed, the water content were measured and found to be 613, 133, 474, 2087, 214, 458, 328, 283 and 288 ppm for [C_2MIm]BF_4, [C_2MIm][DEP], [BC_4MIm]BF_4, [C_4MIm][OAc], [C_4MIm]I, [OMIm]Br, [DEME]BF_4, EAN and PAN by spectrum of NMR (AVANCE III HD, Bruker, 600 MHz) respectively. The ultrapure water used in this study was supplied by a Synergy UV system (Millipore Inc.)

2.2.2 Refractive index measurement

The refractive index at 589 nm of the IL-water systems was determined using a refractometer (Reichert ABBE MARK III, Reichert) that contains built-in illumination provided by long-life light-emitting diodes and a dispersion correction prism for true refractive index measurement at 589 nm. The refractive index measurement range and precision were 1.3106 to 1.7000 n_{D}, respectively. The temperature was controlled to 293 ± 0.1 K using a JULABO F25 water circulator.

2.3 Result and Discussion

The refractive index of ILs, which are combinations of various cations and anions, and water system were investigated. The nine ILs used in this study can be mixed with water in the whole concentration region. The refractive indices of nine ILs-water systems are shown in Figure 2.1 and Table2.2. In all cases, the refractive index increased with increasing IL concentration. The trend observed for $[C_4MIm]BF_4$ is in good agreement with those reported in the study by Chaudhary *et al*. In addition, they were slightly convex upwards from the linear change predicted according to ideal mixing law, Eq. (1),

$$n_{\mathrm{D}}^{\mathrm{id}} = \frac{x n_{\mathrm{D}}^{\mathrm{IL}} + (100 - x) n_{\mathrm{D}}^{\mathrm{w}}}{100} \quad (1)$$

where $n_{\mathrm{D}}^{\mathrm{id}}$, $n_{\mathrm{D}}^{\mathrm{IL}}$, and $n_{\mathrm{D}}^{\mathrm{w}}$ are the refractive indices of the ideal IL-water system, pure IL, and pure water, respectively. Subsequently, we calculated the difference (Δn_{D}) between the experimentally observed refractive indices and those of the ideal solutions, and the results are shown in Figure 2.2 and Table 2.2. The maximum value of Δn_{D} ($\Delta n_{\mathrm{D}}(max)$) varied greatly depending on the IL species, and increased in the following order: $[C_2MIm]BF_4$ < $[DEME]BF_4$ < $[C_4MIm]BF_4$ ≅ EAN < PAN < $[C_2MIm][DEP]$ < $[C_4MIm][OAc]$ < $[C_8MIm]Br$ < $[C_4MIm]I$. This order almost corresponds to the refractive index of the pure ILs. Despite the ILs having different combinations of cations and anions, Δn_{D} had the same concentration dependence for all ILs studied. Furthermore, the IL concentration corresponding to $\Delta n_{\mathrm{D}}(max)$ was around 25 mol% regardless of the IL. Since $\Delta n_{\mathrm{D}}(max)$ increased with increasing $n_{\mathrm{D}}^{\mathrm{IL}}$, $\Delta n_{\mathrm{D}}(max)$ was plotted with respect to $n_{\mathrm{D}}^{\mathrm{IL}}$ in Figure

2.3. Water concentration dependence of the refractive index of other ionic liquids has been reported by González et al. 2012 and Vercher et al. 2011 for 1,2-diethylpyridinium ethylsulfate ([EEPy][ESO_4]), 1-ethyl-3-methylimidazolium trifluoromethanesulfonate ([C_2MIm][TfO]), 3-butyl-1-ethylimidazolium trifluoromethanesulfonate ([BEIM][TfO]), 1-butyl-3-methylimidazolium dicyanamide ([C_4MIm][DCA]), 1-butyl-3-methylimidazolium trifluoromethanesulfonate ([C_4MIm][TfO]), 1-butyl-3-methylpyridinium trifluoromethanesulfonate ([BMPy][TfO]), 1-butyl-1-methylpyrrolidinium trifluoromethanesulfonate ([BMPyr][TfO]), 1-hexyl-3-methylimidazolium dicyanamide ([HMIm][DCA]), 1-butyl-1-methylpyrrolidinium dicyanamide ([BMPyr][DCA]) and 1-methylpyridinium methylsulfate ([MPy][MSO_4]) at 288.15~338.15 K (shown in Table 2.3-2.6). For comparison we have calculated the Δn_{D} of ILs/water system at 293 K for the reference in Table 2-7 using the temperature dependence [González et al. 2012, Vercher et al. 2011] (shown in Figure 2.4-2.13). Then, now the comparison between the calculated and experimental data at 293 K are made in Figure 2.2, 2.3, 2.14. We found that the deviation of Δn_{D} between at 288.15 K and 298.15 K is less than 3% as shown in Figure 2.15-2.24.

As shown in Figure 2.3, the following linear correlation was calculated.

$$\Delta n_D(max) = 0.55574 \cdot \ n_D(pure\ \ IL) - 0.74392 \quad (R^2 = 0.92985) \qquad (2)$$

Finally, Δn_{D} normalized to unity at the IL concentration corresponding to the maximum Δn_{D} is plotted in Figure 2.14 for each IL (this study and the previous study [González et al. 2012 and Vercher et al. 2011]). Interestingly, plots of the IL concentration dependence of the normalized Δn_{D}

($\Delta n_{\mathrm{D}}(min)$= 0 and $\Delta n_{\mathrm{D}}(max)$ = 1) for all ILs studied in this experiment and calculated from previous study overlapped completely. The plots in Figure 2.14 were fitted by the following equation.

$$\text{Normalized } \Delta n_{\mathrm{D}} = \frac{-1.4962}{e^{0.1064x}} - 0.015147x + 1.5198 \qquad (R^2 = 0.99662) \qquad (3)$$

where x is the IL concentration (mol%).

There already has been reported that IL/water systems have unique physicochemical properties such as nano-heterogeneous structure, but at least for the normalized Δn_{D}, the specificity of each IL doesn't almost appear. This finding indicates that the properties of IL/water system doesn't depend on IL species in a macroscopic view.

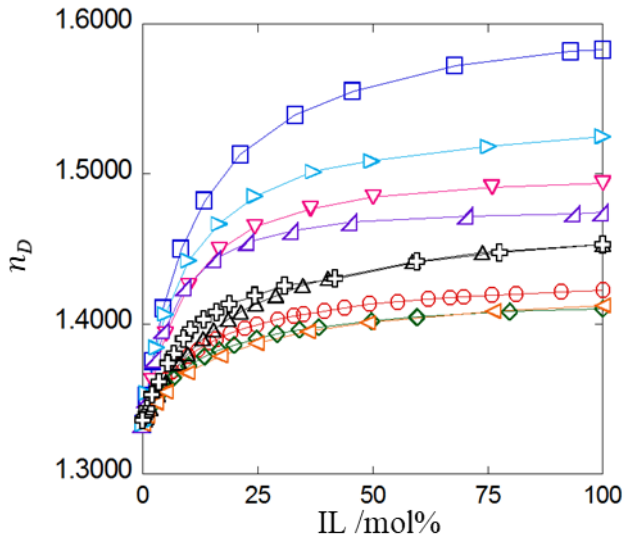

Figure 2.1 Refractive index (n_D) of various IL/water systems as a function of IL concentration at 293 K and 0.1 MPa. Legend: (◿), [C_2MIm][DEP]; (◁), [C_2MIm]BF_4; (▽), [C_4MIm][OAc]; (○), [C_4MIm]BF_4; (□), [C_4MIm]I; (▷), [C_8MIm]Br; (◇), [DEME]BF_4; (▭), PAN; (△), EAN.

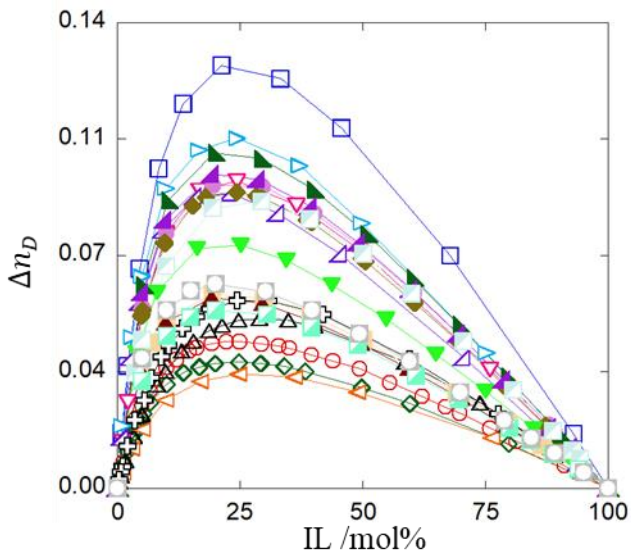

Figure 2.2 Deviation (Δn_D) of refractive index of various IL-water systems from that of the corresponding ideal solution as a function of IL concentration at 293 K. Legend: (◿), [C_2MIm][DEP]; (◁), [C_2MIm]BF_4; (◪), [C_2MIm][TfO]; (▢), [BEIM][TfO]; (▽), [C_4MIm][OAc]; (○), [C_4MIm]BF_4; (□), [C_4MIm]I; (▷), [C_8MIm]Br; (◇), [DEME]BF_4; (▭), PAN; (△), EAN; (●), [C_4MIm][DCA]; (■), [C_4MIm][TfO]; (◢), [HMIm][DCA]; (▼), [BMPy][TfO]; (◆), [BMPyr][DCA]; (▲), [BMPyr][TfO]; (◐), [MPy][MSO_4]; (◣), [EEPy][ESO_4].

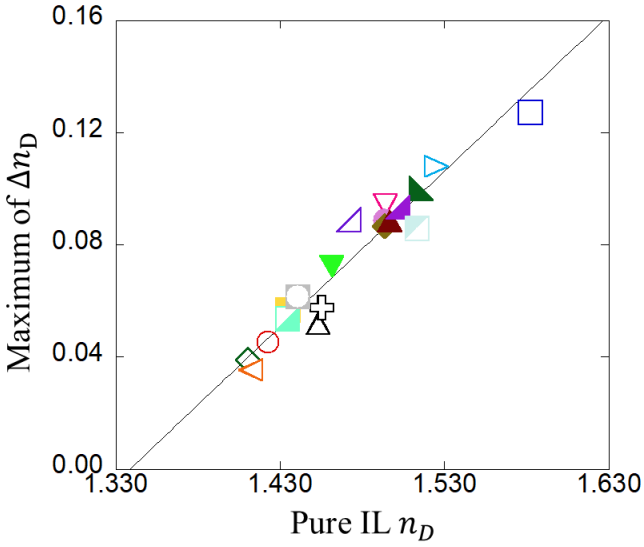

Figure 2.3 Relationship between maximum Δn_D and pure IL n_D for various IL-water systems. Legend: (∠), [C_2MIm][DEP]; (◁), [C_2MIm]BF_4; (◪), [C_2MIm][TfO]; (▢), [BEIM][TfO]; (▽), [C_4MIm][OAc]; (○), [C_4MIm]BF_4; (▫), [C_4MIm]I; (▷), [C_8MIm]Br; (◇), [DEME]BF_4; (▫), PAN; (△), EAN; (●), [C_4MIm][DCA]; (■), [C_4MIm][TfO]; (◢), [HMIm][DCA]; (▼), [BMPy][TfO]; (◆), [BMPyr][DCA]; (▲), [BMPyr][TfO]; (◦), [MPy][MSO_4]; (◣), [EEPy][ESO_4].

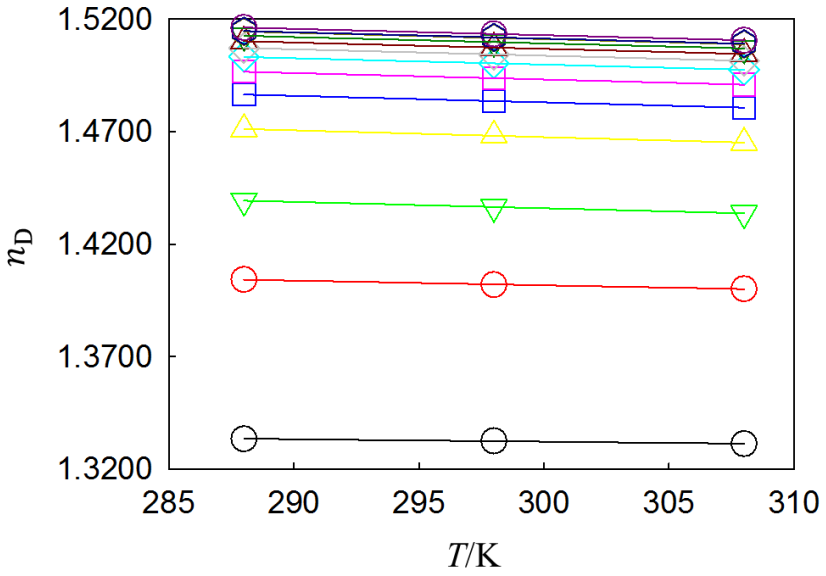

Figure 2.4 Refractive index of [EEPy][ESO_4]/water systems at 288.15 K ~ 308.15 K. The solid lines were calculated by least squares method [Gonzalez et al. 2012]. Legend: (○), pure water; (○), 5.07 mol%; (▽), 10.16 mol%; (△), 19.71 mol%; (□), 29.16 mol%; (□), 39.82 mol%; (◇), 50.78 mol%; (◇), 60.21 mol%; (△), 69.63 mol%; (▽), 79.52 mol%; (○), 89.11 mol%; (○), 90.13 mol%; (○), pure IL.

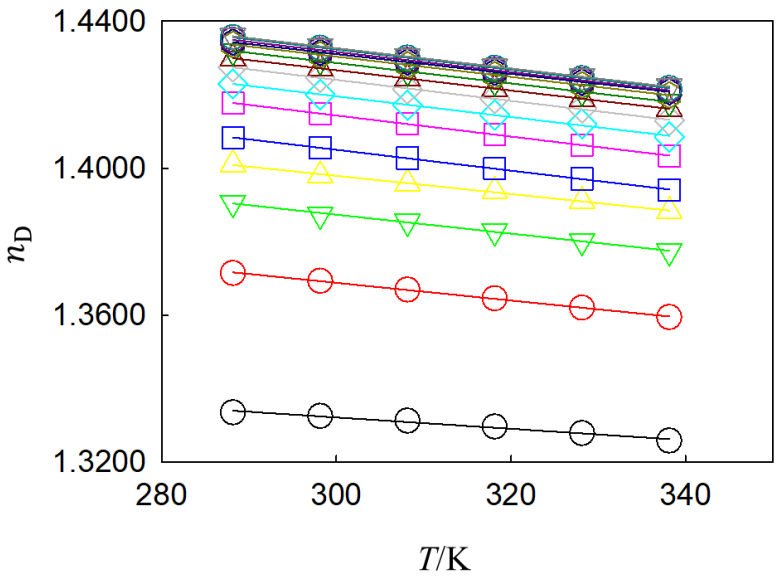

Figure 2.5 Refractive index of [C_2MIm][TfO]/water systems at 288.15 K ~ 338.15K. The solid lines were calculated by least squares method [Gonzalez et al. 2012]. Legend: (○), pure water; (○), 4.954 mol%; (▽), 9.99 mol%; (△), 14.834 mol%; (□), 19.94 mol%; (□), 30.511 mol%; (◇), 39.515 mol%; (◇), 49.028 mol%; (△), 60.800 mol%; (▽), 69.535 mol%; (○), 79.941 mol%; (○), 84.121 mol%; (○), 88.772 mol%; (○), 93.994 mol%; (▽), pure IL.

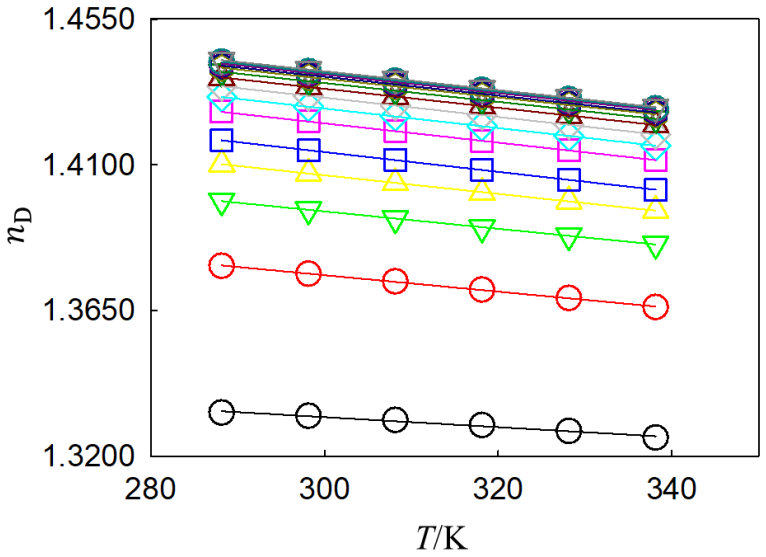

Figure 2.6 Refractive index of [BEIM][TfO]/water systems at 288.15 K ~ 338.15K. The solid lines were calculated by least squares method [Gonzalez et al. 2012]. Legend: (○), pure water; (○), 5.002 mol%; (▽), 9.989 mol%; (△), 15.004 mol%; (□), 19.938 mol%; (□), 30.226 mol%; (◇), 39.626 mol%; (◇), 49.335 mol%; (△), 59.563 mol%; (▽), 69.869 mol%; (○), 78.909 mol%; (○), 84.434 mol%; (○), 89.149 mol%; (○), 95.002 mol%; (▽), pure IL.

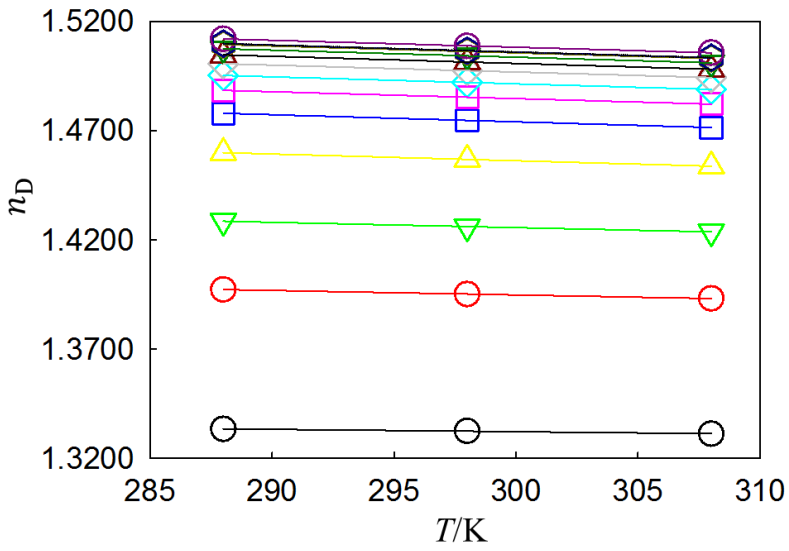

Figure 2.7 Refractive index of [C_4MIm][DCA]/water systems at 288.15 K ~ 308.15 K. The solid lines were calculated by least squares method [Gonzalez et al. 2012]. Legend: (○), pure water; (○), 4.97 mol%; (▽), 9.94 mol%; (△), 19.50 mol%; (□), 29.68 mol%; (□), 40.15 mol%; (◇), 49.70 mol%; (◇), 60.48 mol%; (△), 70.57 mol%; (▽), 79.83 mol%; (○), 87.73 mol%; (○), 89.12 mol%; (○), pure IL.

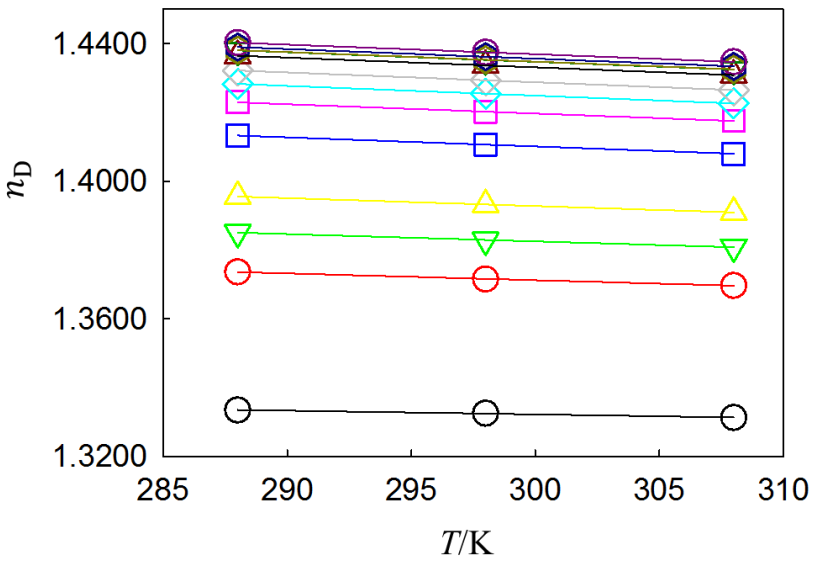

Figure 2.8 Refractive index of [C4MIm][TfO]/water systems at 288.15 K ~ 308.15 K. The solid lines were calculated by least squares method [Gonzalez et al. 2012]. Legend: (○), pure water; (○), 4.52 mol%; (▽), 6.91 mol%; (△), 10.02 mol%; (□), 19.36 mol%; (□), 29.85 mol%; (◇), 39.38 mol%; (◇), 50.15 mol%; (△), 69.17 mol%; (▽), 79.44 mol%; (○), 79.72 mol%; (○), 89.52 mol%; (○), pure IL.

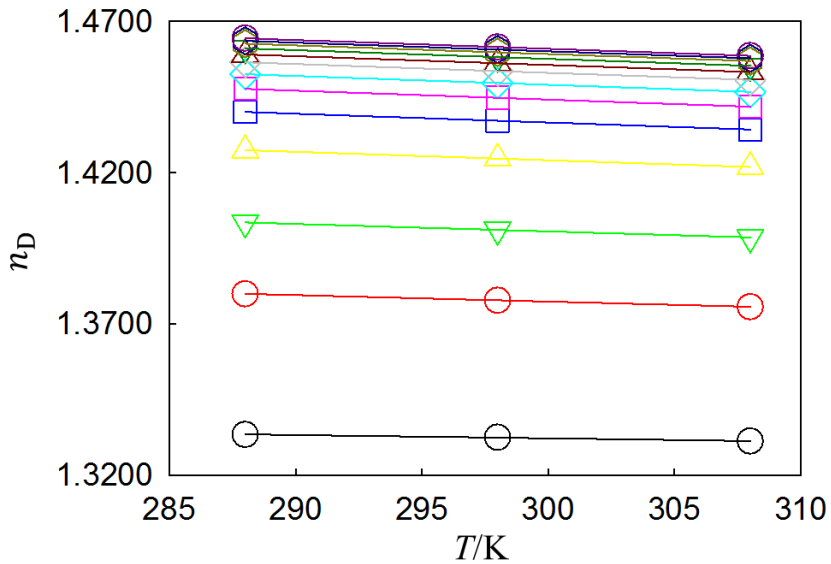

Figure 2.9 Refractive index of [BMPy][TfO]/water systems at 288.15 K ~ 308.15 K. The solid lines were calculated by least squares method [Gonzalez et al. 2012]. Legend: (○), pure water; (○), 3.97 mol%; (▽), 7.99 mol%; (△), 16.17 mol%; (□), 25.06 mol%; (□), 34.39 mol%; (◇), 43.72 mol%; (◇), 54.72 mol%; (△), 64.85 mol%; (▽), 74.98 mol%; (○), 84.83 mol%; (○), 92.06 mol%; (○), pure IL.

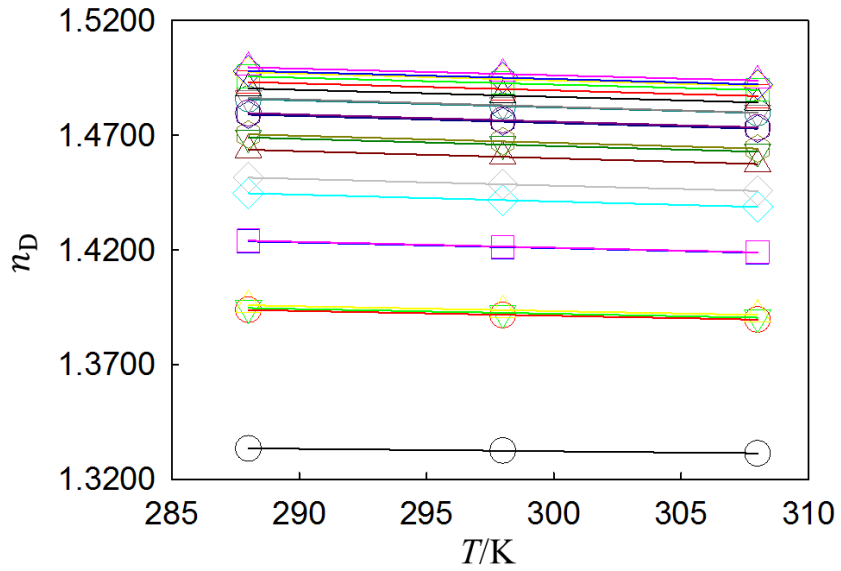

Figure 2.10 Refractive index of [BMPyr][DCA]/water systems at 288.15 K ~ 308.15 K. The solid lines were calculated by least squares method [Gonzalez et al. 2012]. Legend: (○), pure water; (○), 4.83 mol%; (▽), 4.93 mol%; (△), 5.08 mol%; (□), 9.60 mol%; (□), 9.66 mol%; (◇), 15.32 mol%; (◇), 17.92 mol%; (△), 24.29 mol%; (▽), 28.23 mol%; (○), 29.39 mol%; (○), 38.63 mol%; (○), 39.53 mol%; (○), 49.77 mol%; (▽), 50.48 mol%; (△), 60.58 mol%; (□), 69.23 mol%; (□), 78.84 mol%; (◇), 87.23 mol%; (◇), 90.40 mol%; (△), pure IL.

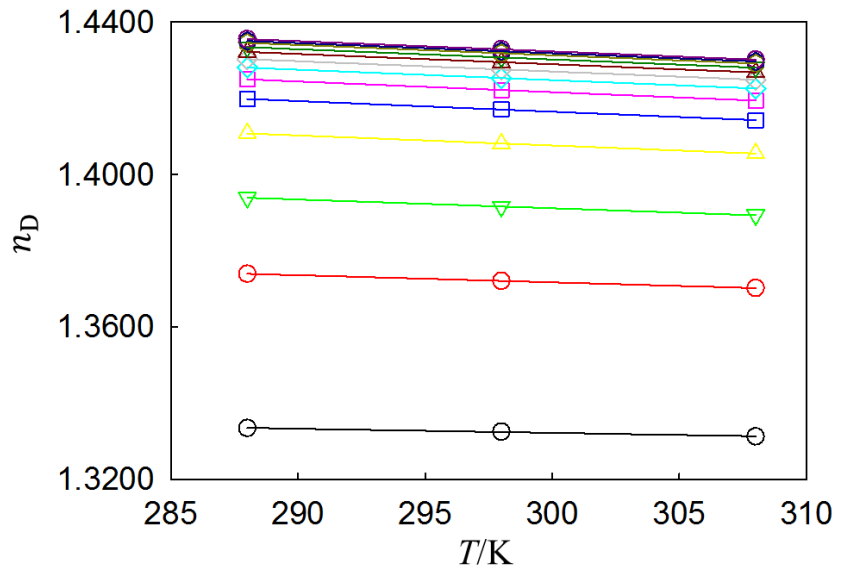

Figure 2.11 Refractive index of [BMPyr][TfO]/water systems at 288.15 K ~ 308.15 K. The solid lines were calculated by least squares method [Gonzalez et al. 2012]. Legend: (○), pure water; (○), 4.67 mol%; (▽), 9.82 mol%; (△), 19.05 mol%; (□), 29.48 mol%; (□), 39.97 mol%; (◇), 49.62 mol%; (◇), 59.20 mol%; (△), 70.03 mol%; (▽), 79.24 mol%; (○), 89.16 mol%; (○), 94.41 mol%; (○), pure IL.

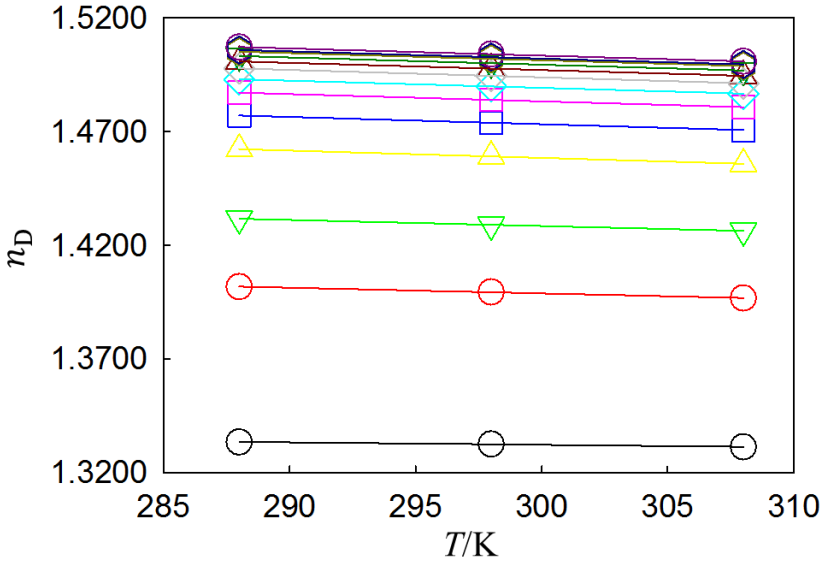

Figure 2.12 Refractive index of [HMIm][DCA]/water systems at 288.15 K ~ 308.15 K. The solid lines were calculated by least squares method [Gonzalez et al. 2012]. Legend: (○), pure water; (○), 5.01 mol%; (▽), 9.69 mol%; (△), 19.33 mol%; (□), 28.77 mol%; (□), 39.31 mol%; (◇), 49.04 mol%; (◇), 59.81 mol%; (△), 69.45 mol%; (▽), 78.76 mol%; (○), 88.09 mol%; (○), 92.15 mol%; (○), pure IL.

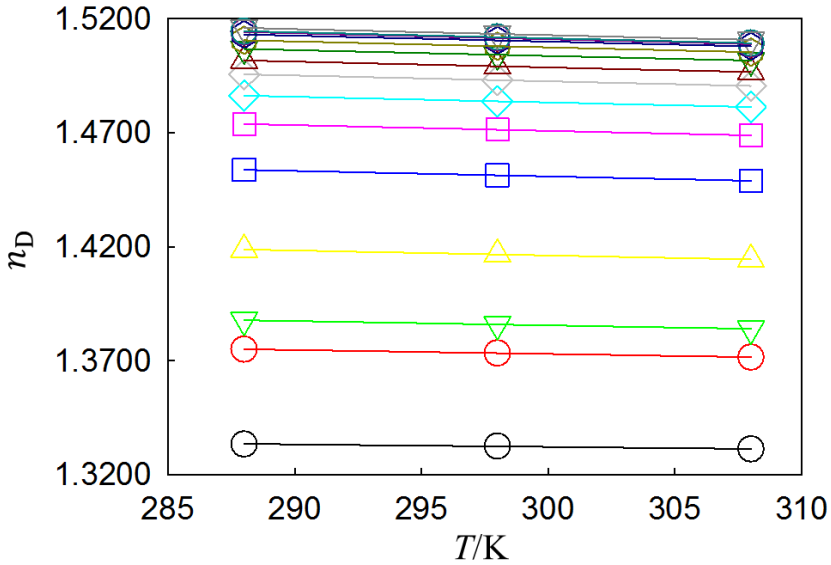

Figure 2.13 Refractive index of [MPy][MSO_4]/water systems at 288.15 K ~ 308.15 K. The solid lines were calculated by least squares method [Gonzalez et al. 2012]. Legend: (○), pure water; (○), 3.55 mol%; (▽), 5.03 mol%; (△), 9.90 mol%; (□), 19.42 mol%; (□), 29.38 mol%; (◇), 39.23 mol%; (◇), 50.04 mol%; (△), 59.95 mol%; (▽), 70.59 mol%; (○), 80.73 mol%; (○), 88.89 mol%; (○), 92.70 mol%; (○), 94.26 mol%; (▽), pure IL.

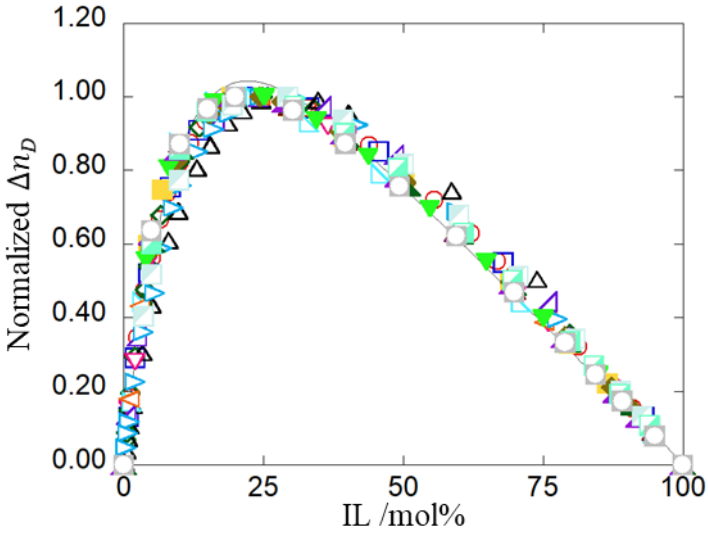

Figure 2.14 Normalized Δn_{D} of various IL-water systems as a function of IL concentration. Legend: (◿), [C_2MIm][DEP]; (◁), [C_2MIm]BF_4; (◪), [C_2MIm][TfO]; (▢), [BEIM][TfO]; (▽), [C_4MIm][OAc]; (○), [C_4MIm]BF_4; (□), [C_4MIm]I; (▷), [C_8MIm]Br; (◇), [DEME]BF_4; (▢), PAN; (△), EAN; (●), [C_4MIm][DCA]; (■), [C_4MIm][TfO]; (◢), [HMIm][DCA]; (▼), [BMPy][TfO]; (◆), [BMPyr][DCA]; (▲), [BMPyr][TfO]; (◿), [MPy][MSO_4]; (◣), [EEPy][ESO_4].

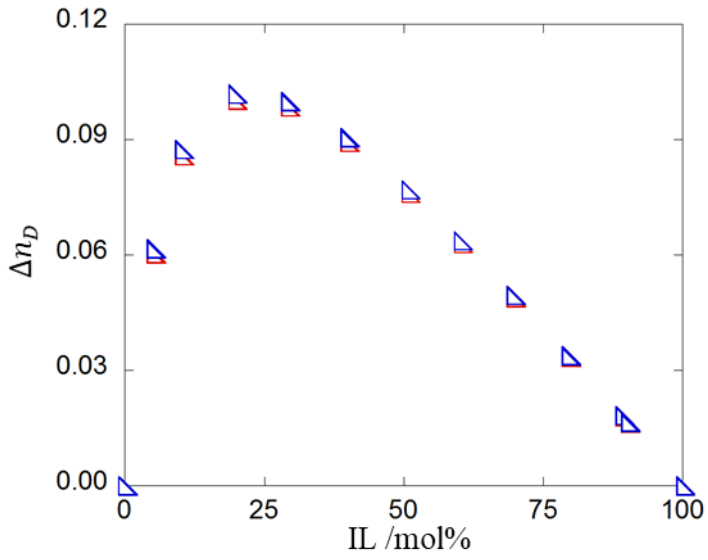

Figure 2.15 Refractive index of [EEPy][ESO_4]/water systems at 288.15 K and 298.15 K [Gonzalez et al. 2012]. Legend: (◺), 288.15 K; (◺), 298.15 K.

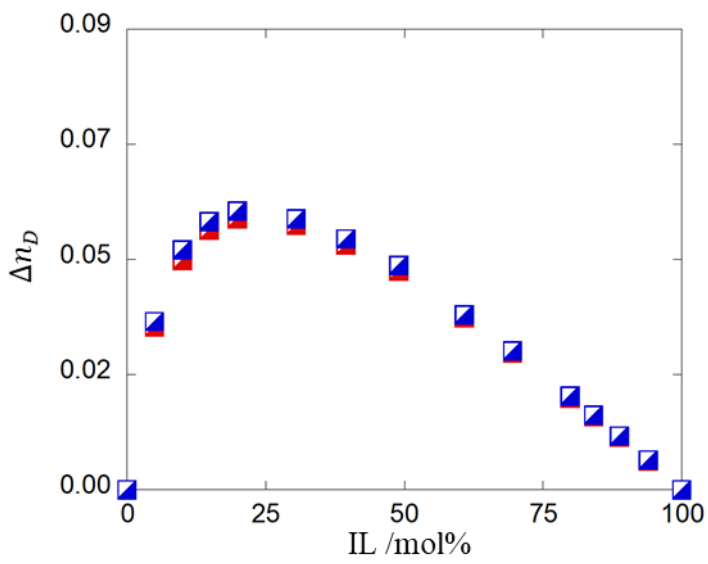

Figure 2.16 Refractive index of [C_2MIm][TfO]/water systems at 288.15 K and 298.15 K [Vercher et al. 2011]. Legend: (◪), 288.15 K; (◪), 298.15 K.

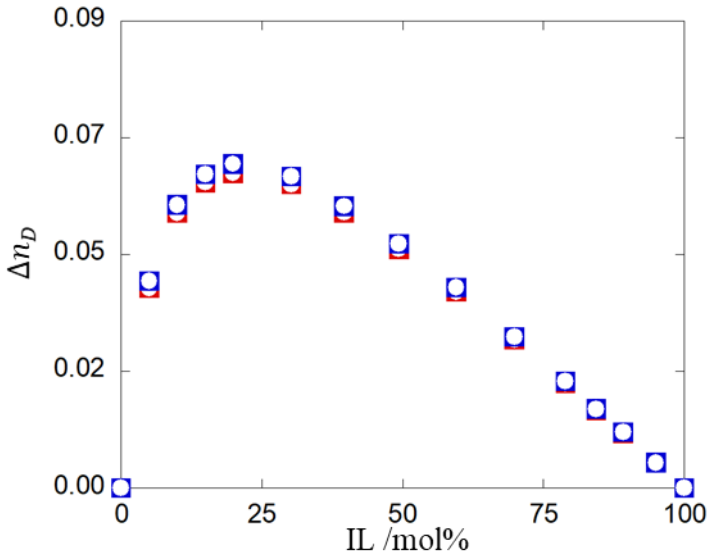

Figure 2.17 Refractive index of [BEIM][TfO]/water systems at 288.15 K and 298.15 K [Vercher et al. 2011]. Legend: (□), 288.15 K; (□), 298.15 K.

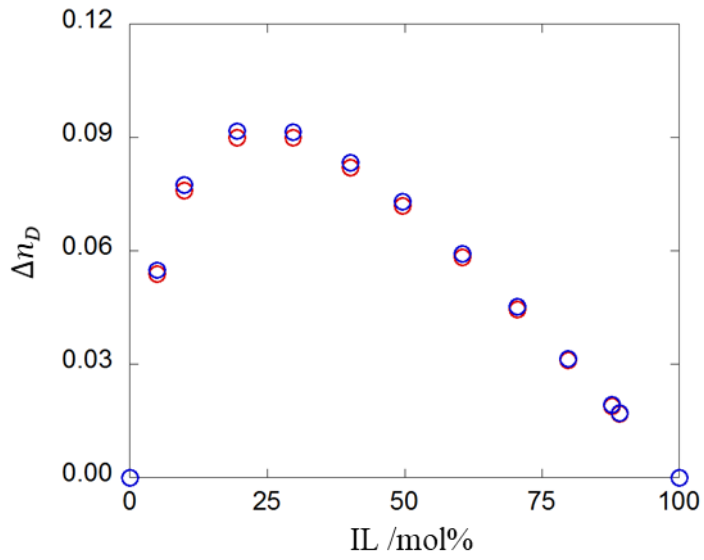

Figure 2.18 Refractive index of [C_4MIm][DCA]/water systems at 288.15 K and 298.15 K [Gonzalez et al. 2012]. Legend: (○), 288.15 K; (○), 298.15 K.

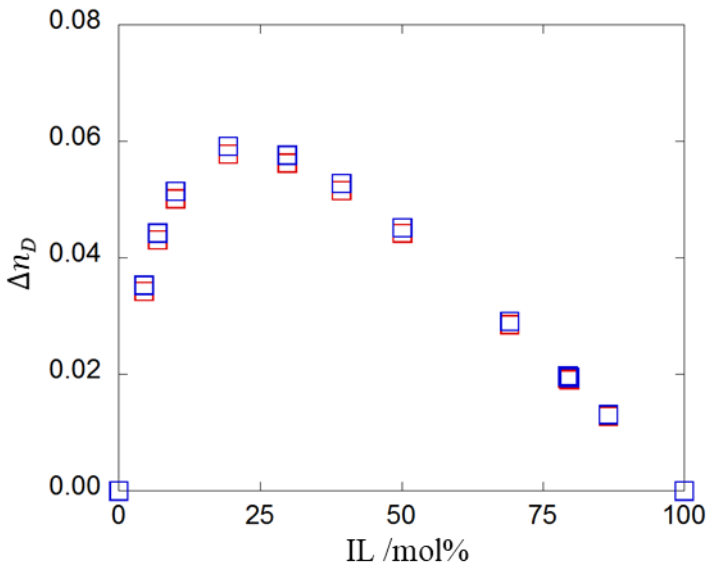

Figure 2.19 Refractive index of [C_4MIm][TfO]/water systems at 288.15 K and 298.15 K [Gonzalez et al. 2012]. Legend: (□), 288.15 K; (□), 298.15 K.

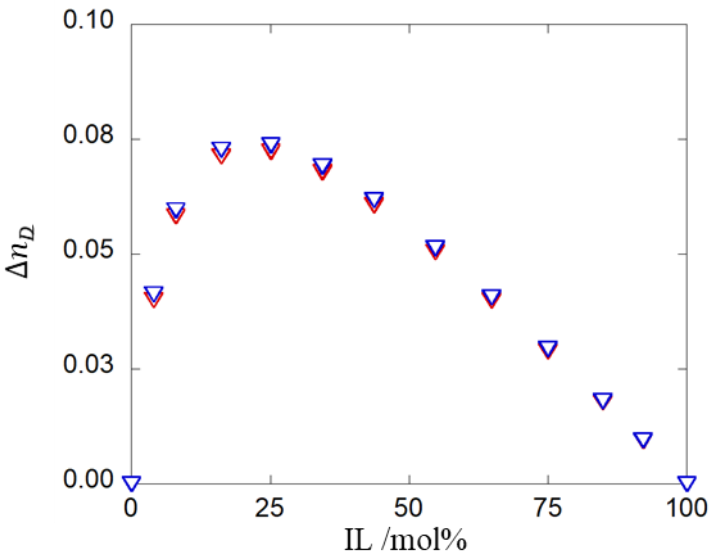

Figure 2.20 Refractive index of [BMPy][TfO]/water systems at 288.15 K and 298.15 K [Gonzalez et al. 2012]. Legend: (▽), 288.15 K; (▽), 298.15 K.

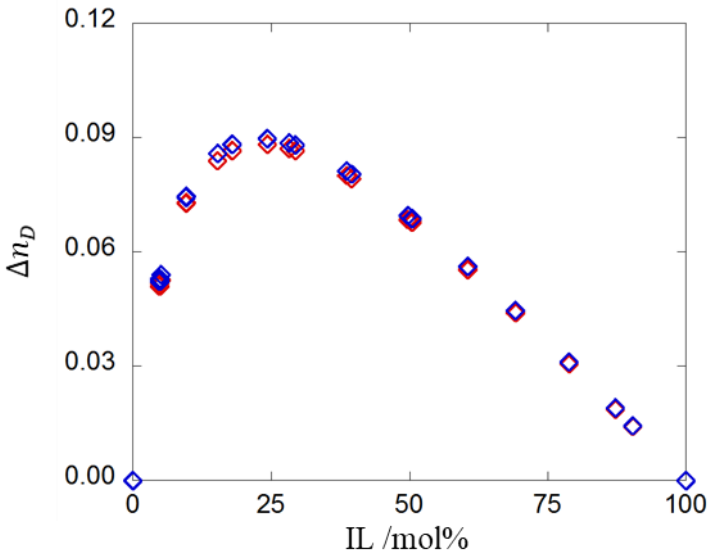

Figure 2.21 Refractive index of [BMPyr][DCA]/water systems at 288.15 K and 298.15 K [Gonzalez et al. 2012]. Legend: (◇), 288.15 K; (◇), 298.15 K.

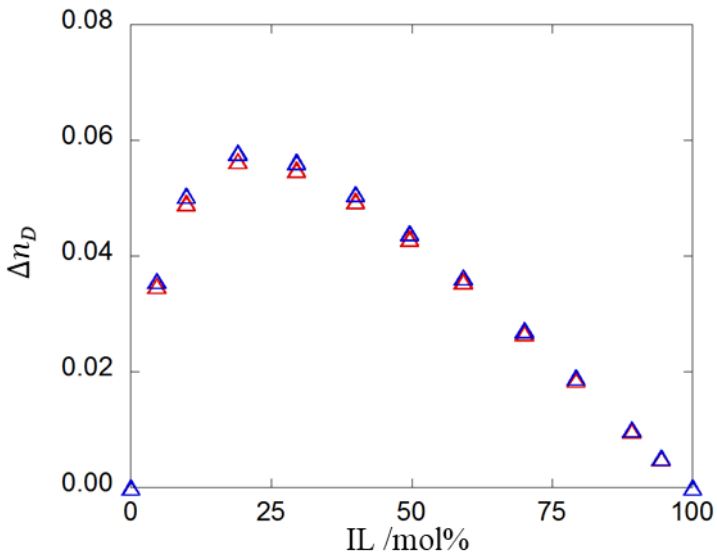

Figure 2.22 Refractive index of [BMPyr][TfO]/water systems at 288.15 K and 298.15 K [Gonzalez et al. 2012]. Legend: (△), 288.15 K; (△), 298.15 K.

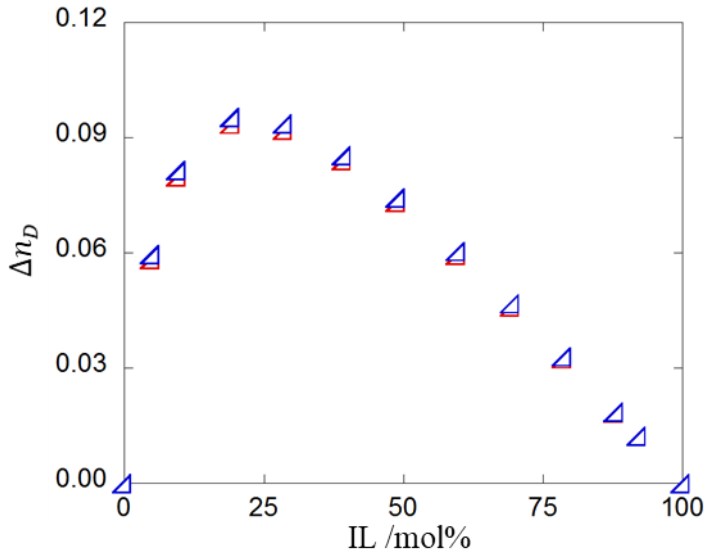

Figure 2.23 Refractive index of [HMIm][DCA]/water systems at 288.15 K and 298.15 K [Gonzalez et al. 2012]. Legend: (◿), 288.15 K; (◿), 298.15 K.

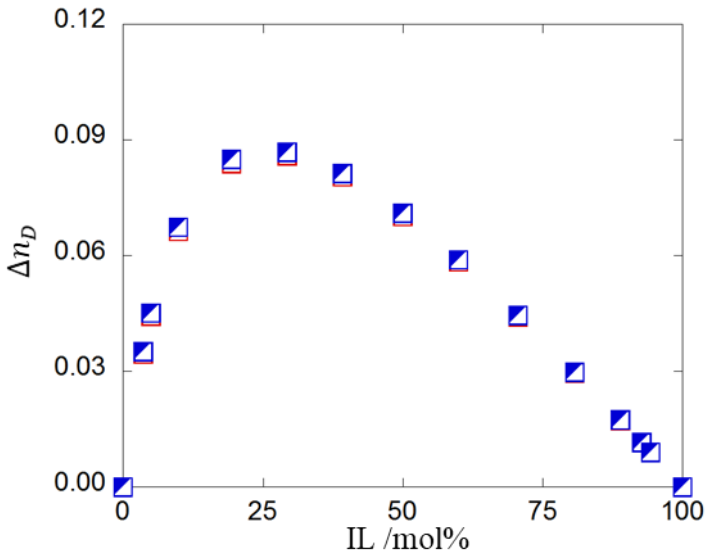

Figure 2.24 Refractive index of [MPy][MSO4]/water systems at 288.15 K and 298.15 K [Gonzalez et al. 2012]. Legend: (◩), 288.15 K; (◩), 298.15 K.

Table 2-1. Ionic liquids used in this study.

ionic liquid	abbreviation	purity	supplier
1-ethyl-3-methylimidazolium diethylphosphate	$[C_4MIm][DEP]$	>0.98	Kanto Chemical Co., Inc
1-ethyl-3-methylimidazolium tetrafluoroborate	$[C_4MIm]BF_4$	>0.95	Kanto Chemical Co., Inc
1-butyl-3-methylimidazolium acetate	$[C_4MIm][OAc]$	>0.95	Sigma Aldrich Co.
1-butyl-3-methylimidazolium tetrafluoroborate	$[C_4MIm]BF_4$	>0.95	Kanto Chemical Co., Inc
1-butyl-3-methylimidazolium iodide	$[C_4MIm]I$	>0.98	Kanto Chemical Co., Inc
1-methyl-3-octylimidazolium bromide	$[C_8MIm]Br$	>0.99	Kanto Chemical Co., Inc
N,*N*-diethyl-*N*-methyl-*N*-(2-methoxyethyl)ammonium tetrafluoroborate	$[DEME]BF_4$	>0.98	Kanto Chemical Co., Inc
ethylammonium nitrate	EAN	>0.97	Kanto Chemical Co., Inc
propylammonium nitrate	PAN	>0.97	Kanto Chemical Co., Inc

Table 2.2. Refractive index (n_D) data of various IL/water systems as a function of IL concentration at 293 K and 0.1 MPa.

T/K =293, *P*=0.1 MPa									
$[C_2MIm]BF_4$		$[C_2MIm]DEP$		$[C_4MIm]BF_4$		$[C_4MIm]I$		$[C_4MIm][OAc]$	
x/mol%	n_D	*x*/mol%	n_D	*x*/mol%	n_D	*x*/mol%	n_D	*x*/mol%	n_D
0	1.3333	0	1.3333	0	1.3333	0.0	1.3333	0	1.3333
1.0	1.3388	0.9	1.3500	1.2	1.3423	0.8	1.3519	1.0	1.3486
2.9	1.3476	2.8	1.3767	2.5	1.3507	2.1	1.3753	2.0	1.3622
5.0	1.3550	4.6	1.3959	3.7	1.3576	4.5	1.4104	5.0	1.3936
9.7	1.3676	9.3	1.4243	5.0	1.3625	8.4	1.4500	9.9	1.4257
16.8	1.3787	15.8	1.4433	6.5	1.3685	13.4	1.4821	16.7	1.4494
24.7	1.3872	23.0	1.4546	7.9	1.3730	21.2	1.5131	24.3	1.4646
35.9	1.3952	32.7	1.4621	10.0	1.3785	33.2	1.5390	36.4	1.4768
48.9	1.4009	45.4	1.4678	11.9	1.3826	45.6	1.5551	50.1	1.4846
76.3	1.4088	70.5	1.4721	14.6	1.3876	67.8	1.5722	75.9	1.4910
100	1.4123	94.0	1.4735	16.1	1.3899	93.0	1.5815	100	1.4940
		100	1.4742	19.1	1.3939	100	1.5824		
				22.1	1.3971				
				24.8	1.3996				
				29.3	1.4029				
				32.8	1.4054				
				35.0	1.4067				
				39.5	1.4087				
				43.9	1.4108				
				49.3	1.4133				
				55.5	1.4147				
				62.1	1.4165				
				66.8	1.4174				
				69.8	1.4183				
				75.9	1.4193				
				81.2	1.4201				
				91.0	1.4214				
				100	1.4226				

The relative standard uncertainty of n_D is ± 0.0001

Table 2.2 Continued

T/K =293, P=0.1 MPa							
[C_8MIm]Br		[DEME]BF_4		EAN		PAN	
x/mol%	n_D	x/mol%	n_D	x/mol%	n_D	x/mol%	n_D
0	1.3333	0	1.3333	0	1.3333	0	1.3333
1.0	1.3541	0.4	1.3362	0.1	1.3338	0.4	1.3363
3.0	1.3845	0.6	1.3371	0.4	1.3358	0.7	1.3389
5.0	1.4066	0.7	1.3382	0.7	1.3378	1.0	1.3410
9.9	1.4425	0.9	1.3397	1.0	1.3399	2.0	1.3484
16.6	1.4668	1.2	1.3417	1.6	1.3435	3.5	1.3579
24.4	1.4853	2.0	1.3460	3.3	1.3528	5.5	1.3663
37.1	1.5015	3.4	1.3526	5.0	1.3615	6.8	1.3748
49.8	1.5086	3.8	1.3543	8.0	1.3740	8.9	1.3836
75.2	1.5184	4.5	1.3573	9.7	1.3801	10.4	1.3888
100	1.5251	5.3	1.3598	13.1	1.3901	13.2	1.3975
		6.7	1.3642	15.4	1.3960	16.0	1.4044
		10.0	1.3723	18.5	1.4029	18.9	1.4102
		13.4	1.3785	21.3	1.4078	24.4	1.4196
		16.7	1.3827	24.6	1.4133	30.8	1.4274
		19.9	1.3862	28.9	1.4189	41.8	1.4368
		24.8	1.3904	34.8	1.4255	59.6	1.4453
		29.2	1.3934	40.2	1.4301	77.6	1.4510
		34.0	1.3962	58.6	1.4415	100	1.4561
		38.3	1.3980	73.9	1.4475		
		49.8	1.4020	100	1.4531		
		59.6	1.4047				
		79.8	1.4083				
		100	1.4104				

Table 2.3 Refractive index (n_D) data of various IL/water systems as a function of IL concentration at 288.15 K.

T/K =288.15									
[EEPy][ESO_4][a]		[C_2MIm][TfO][b]		[BEIM][TfO][b]		[C_4MIm][DCA][a]		[C_4MIm][TfO][a]	
x/mol%	n_D	x/mol%	n_D	x/mol%	n_D	x/mol%	n_D	x/mol%	n_D
0	1.33349	0	1.33351	0	1.33352	0	1.33349	0	1.33349
5.07	1.40430	4.95	1.37143	5.00	1.37880	4.67	1.39733	4.52	1.37365
10.16	1.43938	9.99	1.39058	9.99	1.39889	9.82	1.42867	6.91	1.38516
19.71	1.47121	14.83	1.40106	15.00	1.41026	19.05	1.46004	10.02	1.39564
29.16	1.48656	19.94	1.40835	19.94	1.41759	29.48	1.47799	19.36	1.41332
39.82	1.49668	30.51	1.41770	30.23	1.42638	39.97	1.48855	29.85	1.42301
50.78	1.50325	39.52	1.42298	39.63	1.43092	49.62	1.49536	39.38	1.42835
60.21	1.50723	49.03	1.42752	49.34	1.43425	59.20	1.50075	50.15	1.43224
69.63	1.51023	60.80	1.42996	59.56	1.43696	70.03	1.50476	69.17	1.43654
79.52	1.51266	69.54	1.43186	69.87	1.43871	79.24	1.50758	79.44	1.43810
89.11	1.51458	79.94	1.43369	78.91	1.44000	89.16	1.50953	79.72	1.43815
90.13	1.51478	84.12	1.43434	84.43	1.44063	94.41	1.50990	86.52	1.43903
100	1.51631	88.77	1.43497	89.15	1.44130	100	1.51213	100	1.44032
		93.99	1.43567	95.00	1.44182				
		100	1.43599	100	1.44235				

a: ref. [González et al. 2012], b: ref. [Vercher et al. 2011]

Table 2.3 continued

T/K =288.15									
[BMPy][TfO][a]		[BMPyr][DCA][a]		[BMPyr][TfO][a]		[C_6MIm][DCA][a]		[Mpy][MSO_4][a]	
x/mol%	n_D	x/mol%	n_D	x/mol%	n_D	x/mol%	n_D	x/mol%	n_D
0	1.33349	0	1.33349	0	1.33349	0.00	1.33349	0	1.33349
3.97	1.37998	4.83	1.39390	4.67	1.37399	5.01	1.40179	3.55	1.37506
7.99	1.40357	4.93	1.39472	9.82	1.39398	9.69	1.43179	5.03	1.38778
16.17	1.42747	5.08	1.39597	19.05	1.41085	19.33	1.46233	9.90	1.41884
25.06	1.44008	9.60	1.42386	29.48	1.41987	28.77	1.47716	19.42	1.45378
34.39	1.44770	9.66	1.42419	39.97	1.42501	39.31	1.48721	29.36	1.47388
43.72	1.45257	15.32	1.44481	49.62	1.42809	49.04	1.49312	39.23	1.48632
54.72	1.45651	17.92	1.45158	59.20	1.43031	59.81	1.49784	50.04	1.49567
64.85	1.45910	24.29	1.46368	70.03	1.43221	69.45	1.50096	59.95	1.50177
74.98	1.46111	28.23	1.46905	79.24	1.43345	78.76	1.50333	70.59	1.50679
84.83	1.46266	29.39	1.47041	89.16	1.43458	88.09	1.50525	80.73	1.51059
92.06	1.46358	38.63	1.47901	94.41	1.43506	92.15	1.50599	88.89	1.51315
100	1.46446	39.53	1.47970	100	1.43557	100.0	1.50729	92.70	1.51423
		49.77	1.48580					94.26	1.51462
		50.48	1.48621					100	1.51603
		60.58	1.49044						
		69.23	1.49322						
		78.84	1.49570						
		87.23	1.49752						
		90.40	1.49811						
		100	1.49968						

Table 2.4 Refractive index (n_D) data of various IL/water systems as a function of IL concentration at 298.15 K.

T/K =298.15									
[EEPy][ESO_4][a]		[C_2MIm][TfO][b]		[BEIM][TfO][b]		[C_4MIm][DCA][a]		[C_4MIm][TfO][a]	
x/mol%	n_D	x/mol%	n_D	x/mol%	n_D	x/mol%	n_D	x/mol%	n_D
0	1.33255	0	1.33250	0	1.33250	0	1.33255	0	1.33255
5.07	1.40198	4.954	1.36929	5.00	1.37638	4.67	1.39520	4.52	1.37157
10.16	1.43661	9.99	1.38737	9.99	1.39615	9.82	1.42613	6.91	1.38290
19.71	1.46831	14.834	1.39803	15.00	1.40736	19.05	1.45694	10.02	1.39323
29.16	1.48367	19.94	1.40554	19.94	1.41444	29.48	1.47495	19.36	1.41072
39.82	1.49381	30.511	1.41490	30.23	1.42339	39.97	1.48541	29.85	1.42021
50.78	1.50042	39.515	1.42008	39.63	1.42795	49.62	1.49223	39.38	1.42546
60.21	1.50440	49.028	1.42456	49.34	1.43128	59.20	1.49756	50.15	1.42940
69.63	1.50743	60.8	1.42722	59.56	1.43402	70.03	1.50161	69.17	1.43373
79.52	1.50984	69.535	1.42930	69.87	1.43579	79.24	1.50443	79.44	1.43530
89.11	1.51176	79.941	1.43086	78.91	1.43710	89.16	1.50631	79.72	1.43535
90.13	1.51196	84.121	1.43152	84.43	1.43775	94.41	1.50673	86.52	1.43626
100	1.51350	88.772	1.43210	89.15	1.43833	100	1.50893	100	1.43755
		93.994	1.43277	95.00	1.43890				
		100	1.43320	100	1.43944				

a: ref. [González et al. 2012], b: ref. [Vercher et al. 2011]

Table 2.4 Continued

T/K =298.15									
[BMPy][TfO][a]		[BMPyr][DCA][a]		[BMPyr][TfO][a]		[C_6MIm][DCA][a]		[Mpy][MSO_4][a]	
x/mol%	n_D	x/mol%	n_D	x/mol%	n_D	x/mol%	n_D	x/mol%	n_D
0	1.33255	0	1.33255	0	1.33255	0.00	1.33255	0	1.33255
3.97	1.37782	4.83	1.39161	4.67	1.37210	5.01	1.39945	3.55	1.37336
7.99	1.40118	4.93	1.39249	9.82	1.39161	9.69	1.42902	5.03	1.38593
16.17	1.42474	5.08	1.39362	19.05	1.40814	19.33	1.45924	9.90	1.41670
25.06	1.43724	9.60	1.42118	29.48	1.41708	28.77	1.47400	19.42	1.45141
34.39	1.44482	9.66	1.42145	39.97	1.42221	39.31	1.48405	29.36	1.47142
43.72	1.44968	15.32	1.44172	49.62	1.42536	49.04	1.48997	39.23	1.48384
54.72	1.45363	17.92	1.44870	59.20	1.42762	59.81	1.49467	50.04	1.49314
64.85	1.45623	24.29	1.46078	70.03	1.42951	69.45	1.49780	59.95	1.49921
74.98	1.45822	28.23	1.46612	79.24	1.43075	78.76	1.50016	70.59	1.50426
84.83	1.45982	29.39	1.46748	89.16	1.43187	88.09	1.50210	80.73	1.50803
92.06	1.46073	38.63	1.47610	94.41	1.43240	92.15	1.50284	88.89	1.51052
100	1.46155	39.53	1.47674	100	1.43289	100.0	1.50415	92.70	1.51159
		49.77	1.48284					94.26	1.51199
		50.48	1.48329					100	1.51340
		60.58	1.48751						
		69.23	1.49032						
		78.84	1.49278						
		87.23	1.49459						
		90.40	1.49519						
		100	1.49681						

Table 2.5. Refractive index (n_D) data of various IL/water systems as a function of IL concentration at 308.15 K

T/K =308.15									
[EEPy][ESO_4][a]		[C_2MIm][TfO][b]		[BEIM][TfO][b]		[C_4MIm][DCA][a]		[C_4MIm][TfO][a]	
x/mol%	n_D	*x*/mol%	n_D	*x*/mol%	n_D	*x*/mol%	n_D	*x*/mol%	n_D
0	1.33131	0	1.33351	0	1.33352	0	1.33131	0	1.33131
5.07	1.40013	4.95	1.37143	5.00	1.37880	4.67	1.39322	4.52	1.36969
10.16	1.43375	9.99	1.39058	9.99	1.39889	9.82	1.42382	6.91	1.38091
19.71	1.46515	14.83	1.40106	15.00	1.41026	19.05	1.45386	10.02	1.39103
29.16	1.48071	19.94	1.40835	19.94	1.41759	29.48	1.47147	19.36	1.40803
39.82	1.49094	30.51	1.41770	30.23	1.42638	39.97	1.48225	29.85	1.41759
50.78	1.49759	39.52	1.42298	39.63	1.43092	49.62	1.48897	39.38	1.42268
60.21	1.50156	49.03	1.42752	49.34	1.43425	59.20	1.49443	50.15	1.42655
69.63	1.50461	60.80	1.42996	59.56	1.43696	70.03	1.49821	69.17	1.43090
79.52	1.50705	69.54	1.43186	69.87	1.43871	79.24	1.50114	79.44	1.43253
89.11	1.50896	79.94	1.43369	78.91	1.44000	89.16	1.50321	79.72	1.43259
90.13	1.50914	84.12	1.43434	84.43	1.44063	94.41	1.50348	86.52	1.43343
100	1.51067	88.77	1.43497	89.15	1.44130	100	1.50578	100	1.43475
		93.99	1.43567	95.00	1.44182				
		100	1.43599	100	1.44235				

a: ref. [González et al. 2012], b: ref. [Vercher et al. 2011]

Table 2.5. continued

T/K =308.15									
[BMPy][TfO][a]		[BMPyr][DCA][a]		[BMPyr][TfO][a]		[C_6MIm][DCA][a]		[Mpy][MSO_4][a]	
x/mol%	n_D	x/mol%	n_D	x/mol%	n_D	x/mol%	n_D	x/mol%	n_D
0	1.33131	0	1.33131	0	1.33131	0.00	1.33131	0	1.33131
3.97	1.37570	4.83	1.38970	4.67	1.37023	5.01	1.39679	3.55	1.37158
7.99	1.39863	4.93	1.39055	9.82	1.38937	9.69	1.42645	5.03	1.38397
16.17	1.42192	5.08	1.39175	19.05	1.40557	19.33	1.45590	9.90	1.41447
25.06	1.43429	9.60	1.41891	29.48	1.41430	28.77	1.47076	19.42	1.44897
34.39	1.44183	9.66	1.41909	39.97	1.41943	39.31	1.48083	29.36	1.46886
43.72	1.44673	15.32	1.43884	49.62	1.42262	49.04	1.48679	39.23	1.48134
54.72	1.45069	17.92	1.44577	59.20	1.42490	59.81	1.49131	50.04	1.49057
64.85	1.45331	24.29	1.45746	70.03	1.42683	69.45	1.49462	59.95	1.49665
74.98	1.45535	28.23	1.46281	79.24	1.42808	78.76	1.49698	70.59	1.50170
84.83	1.45694	29.39	1.46424	89.16	1.42918	88.09	1.49894	80.73	1.50539
92.06	1.45784	38.63	1.47289	94.41	1.42970	92.15	1.49962	88.89	1.50794
100	1.45868	39.53	1.47345	100	1.43018	100.0	1.50100	92.70	1.50895
		49.77	1.47973					94.26	1.50937
		50.48	1.47987					100	1.51077
		60.58	1.48432						
		69.23	1.48710						
		78.84	1.48982						
		87.23	1.49162						
		90.40	1.49222						
		100	1.49392						

Table 2.6 Refractive index (n_D) data of various IL/water systems as a function of IL concentration at 318.15 K ~ 338.15 K [Vercher et al. 2011].

T/K =318.15				*T*/K =328.15			
[C_2MIm][TfO]		[BEIM][TfO]		[C_2MIm][TfO]		[BEIM][TfO]	
x/mol%	n_D	*x*/mol%	n_D	*x*/mol%	n_D	*x*/mol%	n_D
0	1.32965	0	1.32966	0	1.32784	0	1.32784
4.95	1.36455	5.00	1.37145	4.95	1.36203	5.00	1.36886
9.99	1.38286	9.99	1.39061	9.99	1.38018	9.99	1.38813
14.83	1.39377	15.00	1.40141	14.83	1.39109	15.00	1.39882
19.94	1.39987	19.94	1.40850	19.94	1.39710	19.94	1.40541
30.51	1.40921	30.23	1.41740	30.51	1.40629	30.23	1.41445
39.52	1.41448	39.63	1.42193	39.52	1.41212	39.63	1.41894
49.03	1.41900	49.34	1.42535	49.03	1.41627	49.34	1.42239
60.80	1.42164	59.56	1.42816	60.80	1.41891	59.56	1.42524
69.54	1.42360	69.87	1.42999	69.54	1.42084	69.87	1.42710
79.94	1.42537	78.91	1.43134	79.94	1.42264	78.91	1.42846
84.12	1.42620	84.43	1.43191	84.12	1.42347	84.43	1.42901
88.77	1.42669	89.15	1.43265	88.77	1.42394	89.15	1.42980
93.99	1.42732	95.00	1.43313	93.99	1.42452	95.00	1.43029
100	1.42767	100	1.43358	100	1.42494	100	1.43073

Table 2.6 Continued

T/K =338.15			
[C_2MIm][TfO]		[BEIM][TfO]	
x/mol%	n_D	*x* / mol%	n_D
0	1.32581	0	1.32581
4.95	1.35943	5.00	1.36608
9.99	1.37739	9.99	1.38556
14.83	1.38829	15.00	1.39592
19.94	1.39415	19.94	1.40227
30.51	1.40338	30.23	1.41150
39.52	1.40853	39.63	1.41593
49.03	1.41302	49.34	1.41941
60.80	1.41621	59.56	1.42231
69.54	1.41807	69.87	1.42420
79.94	1.41989	78.91	1.42562
84.12	1.42083	84.43	1.42616
88.77	1.42121	89.15	1.42697
93.99	1.42181	95.00	1.42744
100	1.42222	100	1.42788

Table 2.7 Refractive index (n_D) data of various IL/water systems at 293 K calculated by the least-squares method from the data reported by Gonzalez et al. 2012 and Vercher et al. 2011.

T/K =293									
[EEPy][ESO_4]		[C_2MIm][TfO]		[BEIM][TfO]		[C_4MIm][DCA]		[C_4MIm][TfO]	
x/mol%	n_D	*x*/mol%	n_D	*x*/mol%	n_D	*x*/mol%	n_D	*x*/mol%	n_D
0	1.33300	0	1.33320	0	1.33321	0	1.33300	0	1.33300
5.07	1.40318	4.95	1.37046	5.00	1.37770	4.67	1.39628	4.52	1.37263
10.16	1.43799	9.99	1.38916	9.99	1.39751	9.82	1.42742	6.91	1.38405
19.71	1.46974	14.83	1.39967	15.00	1.40880	19.05	1.45849	10.02	1.39445
29.16	1.48511	19.94	1.40701	19.94	1.41610	29.48	1.47643	19.36	1.41201
39.82	1.49525	30.51	1.41637	30.23	1.42492	39.97	1.48698	29.85	1.42163
50.78	1.50184	39.52	1.42157	39.63	1.42948	49.62	1.49378	39.38	1.42691
60.21	1.50581	49.03	1.42606	49.34	1.43282	59.20	1.49916	50.15	1.43082
69.63	1.50883	60.80	1.42861	59.56	1.43554	70.03	1.50316	69.17	1.43513
79.52	1.51125	69.54	1.43059	69.87	1.43730	79.24	1.50599	79.44	1.43670
89.11	1.51317	79.94	1.43232	78.91	1.43859	89.16	1.50793	79.72	1.43675
90.13	1.51337	84.12	1.43299	84.43	1.43922	94.41	1.50831	86.52	1.43764
100	1.51490	88.77	1.43358	89.15	1.43986	100	1.51053	100	1.43893
		93.99	1.43428	95.00	1.44038				
		100	1.43462	100	1.44092				

Chapter 3

Physicochemical properties of water confined in the pocket formed in a typical ionic liquid [C_4MIm]BF_4 and the size of the pocket.

3.1 Introduction

In IL structure, the existence of a pocket (cavity) have been suggested [Hung et al. 2005, Cadena et al. 2004, Anthony et al. 2005]. The existence of the pocket has been supported by carbon dioxide absorption experiments. An IL has a smaller volume expansion than that of an organic solvent when dissolving CO_2. Such volume behavior is interpreted to indicate that the IL has a large pocket compared to the molecular solvent, and that CO_2 occupies the pocket. In the case that water is mixed with ILs, water is also confined in the pocket in ILs, and the pocket is called "water pocket". In preceding researches, the size of the water pocket depends on viewpoints and the physicochemical properties of the water confined in the water pocket and the size of the pocket are not elucidated well. The research objectives in this section is estimating the size of a pocket formed in a typical IL and elucidating the physicochemical properties of water confined in a pocket formed in an IL based on chemical shift, self-diffusion coefficient, viscosity and density.

3.2 Material and Method

3.2.1 Samples

$[C_4MIm]BF_4$ was placed under vacuum to less than 4 Pa to remove impurities at room temperature for more than 72 h before use. Twenty alcohols, methanol, ethanol 1-propanol, 1-butanol, 1-pentanol, 1-hexanol, 1-heptanol, 1-octanol, 1-nonanol, 1-decanol, 1-undecanol and 1-dodecanol were used which are summarized in Table 3.1. The ultrapure water used in this study was supplied by a Synergy UV system (Millipore Inc.). Solutions of different concentrations (*x* mol% alcohol or water) were prepared by mixing the required amounts of $[C_4MIm]BF_4$ with water or alcohols.

3.2.2 NMR measurement

NMR measurements were conducted using an AVANCE III HD spectrometer (Bruker, 600 MHz). ^{1}H and ^{19}F spectra were measured using a BBFO probe, and double NMR tubes were employed to avoid mixing the sample and lock solvent (D_2O) containing the chemical shift references; sodium 3-(trimethylsilyl) propionate-2,2,3,3-d_4 for ^{1}H-NMR and 2,2,2-trifluoroacetic acid for ^{19}F-NMR which are summarized in Table 3.1. The ^{1}H-NMR spectroscopy parameters were a 20.0 ppm spectral width, 64k (16k) sample points, 4 (8) scans, 0.37 (1.46) Hz digital resolution, and a 10 s pulse delay. The ^{19}F-NMR spectroscopy parameters were as follows: 237.2 (3.0) ppm spectral width, 520k (8k) sample points, 10 s pulse delay, 4 (8) scans, and 0.18 (0.7) Hz digital resolution. Brackets shows the condition for self-diffusion coefficient measurement. Pulse-gradient spin-echo (PGSE) NMR measurements were performed at 298 K. Measurements of the self-diffusion coefficients for the cations, alcohol, and anion were conducted using ^{1}H and ^{19}F nuclei, respectively.

The self-diffusion coefficient (D) was calculated by plotting the echo attenuation (E) according to Eq. (1) for a single diffusing species [Stejskal et al. 1965]:

$$E = \exp(-\gamma^2 g^2 \delta^2 D(\Delta - \delta/3)) \quad (3.1)$$

where g is the magnetic field gradient strength, Δ is the interval between the gradient pulses, δ is the duration of the gradient pulse, and γ is the gyromagnetic ratio. In the present experiments, δ was set to 1.5 ms, g (16 different points) ranged from 39.1 mT/m to 0.449 T/m, and Δ was set to 15–1000 ms. The gradient settings used were selected to cause sufficient signal attenuation to enable

an accurate estimate of the diffusion coefficients. Accuracy of the measurements was less than 3% standard error in the self-diffusion and chemical shift.

3.2.3 Viscosity measurement

Viscosity measurements were carried out using a SV-10 instrument (A&D Inc.) calibrated with a temperature controlled water bath (Millipore Inc.) at 298.0 K (±0.5 K). The accuracy of the viscosity results was approximately ±3%.

3.2.4 Density measurement

Density measurements were carried out using a Density / Specific Gravity Meter DA-645 calibrated with water and air (0.99705 m^3/kg and 0.00118 m^3/kg) at 298.0 K. The temperature error is ± 0.01 K.

3.3 Result and Discussion

3.3.1 Solubility of alcohol in $[C_4MIm]BF_4$

Water, methanol and ethanol can be dissolved in $[C_4MIm]BF_4$ over the entire concentration range at 298 K; however, the solubility of alcohols with longer alkyl chain lengths than ethanol decreases as the alkyl chain length increases [Wagner et al. 2003, Crosthwaite et al. 2004, Crosthwaite et al. 2005]. The explicit solubilities of each alcohol in $[C_4MIm]BF_4$ at 298 K have not been specifically investigated. Therefore, the saturated solubility of each alcohol in $[C_4MIm]BF_4$ was determined from ^{1}H NMR spectral measurements. For the 1-propanol to 1-dodecanol systems, excess alcohol was added to $[C_4MIm]BF_4$ until phase separation was visually confirmed, and after that, it was left for 24 h or more. The $[C_4MIm]BF_4$-rich saturated solution was then sampled and ^{1}H-NMR spectra were measured. Representative ^{1}H-NMR spectra of the water to ethanol systems at 50 mol% and 1-propanol to 1-hexanol systems at saturation solubility and pure $[C_4MIm]BF_4$ are shown in Figure 3.1a~d.

The saturated solubility was determined from the ratio of the peak area intensity of the alcohol to $[C_4MIm]BF_4$ and the results are shown in Table 3.2 and Figure 3.2. Based on these results, measurements of the chemical shift and the self-diffusion coefficient were performed below the saturation concentration for each alcohol. To investigate the concentration dependence, methanol to 1-hexanol having a solubility of 10 mol% or more were used.

3.3.2 Concentration dependence of density in [C_4MIm]BF_4/water and [C_4MIm]BF_4/alcohol system

If water and alcohol enter into the pockets, it is expected that solution volume has little change even though water or alcohols are added into an IL. In order to investigate the volume change on IL/water and IL/alcohol systems, the density of [C_4MIm]BF_4/alcohol and [C_4MIm]BF_4/water mixture were measured.

The dependence of the density on the alcohol or water concentration in the [C_4MIm]BF_4/alcohol and [C_4MIm]BF_4/water mixtures at 298 K is shown in Figure 3.3 and Table 3.3. As over trend, all the density of [C_4MIm]BF_4/water and [C_4MIM]BF_4]/alcohol systems showed the same concentration dependence. In particular, up to 50 mol% density decrease loosely with increasing concentration whereas over 50 mol% decrease drastically with increasing concentration.

Subsequently, volume expansivity ($\Delta V/V$) was calculated by using Eq. (3.2) in order to investigate solution volume change.

$$\frac{\Delta V}{V} = \frac{V_{\mathrm{mix}} - V_{\mathrm{IL}}}{V_{\mathrm{IL}}} = \frac{1/\rho_{\mathrm{mix}} - 1/\rho_{\mathrm{IL}}}{1/\rho_{\mathrm{IL}}} \quad (3.2)$$

where V_{mix} is volume of IL/water or IL/alcohol system, V_{IL} is volume of pure IL, ρ_{mix} is density of IL/water or IL/alcohol systems, ρ_{IL} is density of pure IL. The dependence of the volume expansivity on the alcohol or water concentration in the [C_4MIm]BF_4/alcohol and [C_4MIm]BF_4/water systems is shown in Figure 3.4 (a) and Table 3.4. In preceding study, the concentration dependence of the volume expansivity on IL/CO_2 system and organic solvent/CO_2 were also reported [Chiehming.

Et al. 1998, Aki, et al. 2004, Blanchard et al. 2001, Kordikowski et al. 1995, Makino et al. 2012], as shown in Figure 3.4 (b). According to this study, the volume expansivity of the IL/CO_2 systems is obviously smaller than the organic solvent systems. This has interpreted by occupying cavity in the ionic liquids. Furthermore, it has been reported from the MD results that the IL structure is maintained by dissolution of CO_2 at low CO_2 concentrations.

As a result, the volume expansivity of [C_4MIm]BF_4/alcohol and [C_4MIm]BF_4/water systems were clearly smaller than that of IL/CO_2 systems and organic solvent/CO_2 systems. Moreover, volume expansivity of [C_4MIm]BF_4/alcohol and [C_4MIm]BF_4/water systems were less than 4 % up to 20 mol%. Therefore, adding water or alcohols into [C_4MIm]BF_4 didn't increase solution volume significantly, indicating that the water and alcohols may enter into the pocket formed in the IL at less than 20 mol%. In other words, the pocket size is more than 1-hexanol size (100 $Å^3$) at least.

3.3.3 Concentration dependence of chemical shift in [C_4MIm]BF_4/water and [C_4MIM]BF_4/alcohol system

In order to investigate interactions between IL structure and water or alcohol in IL, the chemical shift for [C_4MIm]BF_4/alcohol and [C_4MIm]BF_4/water mixture were measured. The dependence of the ^{1}H chemical shift of the cation on the alcohol or water concentration in the [C_4MIm]BF_4/alcohol and [C_4MIm]BF_4/water mixtures at 298 K is shown in Figure 3.5-3.12 and Table 3.5-3.11.

In over trend, all the ^{1}H chemical shift of cation showed the same concentration dependence in [C_4MIm]BF_4/water and [C_4MIM]BF_4]/alcohol systems. At 20 mol% or less, where most alcohol systems are soluble in the IL, differences in chemical shift within 0.05 ppm were observed, despite the addition of alcohol (from methanol to 1-hexanol). Compared to water, the difference between alcohols was very small at 0.1 ppm or less, and thus they were all in good agreement. This result indicated that there is almost no change in the interactions that the cations undergo. Over 20 mol% of alcohol, downfield shifts were also observed with an increase of the alcohol concentration in the methanol and ethanol systems, which can be dissolved in [C_4MIm]BF_4 over the entire concentration range, meaning that the IL structure changes. On the other hand, water system showed significantly downfield shift over the 75 mol%. This results were good agreement with some research of [C_4MIm]BF_4/water system in which nano-heterogenious structure maintains up to ca. 75 mol% of water.[Gao J.et al. (2016)]

Figure 3.13 shows the ^{19}F chemical shift of the anion for the alcohol/[C_4MIm]BF_4 mixtures at 298 K. At 20 mol% or less, only differences within a chemical shift of 0.2 ppm were observed. In terms of both cations and anions, this suggested that the structure of the IL does not change significantly, even if alcohols are added to the IL, as with the water/IL system. In addition, at 20 mol% of alcohol and greater, the chemical shifts of the methanol and ethanol systems clearly moved upfield compared to the water/IL system. On the other hand, water system showed downfield shift over the 75 mol%. This result indicates that there is almost no change in the interactions that the anions undergo up to 20 mol%. Thus, from the result of the ^{1}H chemical shift of cation and the ^{19}F chemical shift of the anion, the addition of an alcohol with an alkyl chain length of 1 to 6 hardly affect the structure of the IL in a static view up to 20 mol%. Over 75 mol% it is expected that the chemical shift deviation was caused by the difference of hydrogen-bond strength between anion and hydroxyl groups of water or alcohol depending on alkyl chain length.

Figure 3.14 also showed the concentration dependence of the ^{1}H chemical shift for the hydroxyl groups of water and alcohol. Both the water/IL system and the alcohol/IL systems showed almost the same concentration dependence over the entire concentration range. At 20 mol% or less, the chemical shift did not change significantly, even if the water or methanol to 1-hexanol concentrations were increased, and there was almost no difference among them. This suggests that water and alcohol may exist in almost the same environment, although characteristics such as the molecular size, hydrophobicity, and shape, are also different. Furthermore, the downfield shift when

a monomer becomes dimers by hydrogen bonding has been reported to be 0.5 ~ 1 ppm. [Eblinger et al. 1996, Aidas et al. 2006, Yamaguchi et al.] In the present experiments, chemical shift change of water and alcohols at 20 mol% or less were within 0.3 ppm. Therefore, it suggests that most of water or alcohols exist as monomers at that low concentration region.

From these results, the pure IL structure maintains and water and alcohols exist as monomer up to 20 mol% in $[C_4MIm]BF_4$/alcohol systems and $[C_4MIm]BF_4$/water system. In other words, monomer water and alcohols in the pockets formed in IL don't affect IL structure significantly in this region.

3.3.4 About limiting effect and NMR self-diffusion coefficient measurement

Self-diffusion coefficient measurement is obtained from the correlation between the change of a nucleus position on a molecule and the attenuation of the NMR spectrum (Figure 3.15) using by Eq. (3.1). For this reason, when a molecular position hardly changes since the molecule move in the restricted space, a value lower than the true self-diffusion coefficient can be obtained. The phenomena is called “limiting effect”. When the self-diffusion coefficient on a sample without limiting effect is measured, a straight line is shown when the square of the gradient pulse intensity and the logarithmic spectrum intensity are plotted (Figure 3.16). On the other hand, when the self-diffusion coefficient on a sample with limiting effect is measured, the same plot as the previous sentence draws a curve. In all the systems measured in this study, no limiting effect was observed.

3.3.5 Concentration dependence of self-diffusion coefficient in $[C_4MIm]BF_4$/water and $[C_4MIm]BF_4$/alcohol system

In order to investigate how water and alcohol in the IL move, the self-diffusion coefficient for $[C_4MIm]BF_4$/alcohol and $[C_4MIm]BF_4$/water mixture were measured. The self-diffusion coefficient (*D*) of protons at the 2H, 4H, 5H, 6H, 7H, 8H, 9H, and 10H positions in the $[C_4MIm]$ cation was determined from ^{1}H-NMR measurements. There was no significant difference in the *D*s at all protons of the cation when compared at the same concentration. Therefore, their average value was taken as the *D*s of the cation. The *D*s of the alcohols were determined using the average values of ethyl and methyl groups of the alkyl chain for the same reason as the $[C_4MIm]$ cation. In this study, the *D*s of cations and alcohols were calculated using only completely separated peaks. The *D* of the anions was measured using ^{19}F-NMR. The concentration dependence of the *D*s of the cations, anions, alcohols and water of the alcohol/$[C_4MIm]BF_4$ mixtures and the water/$[C_4MIm]BF_4$ mixture at 298 K is shown in Figure 3.17-19 and Table 3.12.

As an overall trend, the *D*s of alcohols, anions, cations and water in all the systems increased gradually for alcohol or water concentrations up to 50 mol%. However, the *D*s of alcohol anions, cation, and water then increased rapidly as the alcohol or water concentration was increased to over 70 mol%.

To obtain information on the effect of the alkyl chain length, we focused on the concentration region less than 20 mol%, where most of the alcohols can be dissolved (Figure 3.20-22). The *D*s of

either the IL anions or cations were not dependent on the alkyl chain length of the alcohol at low alcohol concentration. In addition, the *D*s of the anions and cations were almost coincident with each other when comparing the same alcohol or water concentration. Therefore, it is considered that the nano-heterogeneous structure is maintained in this region from a dynamic viewpoint. The results are consistent that [C_4MIm] and BF_4 conformation measured by Raman spectroscopy showed only slightly change at low alcohol concentration (Yoshimura et al. 2019a).

The *D*s of alcohol showed dependence on the alkyl chain length of the alcohol, unlike the cations and anions. The water has a larger *D* than the alcohols, and the *D*s of the alcohols decreases as the number of carbons in the alkyl chain increases.

In the previous research on water/IL systems, water was determined to exist as small domain in the IL-rich region [Rollet et al. 2007, Bernardes et al. 2011, Gao et al. 2016, Feng et al. 2010]. In view of the prior research and the present results, the following solution structures are expected in alcohol/IL systems. In the concentration range of 20 mol% or less, alcohols may move in the nano-heterogeneous structure of the pure IL in terms of the *D* as with the water/IL system, even with the addition of alcohols having 1 to 6 carbon atoms in the alkyl chain.

To compare the movement of the IL and the alcohol in more detail, we calculated the mean distance travelled (*L*) per 1 s by using Eq (3.3) at alcohol or water concentration extrapolated to 0 mol%, as shown in Figure 3.23 and Table 3.13.

$$L = \sqrt{2D\Delta} \quad (3.3)$$

where D is self-diffusion coefficient, Δ is diffusion time. The L of the water was the highest and the L decreased with increasing alkyl chain length of alcohol. Comparing Ls of the water or the alcohols and that of the IL, the L of the water was more than 4 time compared to that of the IL whereas that of 1-hexanol was about 1.5 times compared to that of the IL. Interestingly, the Ls of 1-butanol to 1-hexanol decrease loosely compare with that of water to 1-propanol and the difference between the Ls of IL and that of alcohols were the almost same. Since limiting effect was not observed, the movements of the water and the alcohols can be treated as not in restricted space, meaning that the water and small alcohols which move clearly faster than IL don't move fast only in the pocket but move between the pockets.

Typically, the self-diffusion coefficient of a molecule in solution is generally correlated with the molecular radius. This relationship is expressed by the Stokes-Einstein equation,[Einstein et al. 1956] represented by Eq. (3.4):

$$D = \frac{kT}{C\pi\eta r} \qquad (3.4)$$

where k is the Boltzmann constant, T is the absolute temperature, D is the self-diffusion coefficient, c is a constant depending on boundary condition, r is the molecular radius, and η is the viscosity. From Eq. (3.4) we find that there is an inverse relationship between the self-diffusion coefficient and the particle radius, indicating that the smaller the particle, the larger the self-diffusion coefficient. Thus, the fact that L for water and alcohols are higher than that for the anion and cation may simply reflect the molecular radii difference. From Eq (3.4), if D is proportional to inverse r, the

D ratio of water or alcohols to anion or cation ($D_{\mathrm{solvent}}/D_{\mathrm{anion}}$, $D_{\mathrm{solvent}}/D_{\mathrm{cation}}$) is proportional to *r* ratio of anion or cation to water or alcohols ($r_{\mathrm{anion}}/r_{\mathrm{solvent}}$, $r_{\mathrm{cation}}/r_{\mathrm{solvent}}$). Therefore, we checked the relationship between the *D* ratio and *r* ratio at alcohol or water concentration extrapolated to 0 mol% shown in Figure 3.24 (information on molecular size shown in Table 3.14 [Yoshimura et al. 2019a, Tokuda et al. 2005]). The *D* ratio was determined to have the following order: water > methanol > ethanol > 1-propanol, and no significant differences were observed for the alcohols above 1-propanol. On the contrary, the *r* ratio had no significant difference between water to 1-hexanol compared the *D* ratio. It means that *D* ratio isn't simply proportional to the *r* ratio. In other words, the *D*s of water and alcohols in the IL don't simply depends on molecular size. From the result of the IL structure maintaining up to 20 mol% from dynamic and static views, water and alcohols move in pure IL structure. Therefore, it is expected that local interaction between the alcohols and the IL does not directly reflect the bulk solution viscosity. For this reason, the relationship between viscosity, which is a macroscopic property, and self-diffusion coefficient, which is a microscopic property, is discussed in next section.

3.3.6 Relationship between self-diffusion coefficient and viscosity in $[C_4MIm]BF_4$/water and $[C_4MIm]BF_4$/alcohol system

Generally, the diffusion of molecules is highly correlated to the macroscopic viscosity (η) of the fluid, and the Stokes−Einstein (SE) equation Eq. (3.4) is often applied. According to this equation, the self-diffusion coefficient is proportional to the inverse of the viscosity of the solution. This equation can be expressed as Eq. (3.5) by logarithmizing both sides.

$$\log(D) = \log\left(\frac{1}{\eta}\right) + \log\left(\frac{kT}{c\pi r}\right) \qquad (3.5)$$

From Eq. (3.5), the slope on $\log(D)$ vs. $\log\left(\frac{1}{\eta}\right)$ is simply reflected the relationship between the macroscopic viscosity and microscopic diffusion since $\log\left(\frac{kT}{c\pi r}\right)$ is an intercept. The relationship between the D and η were investigated in water to 1-hexanol systems at less than 50 mol% shown in Figure 3.25-27 (viscosity value summarized in Table 3.15). The dependence of the Ds of the cation and that of the anion with respect to the η were same at low concentrations regardless of water to 1-hexanol systems. The slope of anions and cations calculated using least squares method showed around 0.9, meaning that the movements of cation and anion are almost proportional to bulk solution movement. On the other hand, the slope of water had the lowest value and Ds of alcohols became more sensitive to the viscosity change as the carbon number of alcohol increased, as shown in Figure 3.28 and Table 3.16. It means that the movements of the water and the alcohols were not simply proportional to bulk solution movement. The slope of water to 1-propanol were clearly lower than that of anion and cation, suggesting that the movements of the water and the alcohols doesn't reflect

the movement of bulk solution. In other words, they moves independently to the movement of the bulk solution to some extent. On the contrary, the slope of 1-butanol to 1-hexanol had no significantly difference with anion and cation, suggesting that the movements of the alcohols are in good agreement with the movement of bulk solution.

In summary, the following dynamic model could be obtained for the water and alcohols in the IL as shown in Figure 3.29. The IL structure hardly change from the view of the dynamic (self-diffusion coefficient) and static (chemical shift) properties, even though 1-hexanol was added up to 20 mol%. The pocket size in the IL structure is at least more than 1-hexanol size (100 $Å^3$) from the density data. Moreover, from macroscopic (viscosity) and microscopic (self-diffusion coefficient) dynamic views, the movement of water and small alcohols in the IL isn't restricted in the pocket and move between the pockets whereas that of large alcohols are restricted in the pocket compared to water and small alcohols.

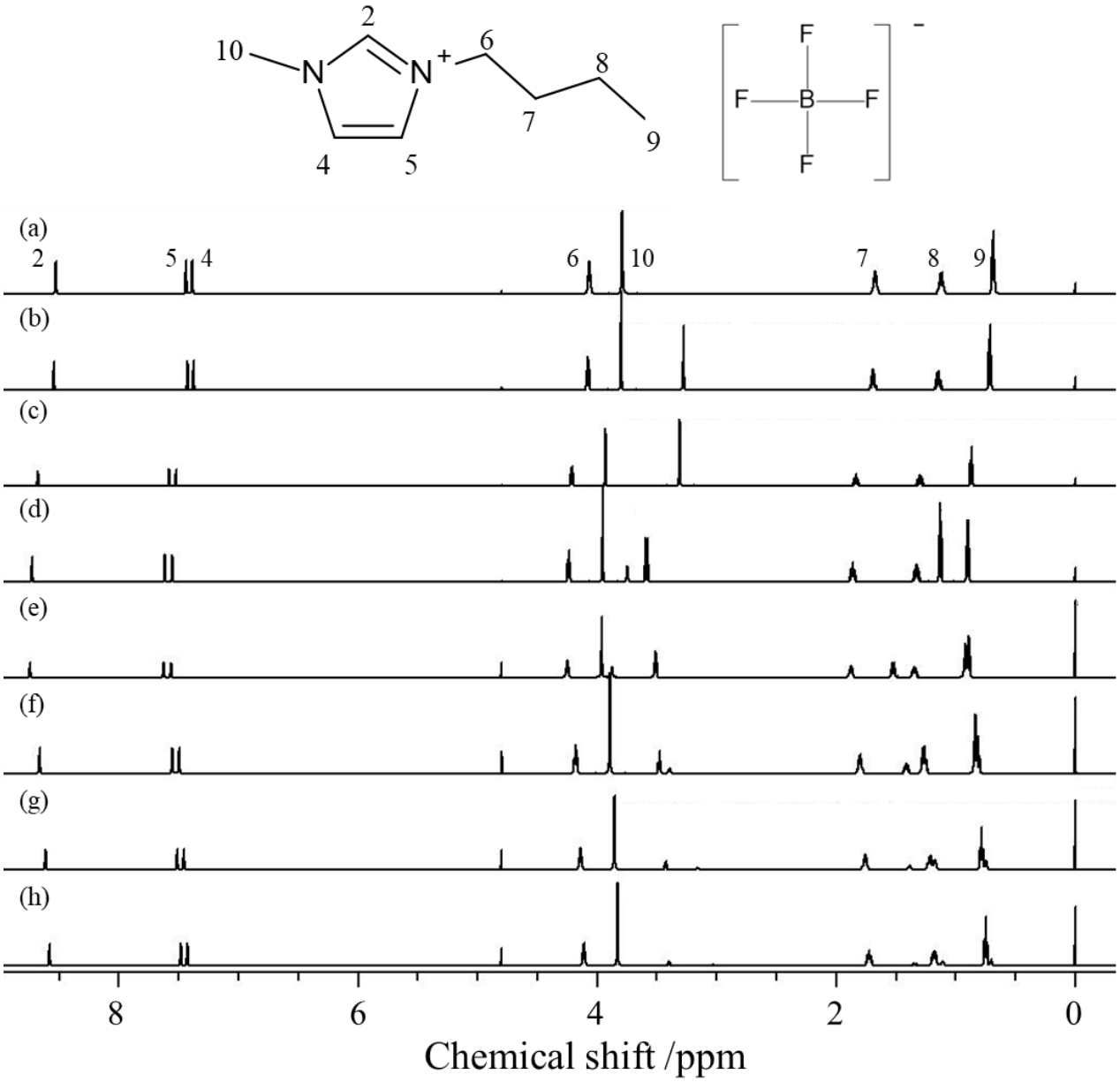

Figure 3.1a Structure of $[C_4MIm]BF_4$ and representative ^1H spectra of the water to ethanol systems at 50 mol% and 1-propanol to 1-hexanol systems at saturation solubility and pure $[C_4MIm]BF_4$. The peak around 4.8 ppm is H_2O in an internal standard solution.: (a) pure $[C_4MIm]BF_4$, (b) $[C_4MIm]BF_4$/water system at 50 mol%, (c) $[C_4MIm]BF_4$/methanol system at 50 mol%, (d) $[C_4MIm]BF_4$/ethanol system at 50 mol%, (e) $[C_4MIm]BF_4$/1-propanol system at 53 mol%, (f) $[C_4MIm]BF_4$/1-butanol system at 34 mol%, (g) $[C_4MIm]BF_4$/1-pentanol system at 21 mol%, (h) $[C_4MIm]BF_4$/1-hexanol system at 12 mol%.

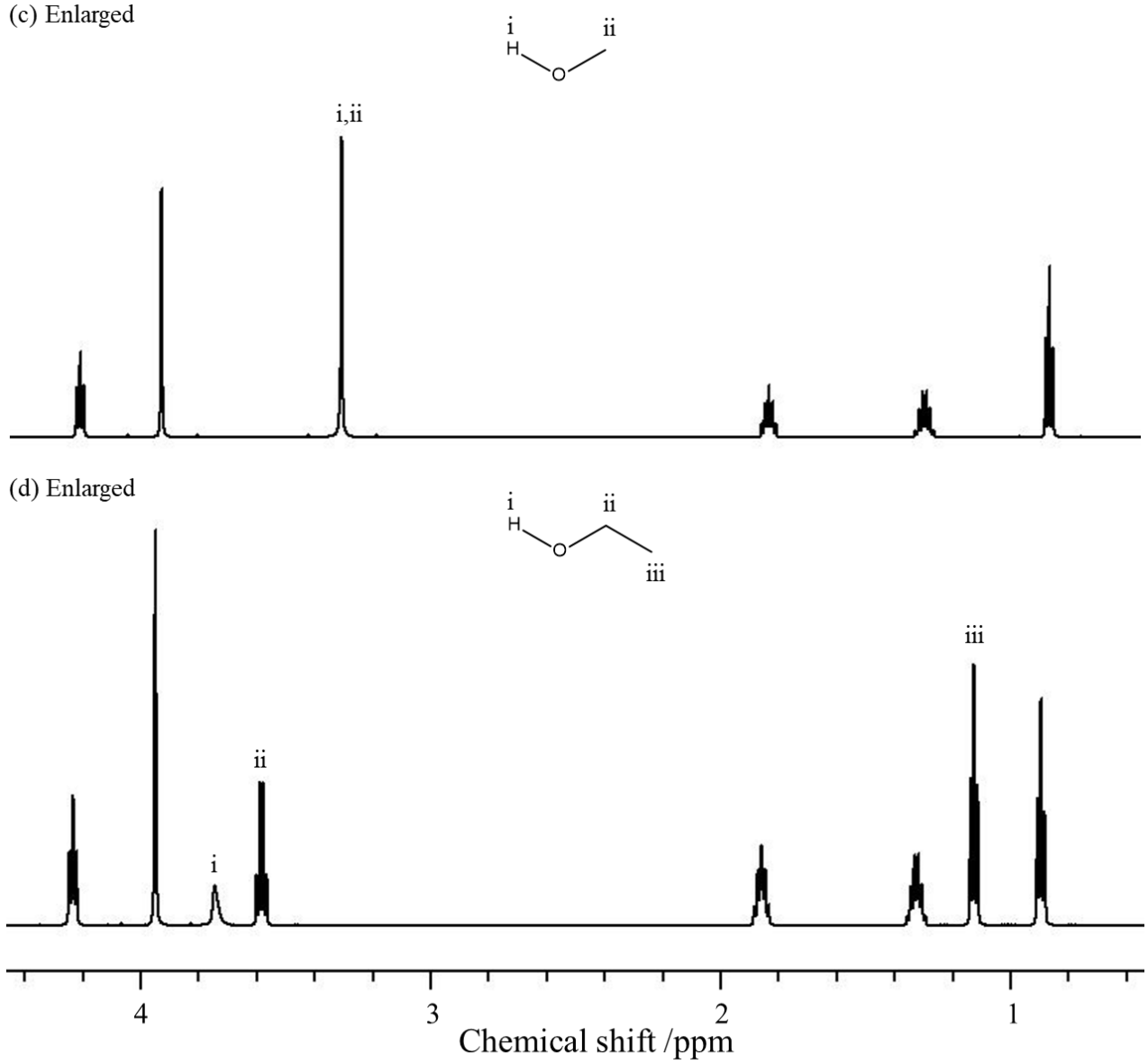

Figure 3.1b Structure of $[C_4MIm]BF_4$ and representative ^1H spectra of the water to ethanol systems at 50 mol% and 1-propanol to 1-hexanol systems at saturation solubility and pure $[C_4MIm]BF_4$. The peak around 4.8 ppm is H_2O in an internal standard solution.: (c) $[C_4MIm]BF_4$/methanol system at 50 mol%, (d) $[C_4MIm]BF_4$/ethanol system at 50 mol%,

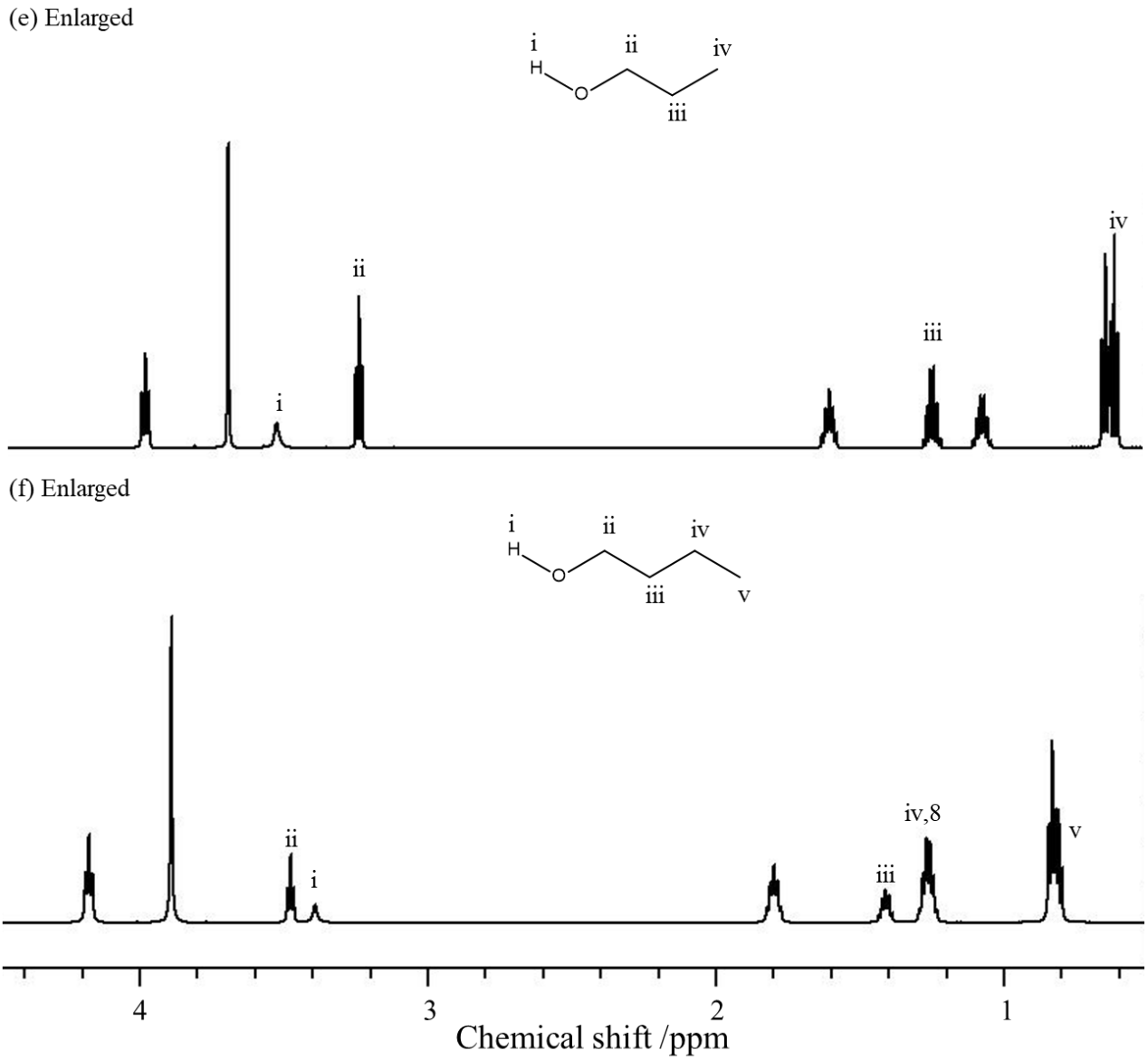

Figure 3.1c Structure of $[C_4MIm]BF_4$ and representative ^1H spectra of the water to ethanol systems at 50 mol% and 1-propanol to 1-hexanol systems at saturation solubility and pure $[C_4MIm]BF_4$. The peak around 4.8 ppm is H_2O in an internal standard solution.: (e) $[C_4MIm]BF_4$/1-propanol system at 53 mol%, (f) $[C_4MIm]BF_4$/1-butanol system at 34 mol%.

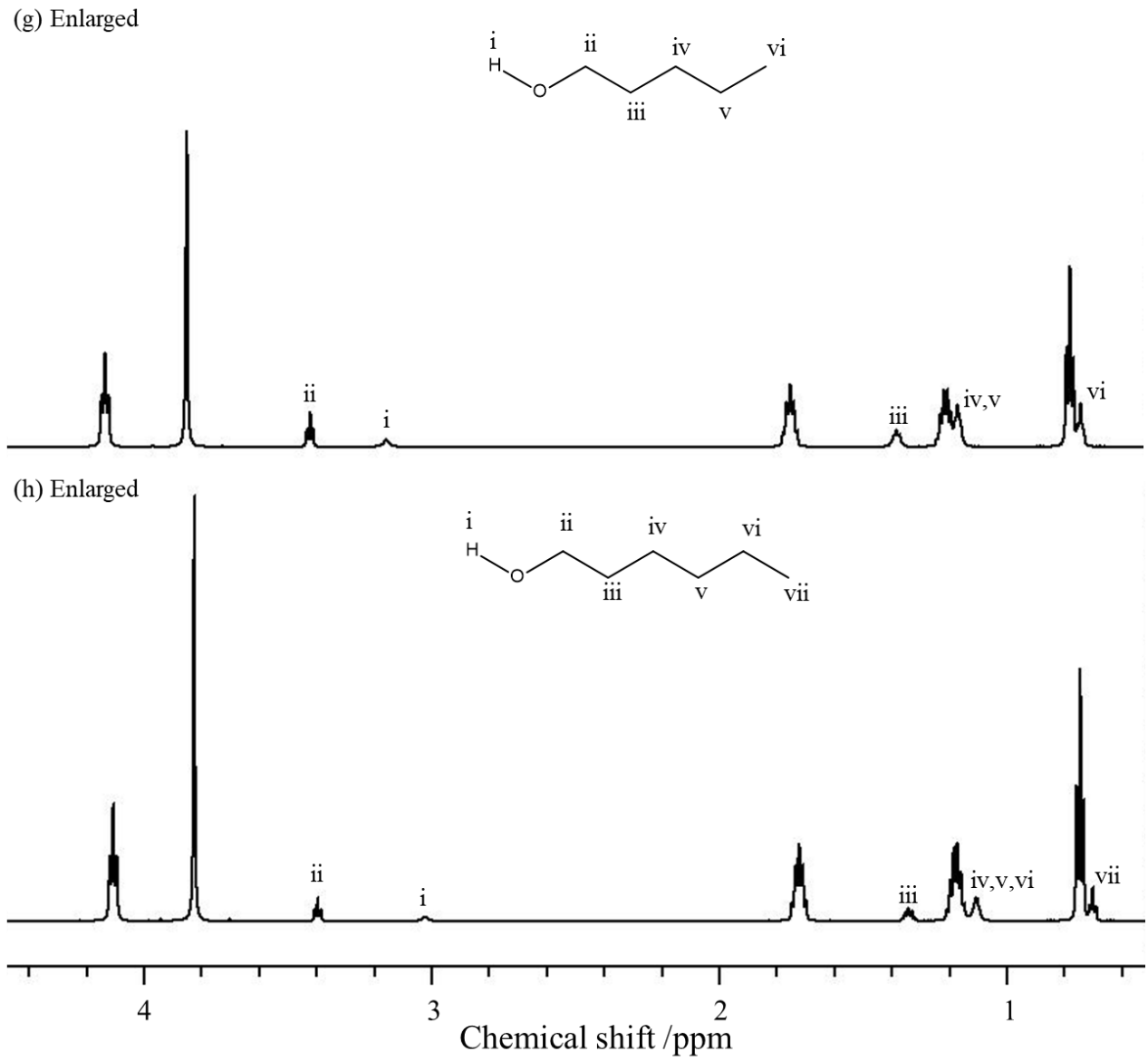

Figure 3.1d Structure of $[C_4MIm]BF_4$ and representative ^1H spectra of the water to ethanol systems at 50 mol% and 1-propanol to 1-hexanol systems at saturation solubility and pure $[C_4MIm]BF_4$. The peak around 4.8 ppm is H_2O in an internal standard solution.: (g) $[C_4MIm]BF_4$/1-pentanol system at 21 mol%, (h) $[C_4MIm]BF_4$/1-hexanol system at 12 mol%.

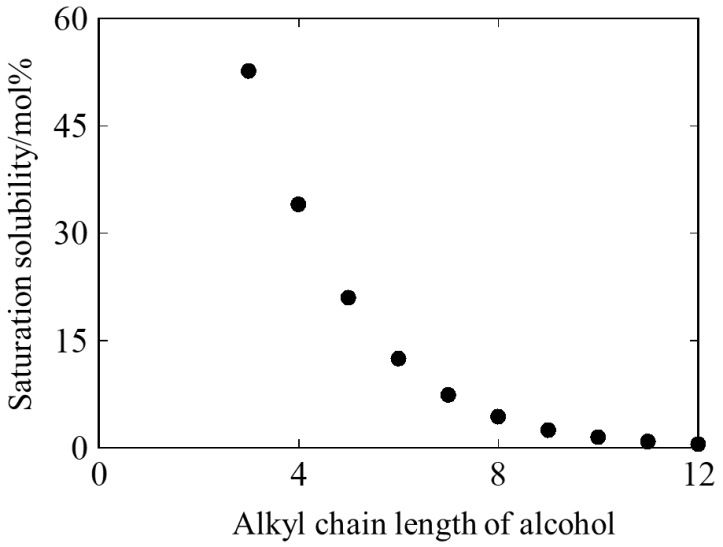

Figure 3.2 Alkyl chain length dependence of saturation solubility of alcohols to $[C_4MIm]BF_4$ at 298 K.

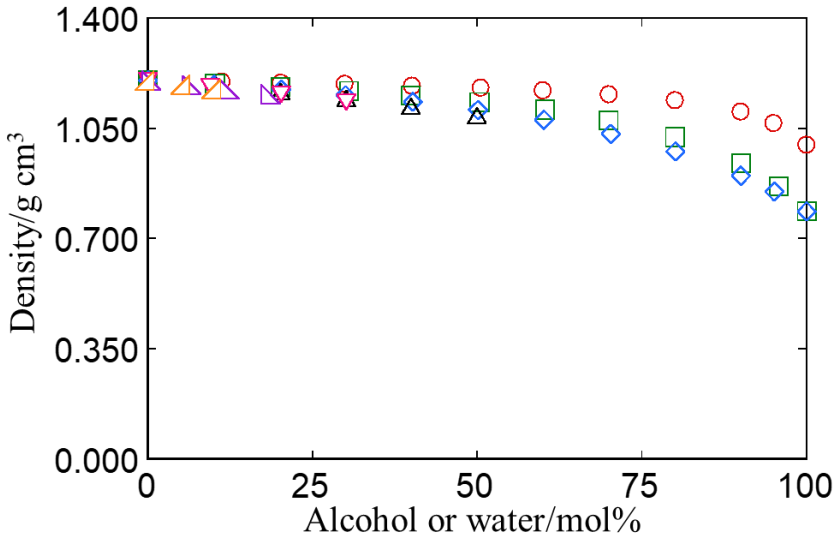

Figure 3.3 Density of $[C_4MIM]BF_4$/alcohol and $[C_4MIM]BF_4$/water systems at various concentrations of alcohol or water at 298 K: Legend: water (○), methanol (□), ethanol (◇), 1-propanol (△), 1-butanol (▽), 1-pentanol (◺), and 1-hexanol (◿).

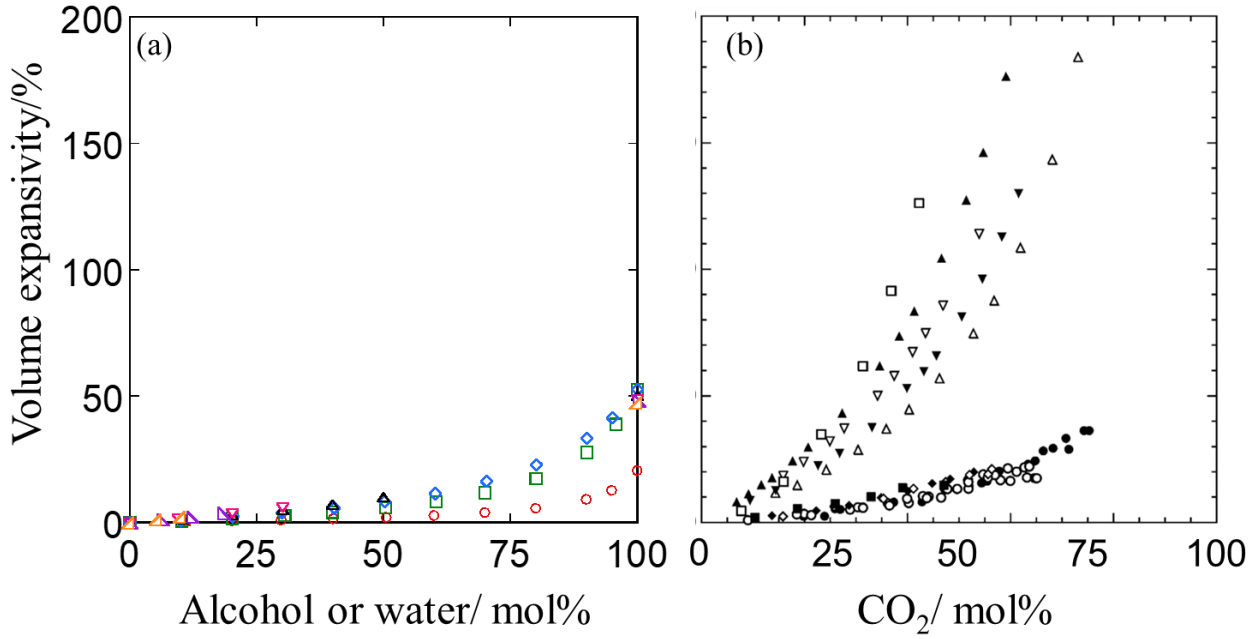

Figure 3.4 Volume expantivities of $[C_4MIM]BF_4$/alcohol and $[C_4MIM]BF_4$/water systems at various concentrations at 298 K and that of IL/CO_2 and organic solvent/CO_2 systems at various concentrations at 313 K [Chiehming. Et al. 1998, Aki, et al. 2004, Blanchard et al. 2001, Kordikowski et al. 1995, Makino et al. 2012]: (a) $[C_4MIM]BF_4$/alcohol and $[C_4MIM]BF_4$/water systems, (b) IL/CO_2 and organic solvent/CO_2 systems Legend: water (○), methanol (□), ethanol (◇), 1-propanol (△), 1-butanol (▽), 1-pentanol (◺), and 1-hexanol (◿), 1-butyl-3-methylimidazolium bis(trifuoromethanesulfonyl) amide (●), 1-butyl-3-methylimidazolium hexafuorophosphate (○), 1-butyl-3-methylimidazolium tetrafluoroborate (◆), 1-butyl-3-methylimidazolium dicyanamide (◇), 1-butyl-3-methylimidazolium nitrate (■), methanol (▲), acetone (△), acetonitrile (▼), ethyl acetate (▽), *N*,*N*-dimethylformamide (□).

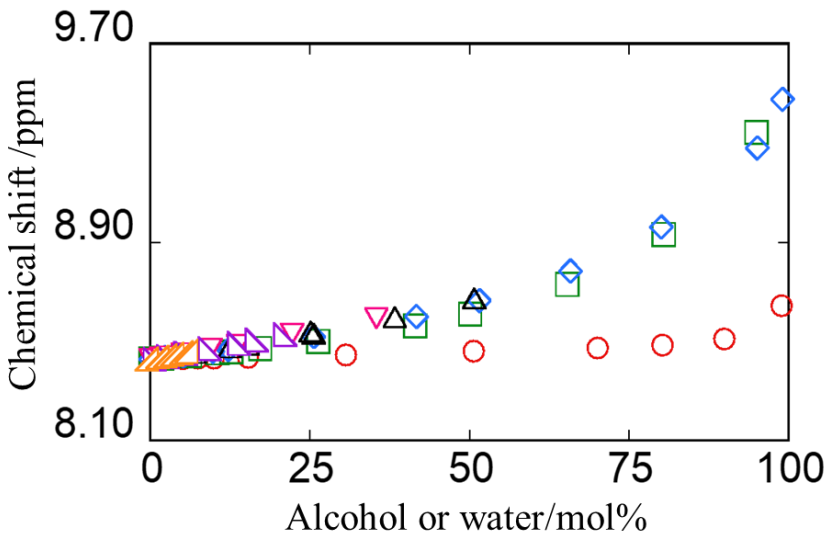

Figure 3.5 ^{1}H chemical shift for 2H of [C_4MIm] cation at various concentrations of alcohol and water at 298 K: Legend: water (○), methanol (□), ethanol (◇), 1-propanol (△), 1-butanol (▽), 1-pentanol (◺), and 1-hexanol (◿).

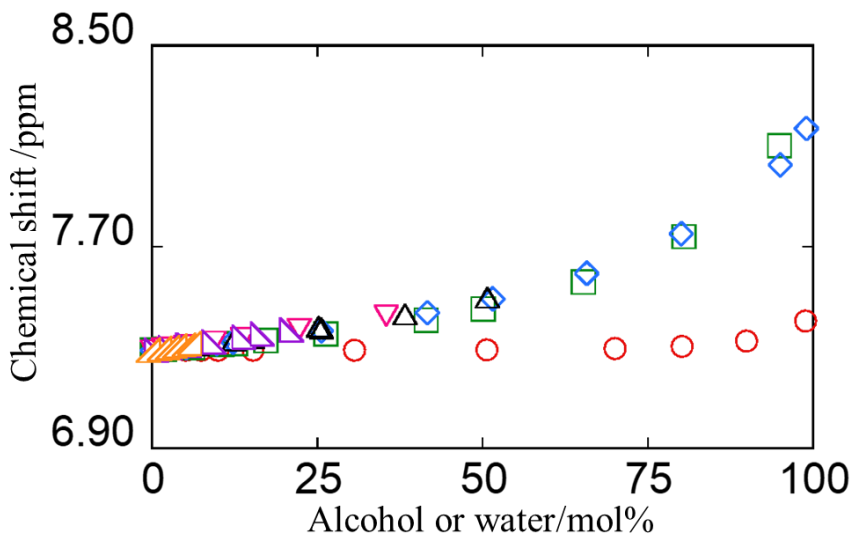

Figure 3.6 ^{1}H chemical shift for 4H of [C_4MIm] cation at various concentrations of alcohol and water at 298 K: Legend: water (○), methanol (□), ethanol (◇), 1-propanol (△), 1-butanol (▽), 1-pentanol (◺), and 1-hexanol (◿).

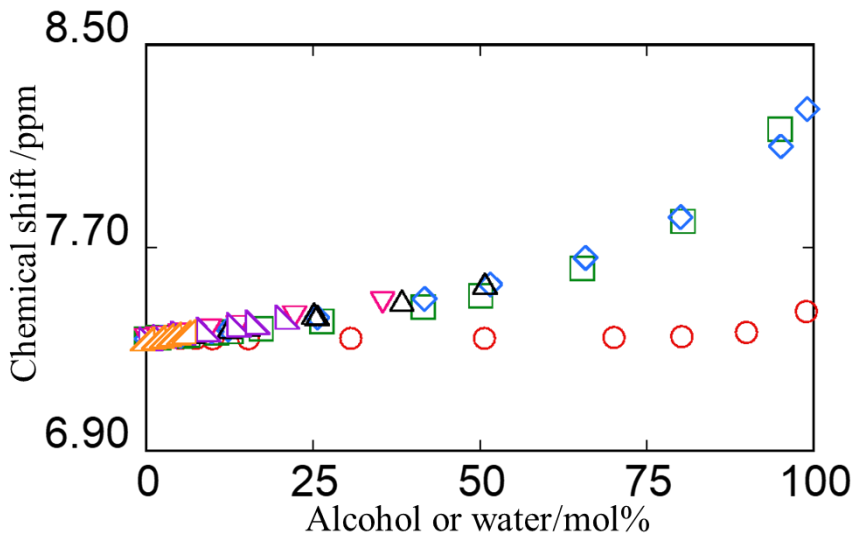

Figure 3.7 ^{1}H chemical shift for 5H of [C_4MIm] cation at various concentrations of alcohol and water at 298 K: Legend: water (○), methanol (□), ethanol (◇), 1-propanol (△), 1-butanol (▽), 1-pentanol (◺), and 1-hexanol (◿).

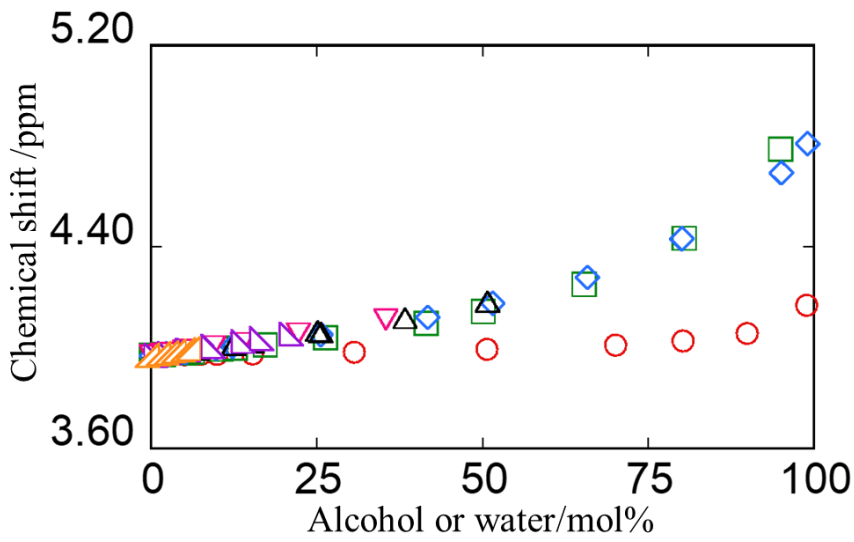

Figure 3.8 ^{1}H chemical shift for 6H of [C_4MIm] cation at various concentrations of alcohol and water at 298 K: Legend: water (○), methanol (□), ethanol (◇), 1-propanol (△), 1-butanol (▽), 1-pentanol (◺), and 1-hexanol (◿).

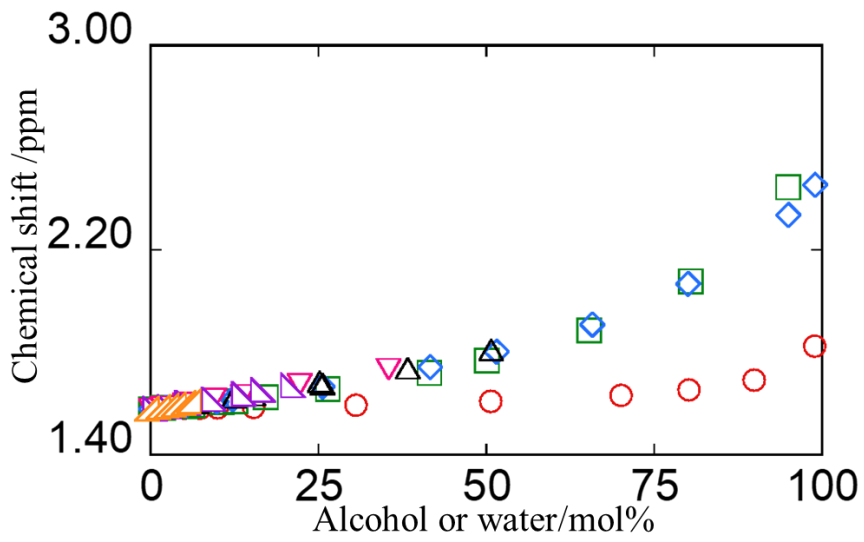

Figure 3.9 ^{1}H chemical shift for 7H of [C_4MIm] cation at various concentrations of alcohol and water at 298 K: Legend: water (○), methanol (□), ethanol (◇), 1-propanol (△), 1-butanol (▽), 1-pentanol (◺), and 1-hexanol (◿).

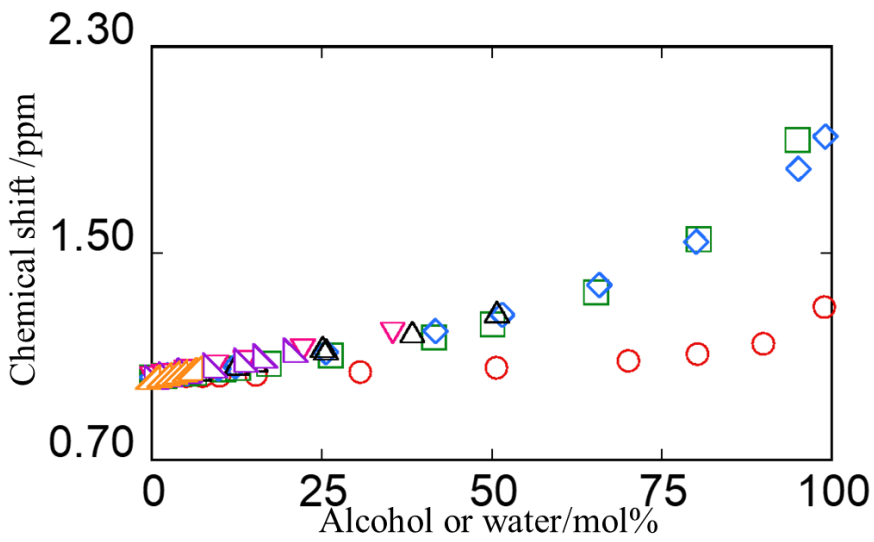

Figure 3.10 ^{1}H chemical shift for 8H of [C_4MIm] cation at various concentrations of alcohol and water at 298 K: Legend: water (○), methanol (□), ethanol (◇), 1-propanol (△), 1-butanol (▽), 1-pentanol (◺), and 1-hexanol (◿).

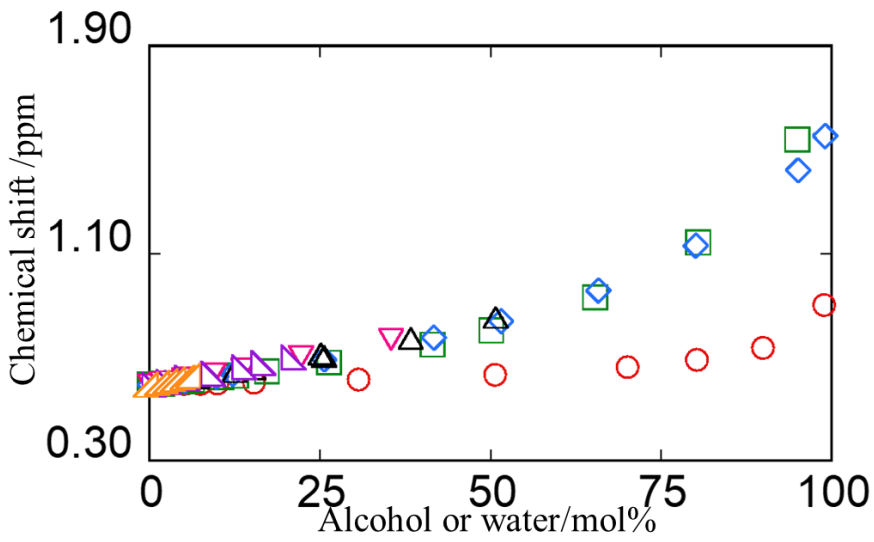

Figure 3.11 ^{1}H chemical shift for 9H of [C_4MIm] cation at various concentrations of alcohol and water at 298 K: Legend: water (○), methanol (□), ethanol (◇), 1-propanol (△), 1-butanol (▽), 1-pentanol (◺), and 1-hexanol (◿).

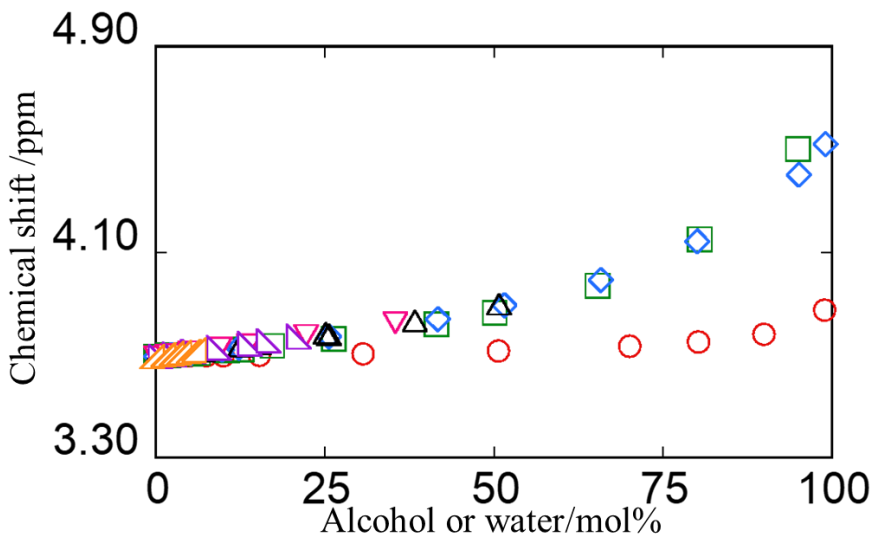

Figure 3.12 ^{1}H chemical shift for 10H of [C_4MIm] cation at various concentrations of alcohol and water at 298 K: Legend: water (○), methanol (□), ethanol (◇), 1-propanol (△), 1-butanol (▽), 1-pentanol (◺), and 1-hexanol (◿).

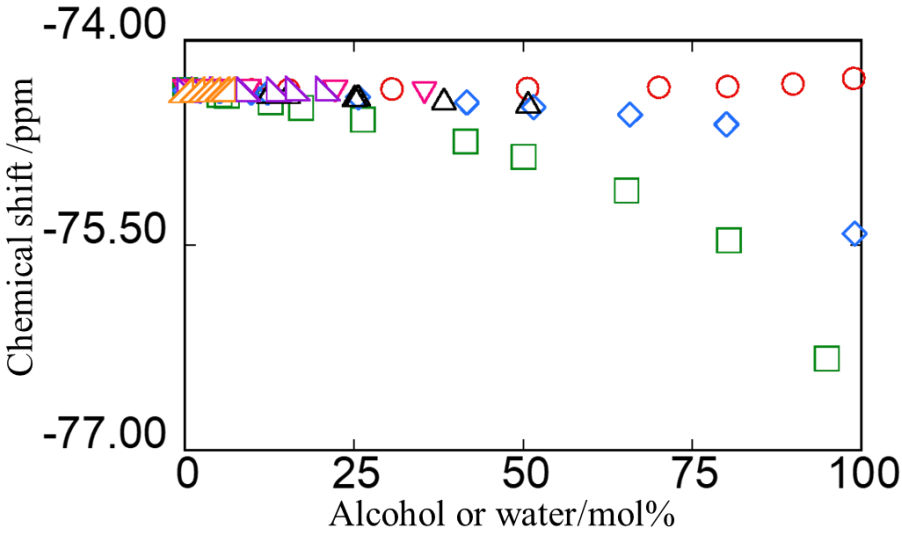

Figure 3.13 ^{19}F chemical shift of BF_4 anion at various concentrations of alcohol or water at 298 K: Legend: water (○), methanol (□), ethanol (◇), 1-propanol (△), 1-butanol (▽), 1-pentanol (◺), and 1-hexanol (◿).

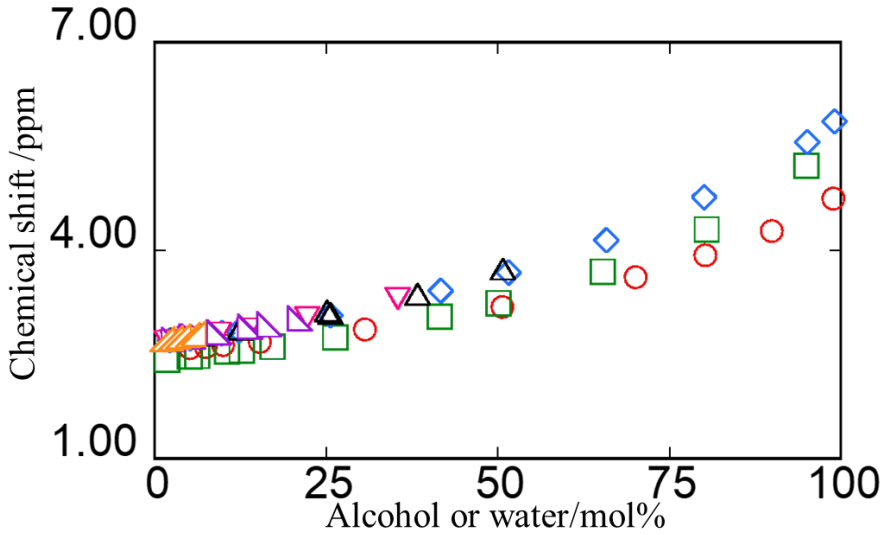

Figure 3.14 ^{1}H chemical shift of hydroxyl proton on alcohols and water at various concentrations of alcohol or water at 298 K: Legend: water (○), methanol (□), ethanol (◇), 1-propanol (△), 1-butanol (▽), 1-pentanol (◺), and 1-hexanol (◿).

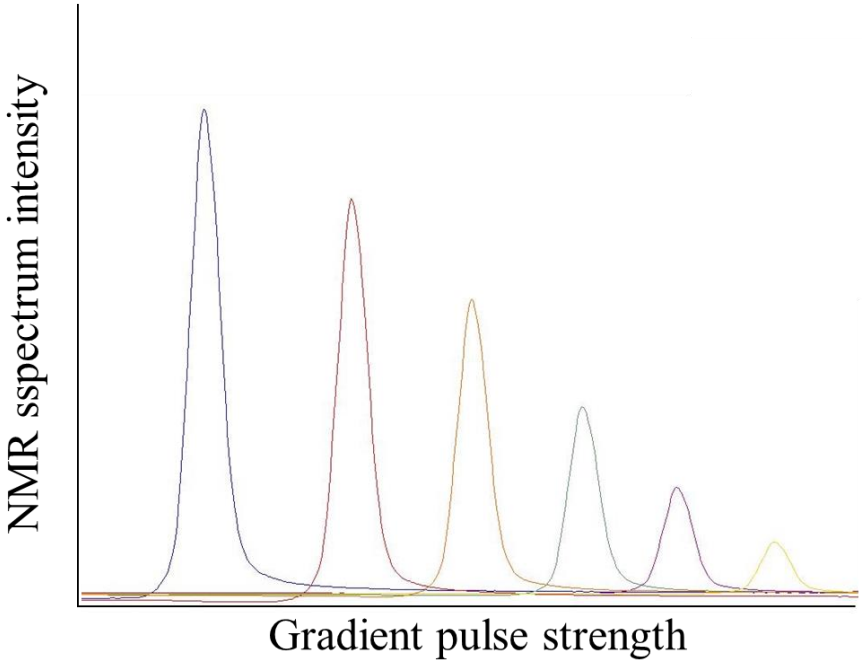

Figure 3.15 Reduction of NMR spectrum intensity by gradient pulse.

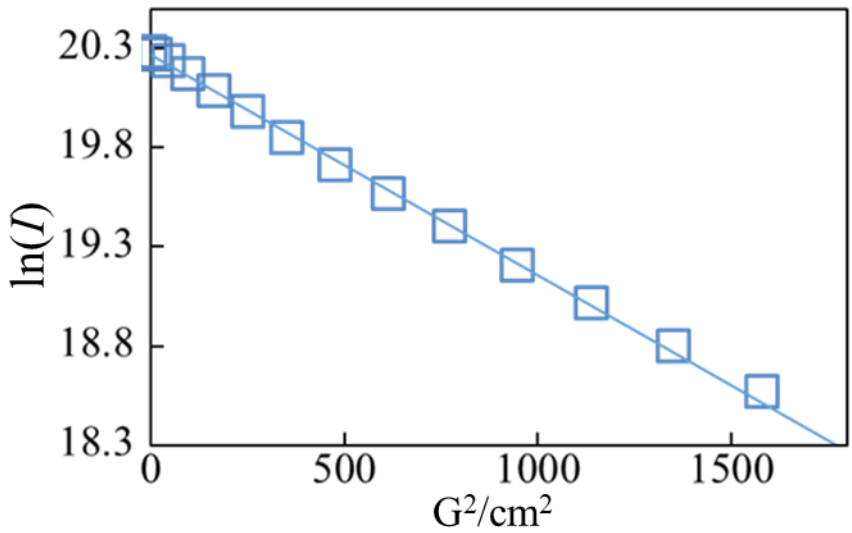

Figure 3.16 The square of gradient pulse strength vs. the natural logarithm of ^{1}H NMR signal intensity of hydroxyl groups of water in $[C_4MIm]BF_4$/5 mol% water system.

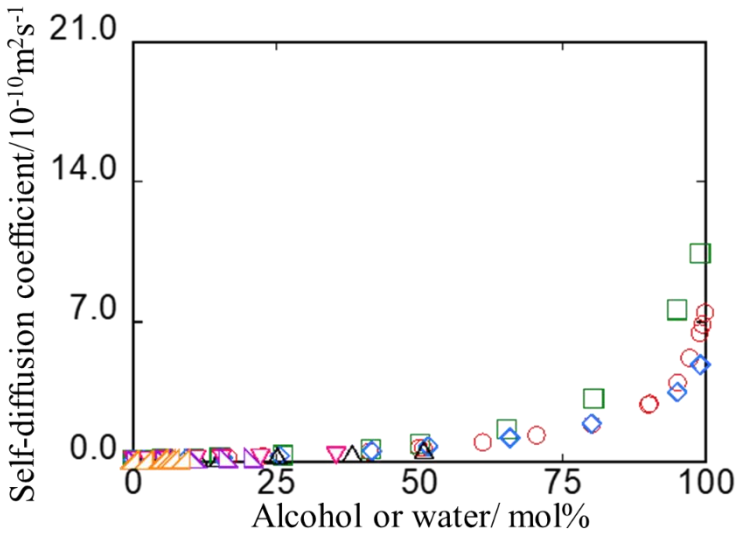

Figure 3.17 Self-diffusion coefficients of [C_4MIm] at various concentrations of alcohol and water at 298 K. Legend: water (○), methanol (□), ethanol (◇), 1-propanol (△), 1-butanol (▽), 1-pentanol (◺), and 1-hexanol (◿).

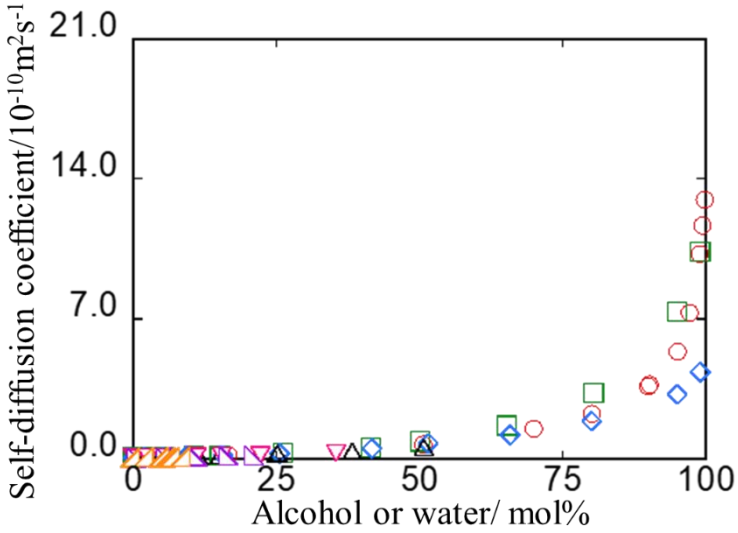

Figure 3.18 Self-diffusion coefficients of BF_4 at various concentrations of alcohol and water at 298 K. Legend: water (○), methanol (□), ethanol (◇), 1-propanol (△), 1-butanol (▽), 1-pentanol (◺), and 1-hexanol (◿).

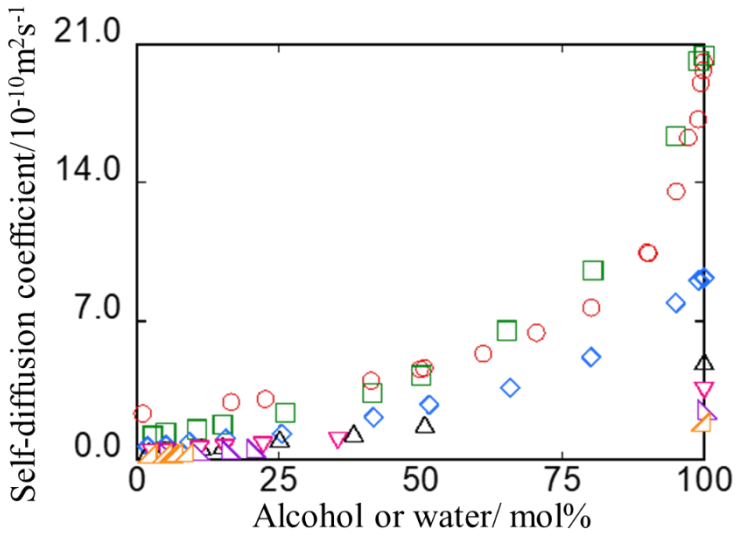

Figure 3.19 Self-diffusion coefficients of solvent at various concentrations of alcohol and water at 298 K. Legend: water (○), methanol (□), ethanol (◇), 1-propanol (△), 1-butanol (▽), 1-pentanol (◺), and 1-hexanol (◿).

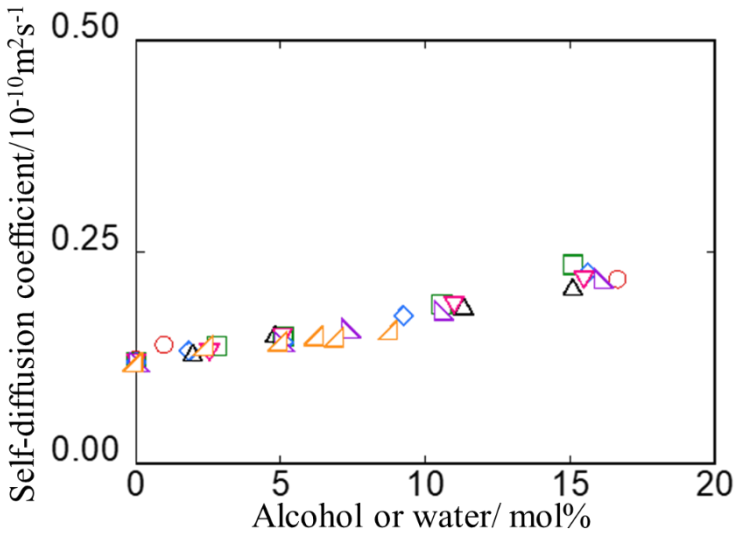

Figure 3.20 Self-diffusion coefficients of [C_4MIm] at various concentrations of alcohol and water at less than 20 mol% at 298 K: Legend: water (○), methanol (□), ethanol (◇), 1-propanol (△), 1-butanol (▽), 1-pentanol (◺), and 1-hexanol (◿).

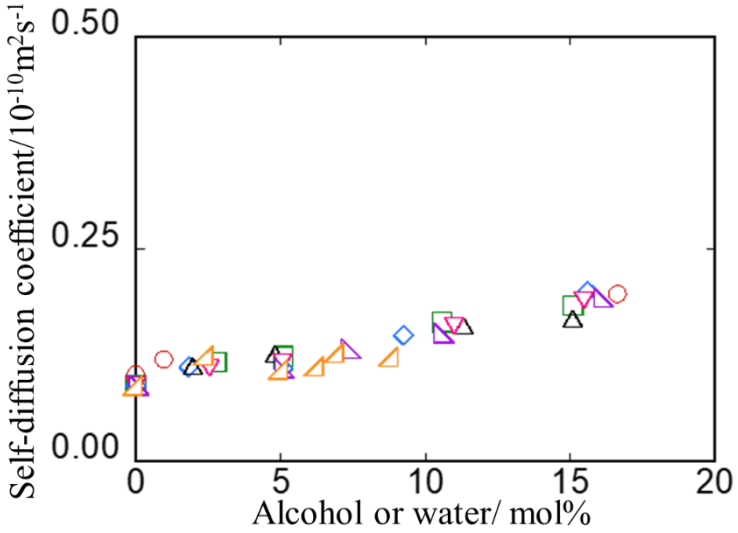

Figure 3.21 Self-diffusion coefficients of BF_4 at various concentrations of alcohol and water at less than 20 mol% at 298 K: Legend: water (○), methanol (□), ethanol (◇), 1-propanol (△), 1-butanol (▽), 1-pentanol (◺), and 1-hexanol (◿).

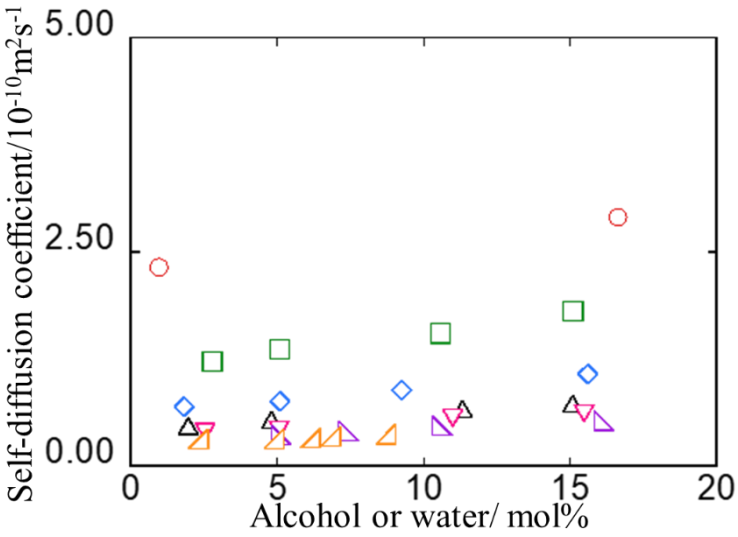

Figure 3.22 Self-diffusion coefficients of solvent at various concentrations of alcohol and water at less than 20 mol% at 298 K. Legend: water (○), methanol (□), ethanol (◇), 1-propanol (△), 1-butanol (▽), 1-pentanol (◺), and 1-hexanol (◿).

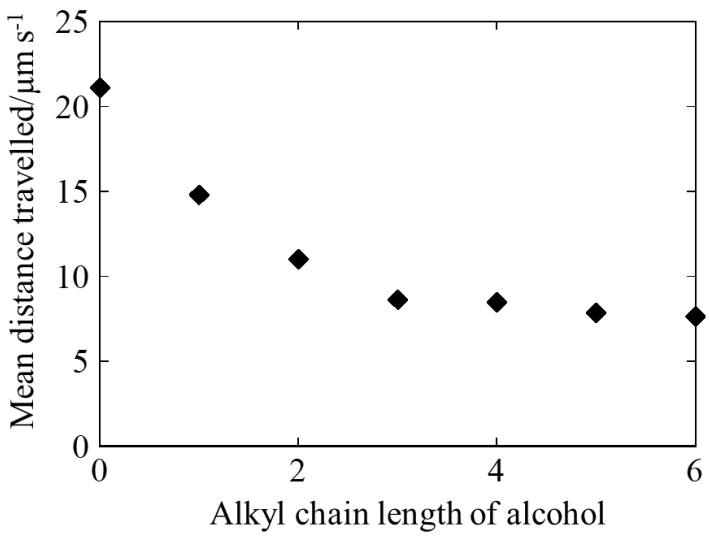

Figure 3.23 Mean distance travelled of water and alcohol in $[C_4MIm]BF_4$/water and $[C_4MIm]BF_4$/alcohol systems at alcohol or water concentration extrapolated to 0 mol% at 298 K.

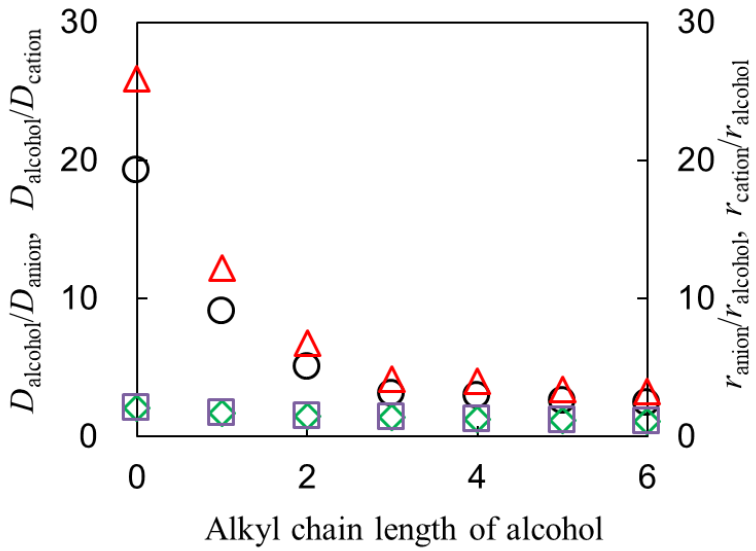

Figure 3.24 Alkyl chain length dependence of $D_{solvent}/D_{anion}$ or $D_{solvent}/D_{cation}$ at alcohol or water concentration extrapolated to 0 mol% and $r_{anion}/r_{alcohol}$ or $r_{cation}/r_{alcohol}$ in the pure IL at 298 K [Yoshimura et al. (b), Tokuda et al. 2005]. Legend: $D_{alcohol}/D_{anion}$ (△), $D_{alcohol}/D_{cation}$ (○), $r_{anion}/r_{alcohol}$ (□), and $r_{cation}/r_{alcohol}$ (◇).

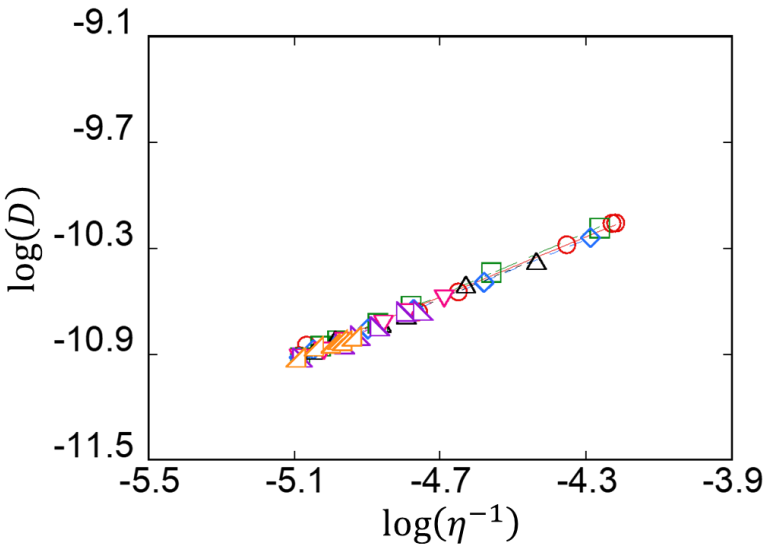

Figure 3.25 Relationships between logarithm reciprocal of viscosity and logarithm self-diffusion coefficient of [C_4MIm] at less than 50 mol% at 298 K. The viscosity was calculated using a polynomial approximation function. Legend: water (○), methanol (□), ethanol (◇), 1-propanol (△), 1-butanol (▽), 1-pentanol (◺), and 1-hexanol (◿).

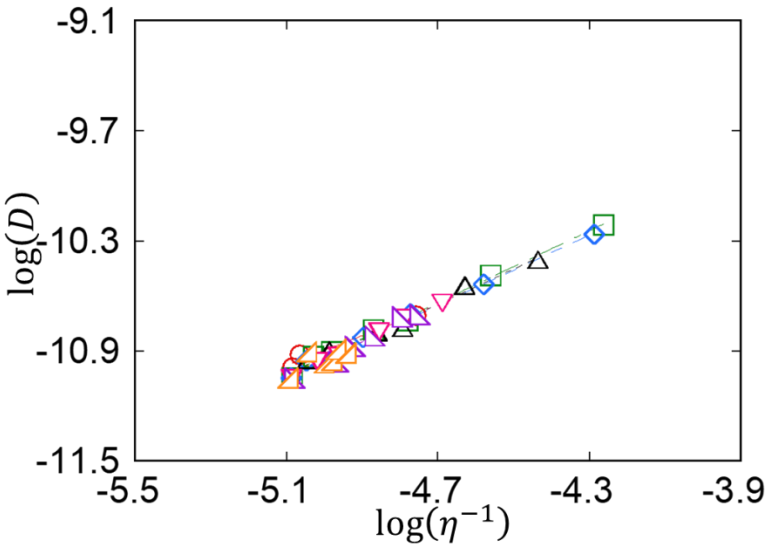

Figure 3.26 Relationships between logarithm reciprocal of viscosity and logarithm self-diffusion coefficient of BF_4 at less than 50 mol% at 298 K. The viscosity was calculated using a polynomial approximation function. Legend: water (○), methanol (□), ethanol (◇), 1-propanol (△), 1-butanol (▽), 1-pentanol (◺), and 1-hexanol (◿).

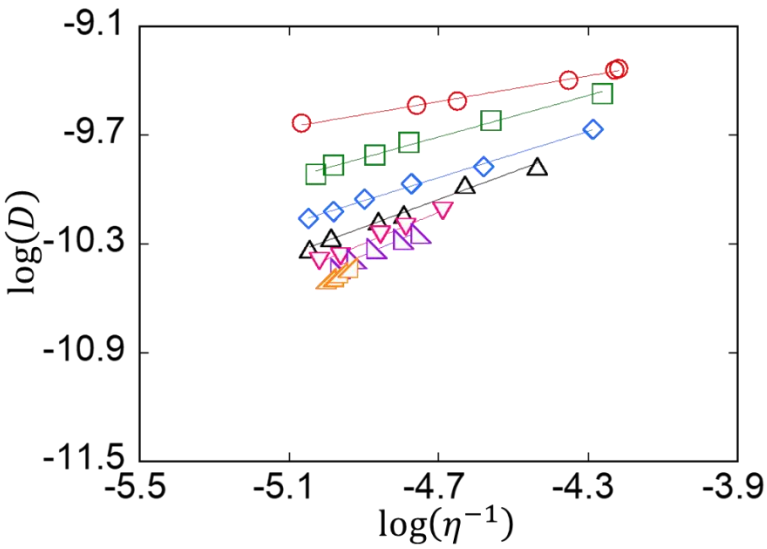

Figure 3.27 Relationships between logarithm reciprocal of viscosity and logarithm self-diffusion coefficient of water and alcohols at less than 50 mol% at 298 K. The viscosity was calculated using a polynomial approximation function. Legend: water (○), methanol (□), ethanol (◇), 1-propanol (△), 1-butanol (▽), 1-pentanol (◺), and 1-hexanol (◿).

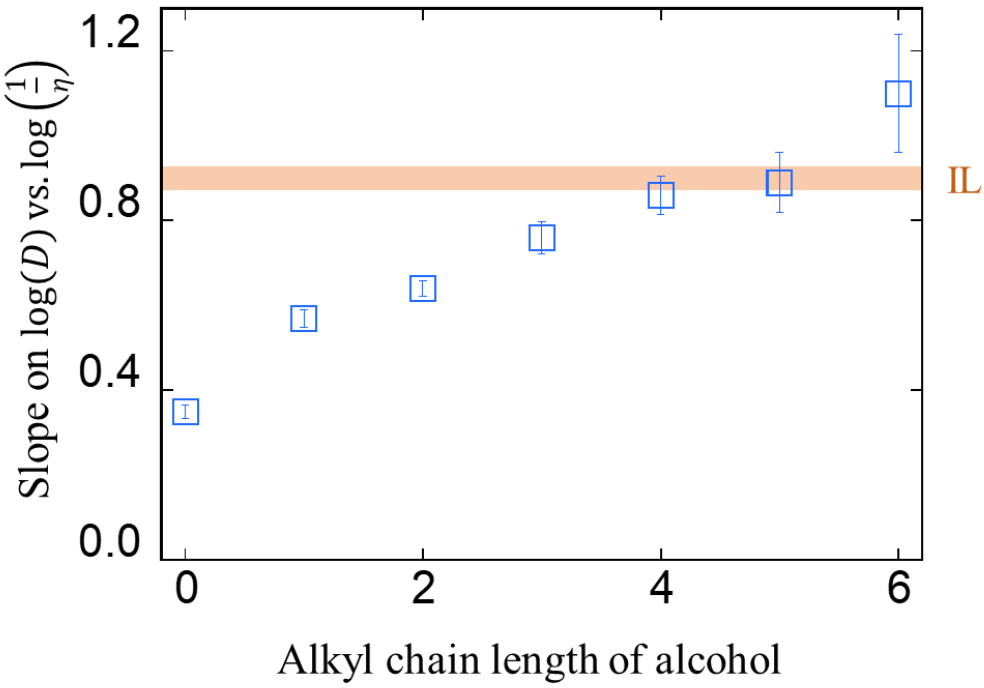

Figure 3.28 Relationship between Slopes on $\log(D)$ vs. $\log\left(\frac{1}{\eta}\right)$ and alkyl chain length of alcohols.

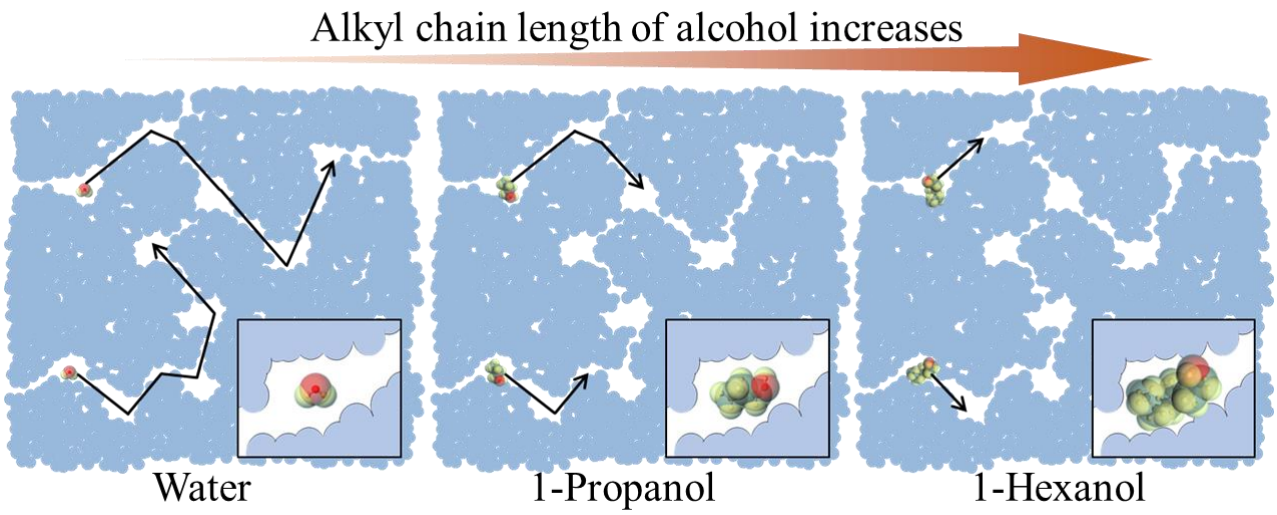

Figure 3.29 Dynamic model of a pocket in $[C_4MIm]BF_4$/water and $[C_4MIm]BF_4$/alcohol systems with the least amount of water or alcohol. Arrows show the mean distance travelled.

Table 3.1 Samples, internal standard and lock solvent information

sample	abbreviation	mass fraction purity	supplier
1-Butyl-3-methylimidazolium tetrafluoroborate	$[C_4MIm]BF_4$	>0.99	Sigma Aldrich Co.
Methanol		>0.998	Kanto Chemical Co., Inc
Ethanol		>0.995	Fujifilm Wako Pure Chemical Co.
1-Propanol		>0.995	Fujifilm Wako Pure Chemical Co.
1-Butanol		>0.99	Fujifilm Wako Pure Chemical Co.
1-Pentanol		>0.98	Fujifilm Wako Pure Chemical Co.
1-Hexanol		>0.97	Fujifilm Wako Pure Chemical Co.
1-Heptanol		>0.98	Kanto Chemical Co., Inc
1-Octanol		>0.98	Kanto Chemical Co., Inc
1-Nonanol		>0.99	Tokyo Chemical Inductry Co., Ltd.
1-Decanol		>0.98	Tokyo Chemical Inductry Co., Ltd.
1-Undecanol		>0.99	Tokyo Chemical Inductry Co., Ltd.
1-Dodecanol		>0.99	Tokyo Chemical Inductry Co., Ltd.
D_2O, 99%D		>0.97	Kanto Chemical Co., Inc
Sodium 3-(trimethylsilyl) propionate-2,2,3,3-d_4	TSP		Fujifilm Wako Pure Chemical Co.
2,2,2-Trifluoroacetic acid	TFA	>0.99	Watanabe Chemical Industries, ltd.

Table 3.2 Saturated solubility of alcohols in $[C_4MIm]BF_4$ at 298 K.

Alcohol	*x*/mol%
1-Propanol	52.68
1-Bbutanol	33.99
1-Pentanol	20.99
1-Hexanol	12.45
1-Heptanol	7.36
1-Octanol	4.32
1-Nonanol	2.46
1-Ddecanol	1.49
1-Undecanol	0.88
1-Dodecanol	0.51

Table 3.3 Concentration dependence of density in $[C_4MIM]BF_4$/alcohol and $[C_4MIM]BF_4$/water systems at 298 K.

Water		Methanol		Ethanol		1-Propanol	
x/mol%	ρ/gcm^{-3}	x/mol%	ρ/gcm^{-3}	x/mol%	ρ/gcm^{-3}	x/mol%	ρ/gcm^{-3}
0	1.2022	0	1.2022	0	1.2022	0	1.2022
11.21	1.1985	10.17	1.1929	10.02	1.1892	10.37	1.1840
20.21	1.1937	20.14	1.1819	20.25	1.1729	20.17	1.1667
29.87	1.1905	30.53	1.1688	29.98	1.1556	30.08	1.1452
40.11	1.1849	39.89	1.1541	40.23	1.1347	39.91	1.1203
50.54	1.1785	50.34	1.1335	50.11	1.1084	49.93	1.0914
59.96	1.1698	60.28	1.1095	60.14	1.0780	100	0.8005
70.00	1.1574	69.98	1.0752	70.24	1.0330		
80.02	1.1383	80.01	1.0224	80.11	0.9773		
90.00	1.1020	90.02	0.9399	90.03	0.9003		
95.00	1.0666	95.75	0.8653	95.09	0.8489		
100	0.9971	100	0.7878	100	0.7866		

1-Butanol		1-Pentanol		1-Hexanol	
x/mol%	ρ/gcm^{-3}	x/mol%	ρ/gcm^{-3}	x/mol%	ρ/gcm^{-3}
0	1.2022	0	1.20215	0	1.2022
9.51	1.1821	6.11	1.18774	5.40	1.1885
20.23	1.1590	11.93	1.17424	10.13	1.1756
30.11	1.1339	18.12	1.15805	100	0.8154
100	0.8078	100	0.81137		

Table 3.4 Concentration dependence of volume expansivity in $[C_4MIM]BF_4$/alcohol and $[C_4MIM]BF_4$/water systems at 298 K.

Water		Methanol		Ethanol		1-Propanol	
x/mol%	$\Delta V/\%$	x/mol%	$\Delta V/\%$	x/mol%	$\Delta V/\%$	x/mol%	$\Delta V/\%$
0	0.0	0	0.0	0	0.0	0	0.0
11.21	0.3	10.17	0.8	10.02	1.1	10.37	1.5
20.21	0.7	20.14	1.7	20.25	2.5	20.17	3.0
29.87	1.0	30.53	2.8	29.98	4.0	30.08	5.0
40.11	1.5	39.89	4.2	40.23	5.9	39.91	7.3
50.54	2.0	50.34	6.1	50.11	8.5	49.93	10.1
59.96	2.8	60.28	8.4	60.14	11.5	100	50.2
70.00	3.9	69.98	11.8	70.24	16.4		
80.02	5.6	80.01	17.6	80.11	23.0		
90.00	9.1	90.02	27.9	90.03	33.5		
95.00	12.7	95.75	38.9	95.09	41.6		
100	20.6	100	52.6	100	52.8		

1-Butanol		1-Pentanol		1-Hexanol	
x/mol%	$\Delta V/\%$	x/mol%	$\Delta V/\%$	x/mol%	$\Delta V/\%$
0	0.0	0	0.0	0	0.0
9.51	1.7	6.11	1.2	5.40	1.2
20.23	3.7	11.93	2.4	10.13	2.3
30.11	6.0	18.12	3.8	100	47.4
100	48.8	100	48.2		

Table 3.5 Concentration dependence of chemical shift in $[C_4MIm]BF_4$/water system at 298 K.

	Chemical Shift /ppm									
x/mol%	2H	4H	5H	6H	7H	8H	9H	10H	F	OH
0	8.429	7.290	7.342	3.970	1.580	1.021	0.593	3.694	-74.362	
5.15	8.430	7.290	7.342	3.971	1.581	1.023	0.595	3.695	-74.363	2.589
7.49	8.431	7.289	7.341	3.971	1.581	1.024	0.595	3.695	-74.361	2.603
10.01	8.432	7.288	7.340	3.972	1.582	1.025	0.597	3.695	-74.362	2.631
15.36	8.434	7.288	7.341	3.974	1.585	1.028	0.600	3.697	-74.362	2.677
30.66	8.444	7.288	7.342	3.981	1.593	1.038	0.611	3.703	-74.358	2.857
50.71	8.458	7.290	7.343	3.992	1.607	1.056	0.630	3.714	-74.353	3.181
70.13	8.473	7.296	7.344	4.009	1.631	1.083	0.659	3.731	-74.343	3.612
80.26	8.484	7.305	7.348	4.026	1.653	1.108	0.688	3.748	-74.336	3.929
89.97	8.509	7.326	7.364	4.055	1.690	1.149	0.734	3.778	-74.321	4.273
98.99	8.643	7.405	7.448	4.169	1.824	1.290	0.898	3.872	-74.278	4.740
100										4.819

Table 3.6 Concentration dependence of chemical shift in $[C_4MIm]BF_4$/methanol system at 298 K.

	Chemical Shift /ppm									
x/mol%	2H	4H	5H	6H	7H	8H	9H	10H	F	OH
0	8.429	7.290	7.342	3.970	1.580	1.021	0.593	3.694	-74.362	
1.77	8.433	7.294	7.346	3.974	1.585	1.026	0.598	3.698		2.423
5.10	8.440	7.301	7.353	3.981	1.593	1.035	0.607	3.705	-74.398	2.474
6.15	8.443	7.303	7.355	3.983	1.595	1.037	0.609	3.707	-74.404	2.480
10.55	8.454	7.313	7.365	3.994	1.607	1.051	0.623	3.718		2.544
12.60	8.458	7.317	7.370	3.999	1.612	1.056	0.628	3.723	-74.451	2.556
17.17	8.471	7.329	7.383	4.012	1.626	1.071	0.644	3.735	-74.492	2.617
26.30	8.501	7.356	7.410	4.040	1.658	1.105	0.679	3.763	-74.577	2.753
41.48	8.563	7.411	7.468	4.099	1.721	1.174	0.749	3.820	-74.736	3.050
50.09	8.611	7.454	7.512	4.143	1.770	1.226	0.803	3.863	-74.847	3.242
65.27	8.729	7.560	7.620	4.252	1.886	1.350	0.930	3.969	-75.098	3.693
80.43	8.933	7.743	7.805	4.436	2.079	1.555	1.142	4.149	-75.462	4.306
94.96	9.343	8.104	8.168	4.790	2.446	1.940	1.541	4.502	-76.327	5.221
100										5.743

Table 3.7 Concentration dependence of chemical shift in $[C_4MIm]BF_4$/ethanol system at 298 K.

	Chemical Shift /ppm									
x/mol%	2H	4H	5H	6H	7H	8H	9H	10H	F	OH
0	8.429	7.291	7.342	3.970	1.580	1.021	0.593	3.694	-74.362	
2.24	8.435	7.296	7.348	3.976	1.586	1.028	0.600	3.700	-74.366	2.710
5.10	8.442	7.302	7.354	3.982	1.593	1.036	0.607	3.706	-74.369	2.740
5.25	8.445	7.304	7.356	3.984	1.595	1.038	0.610	3.708	-74.371	2.750
9.78	8.460	7.317	7.370	3.998	1.610	1.054	0.626	3.721	-74.379	2.812
12.21	8.468	7.325	7.378	4.005	1.618	1.063	0.635	3.728	-74.383	2.846
25.58	8.521	7.369	7.425	4.051	1.668	1.117	0.690	3.772	-74.411	3.069
41.65	8.602	7.439	7.499	4.122	1.745	1.200	0.774	3.840	-74.455	3.421
51.54	8.666	7.495	7.556	4.178	1.803	1.263	0.839	3.893	-74.485	3.688
65.77	8.784	7.597	7.661	4.279	1.910	1.377	0.957	3.992	-74.542	4.151
80.06	8.961	7.753	7.820	4.433	2.069	1.545	1.129	4.142	-74.611	4.770
95.02	9.281	8.028	8.100	4.695	2.338	1.828	1.420	4.402		5.567
99.00	9.478	8.172	8.248	4.811	2.456	1.953	1.553	4.520	-75.412	5.863
100										5.962

Table 3.8 Concentration dependence of chemical shift in $[C_4MIm]BF_4$/1-propanol system at 298 K.

	Chemical Shift /ppm									
x/mol%	2H	4H	5H	6H	7H	8H	9H	10H	F	OH
0	8.430	7.291	7.342	3.971	1.580	1.022	0.593	3.695	-74.361	
2.39	8.437	7.297	7.349	3.977	1.588	1.030	0.602	3.701	-74.365	2.727
6.83	8.454	7.311	7.364	3.992	1.604	1.047	0.619	3.715	-74.370	2.788
12.35	8.476	7.330	7.384	4.011	1.625	1.071	0.643	3.733	-74.379	2.870
15.21	8.486	7.340	7.394	4.021	1.635	1.082	0.654	3.742	-74.382	2.911
25.12	8.540	7.384	7.441	4.067	1.686	1.138	0.712	3.785	-74.405	3.131
25.56	8.532	7.378	7.434	4.060	1.678	1.129	0.703	3.779	-74.399	3.092
38.25	8.598	7.433	7.492	4.117	1.739	1.196	0.772	3.833	-74.424	3.372
50.71	8.675	7.499	7.560	4.184	1.811	1.274	0.852	3.896	-74.449	3.733
100										5.854

Table 3.9 Concentration dependence of chemical shift in $[C_4MIm]BF_4$/1-butanol system at 298 K.

	Chemical Shift /ppm									
x/mol%	2H	4H	5H	6H	7H	8H	9H	10H	F	OH
0	8.430	7.291	7.342	3.970	1.580	1.022	0.593	3.695	-74.361	
1.73	8.436	7.297	7.348	3.976	1.587	1.029	0.600	3.700	-74.362	2.696
1.80	8.437	7.297	7.349	3.977	1.587	1.029	0.601	3.700	-74.362	-0.090
2.54	8.440	7.300	7.352	3.980	1.590	1.033	0.605	3.703	-74.362	2.710
5.07	8.451	7.309	7.362	3.990	1.601	1.045	0.617	3.712	-74.362	2.747
5.73	8.453	7.311	7.364	3.991	1.603	1.047	0.619	3.714	-74.366	2.757
9.40	8.471	7.326	7.379	4.006	1.620	1.065	0.637	3.728	-74.363	2.814
13.69	8.486	7.338	7.393	4.020	1.634	1.082	0.655	3.740		2.873
22.21	8.532	7.376	7.432	4.059	1.677	1.128	0.703	3.776	-74.370	3.036
35.41	8.594	7.428	7.486	4.113	1.735	1.193	0.769	3.827	-74.378	3.315
100										5.769

Table 3.10 Concentration dependence of chemical shift in $[C_4MIm]BF_4$/1-pentanol system at 298 K.

	Chemical Shift /ppm									
x/mol%	2H	4H	5H	6H	7H	8H	9H	10H	F	OH
0	8.430	7.291	7.342	3.971	1.580	1.022	0.593	3.695	-74.361	
2.06	8.440	7.299	7.351	3.979	1.590	1.032	0.604	3.703	-74.358	2.719
4.74	8.453	7.310	7.363	3.990	1.602	1.046	0.618	3.713	-74.357	2.764
5.02	8.453	7.311	7.363	3.991	1.603	1.047	0.619	3.713	-74.358	2.764
8.71	8.470	7.325	7.378	4.005	1.619	1.065	0.637	3.726	-74.355	2.825
13.22	8.493	7.343	7.397	4.024	1.640	1.088	0.661	3.744	-74.353	2.903
16.03	8.508	7.354	7.409	4.037	1.653	1.104	0.677	3.756	-74.352	2.936
20.51	8.528	7.372	7.427	4.055	1.673	1.125	0.699	3.772	-74.350	3.025
100										5.721

Table 3.11 Concentration dependence of chemical shift in $[C_4MIM]BF_4$/1-hexanol system at 298 K.

	Chemical Shift /ppm									
x/mol%	2H	4H	5H	6H	7H	8H	9H	10H	F	OH
0	8.430	7.291	7.342	3.971	1.580	1.022	0.593	3.695	-74.361	
1.71	8.438	7.297	7.349	3.977	1.588	1.030	0.602	3.700	-74.359	2.726
2.98	8.443	7.302	7.354	3.981	1.593	1.036	0.607	3.704	-74.357	2.741
4.05	8.449	7.306	7.359	3.986	1.598	1.042	0.614	3.709	-74.356	2.762
5.42	8.455	7.312	7.364	3.992	1.604	1.049	0.621	3.714	-74.353	2.785
6.25	8.462	7.317	7.370	3.998	1.610	1.056	0.628	3.719	-74.355	2.798
100										5.670

Table 3.12 Self-diffusion coefficients of the anions, cations, alcohols and water in $[C_4Mim]BF_4$/alcohol and $[C_4Mim]BF_4$/water systems at 298 K.

Water				Methanol			
	$D/10^{-10}m^2s^{-1}$				$D/10^{-10}m^2s^{-1}$		
x/mol%	$[C_4MIm]$	BF_4	water	x/mol%	$[C_4MIm]$	BF_4	alcohol
0	0.123	0.102		0.0	0.121	0.090	
1.0	0.141	0.120	2.323	2.8	0.139	0.117	1.218
16.6	0.218	0.197	2.907	5.1	0.150	0.124	1.363
22.7	0.283		3.072	10.6	0.189	0.164	1.551
41.3	0.522		3.998	15.1	0.235	0.184	1.817
50.0	0.691		4.559	26.2	0.365	0.325	2.403
50.7	0.693	0.734	4.627	41.5	0.653	0.613	3.390
61.1	0.971		5.363	50.1	0.906	0.894	4.284
70.0		1.515		65.3	1.679	1.689	6.529
70.5	1.331		6.418	80.4	3.205	3.326	9.566
80.2	1.877	2.267	7.679	95.0	7.627	7.395	16.360
90.0	2.869	3.617	10.470	99.0	10.455	10.385	20.160
90.3	2.905	3.714	10.440	100.0			20.440
95.1	3.964	5.363	13.560				
97.3	5.193	7.317	16.280				
99.0	6.448	10.240	17.200				
99.5	6.874	11.670	19.030				
99.9	7.468	12.955	19.680				
100			20.100				

Table 3.12 Continued

Ethanol				1-Propanol			
	$D/10^{-10}m^2s^{-1}$				$D/10^{-10}m^2s^{-1}$		
x/mol%	$[C_4MIm]$	BF_4	alcohol	x/mol%	$[C_4MIm]$	BF_4	alcohol
0.0	0.121	0.090		0.0	0.121	0.090	
1.8	0.134	0.111	0.692	2.0	0.131	0.112	0.468
5.1	0.144	0.109	0.758	4.8	0.153	0.126	0.543
9.2	0.175	0.149	0.890	11.3	0.187	0.160	0.669
15.6	0.226	0.200	1.077	15.1	0.209	0.168	0.729
25.6	0.321	0.291	1.339	25.1	0.312	0.286	1.067
41.7	0.576	0.545	2.157	38.3	0.425	0.396	1.349
51.5	0.802	0.802	2.794	50.7	0.604	0.597	1.816
65.8	1.234	1.212	3.661	100.0			4.969
80.1	1.947	1.908	5.206				
95.0	3.508	3.243	7.945				
99.0	4.878	4.366	9.074				
100.0			9.216				

1-Butanol				1-Pentanol			
	$D/10^{-10}m^2s^{-1}$				$D/10^{-10}m^2s^{-1}$		
x/mol%	$[C_4MIm]$	BF_4	alcohol	x/mol%	$[C_4MIm]$	BF_4	alcohol
0.0	0.121	0.090		0.0	0.121	0.090	
2.5	0.132	0.110	0.404	5.0	0.144	0.110	0.366
5.1	0.150	0.118	0.430	7.3	0.160	0.133	0.415
11.0	0.188	0.160	0.566	10.5	0.181	0.152	0.475
15.5	0.218	0.190	0.624	16.0	0.219	0.193	0.532
22.2	0.261	0.230	0.765	20.5	0.222	0.198	0.573
35.4	0.360	0.327	1.009	100.0			2.552
100.0			3.539				

Table 3.12 Continued

1-Hexanol			
	$D/10^{-10}m^2s^{-1}$		
x/mol%	[C_4MIm]	BF_4	alcohol
0.0	0.121	0.090	
2.4	0.140	0.125	0.321
5.0	0.145	0.108	0.322
6.3	0.152	0.112	0.331
7.0	0.150	0.128	0.348
8.8	0.159	0.123	0.371
100.0			1.926

Table 3.13 Mean distance travelled (L) of [C_4MIm], BF_4, alcohols and water at alcohol or water concentration extrapolated to 0 mol% at 298 K.

	L/μm s^{-1}
Water	21.12
Methanol	14.82
Ethanol	11.01
1-Propanol	8.65
1-Butanol	8.48
1-Pentanol	7.87
1-Hexanol	7.64
[C_4MIm]	4.91
BF_4	4.23

Table 3.14 Molecular volume and radii of [C_4MIm], BF_4, alcohols and water [Yoshimura et al. 2019 a, Tokuda et al. 2005].

	V/Å^3	radii/Å		V/Å^3	radii/Å
Water	17.7	1.6	[C_4MIm]		3.3[a]
Methanol	29.7	1.9	BF_4	77.6[b]	2.6
Ethanol	45.7	2.2			
1-Propanol	54.8	2.4			
1-Butanol	76.4	2.6			
1-Pentanol	84.9	2.7			
1-Hexanol	100.7	2.9			
1-Heptanol	110.0	3.0			
1-Octanol	125.9	3.1			
1-Nonanol	142.1	3.2			
1-Decanol	158.0	3.4			

Table 3.15 Concentration dependence of viscosity in $[C_4MIM]BF_4$/alcohol and $[C_4MIM]BF_4$/water systems at 298 K.

Water		Methanol		Ethanol		1-Propanol	
x/mol%	η/mPas	x/mol%	η/mPas	x/mol%	η/mPas	x/mol%	η/mPas
0	122.01	0	122.04	0	122.12	0	122.28
11.21	71.83	10.17	74.54	10.02	76.37	10.37	75.39
20.21	50.10	20.14	48.28	20.25	47.94	20.17	51.71
29.87	33.41	30.53	30.77	29.98	31.52	30.08	35.80
40.11	24.44	39.89	19.52	40.23	20.64	39.91	25.42
50.54	16.32	50.34	12.26	50.11	14.16	49.93	18.50
59.96	12.14	60.28	7.82	60.14	9.29	100	2.15
70.00	8.18	69.98	4.47	70.24	5.78		
80.02	5.23	80.01	2.49	80.11	3.85		
90.00	3.42	90.02	1.27	90.03	2.33		
95.00	2.08	95.75	0.85	95.09	1.69		
100	0.89	100	0.60	100	1.23		

1-Butanol		1-Pentanol		1-Hexanol	
x/mol%	η/mPas	x/mol%	η/mPas	x/mol%	η/mPas
0	122.20	0	122.26	0	122.27
9.51	75.83	6.11	89.26	5.40	96.76
20.23	52.36	11.93	71.66	10.13	82.70
30.11	36.12	18.12	60.33	100	4.88
100	2.71	100	3.73		

Table 3.16 Slopes on $\log(D)$ vs. $\log\left(\frac{1}{\eta}\right)$ at less than 50 mol%

	Slope
Water	0.35 ± 0.02
Methanol	0.57 ± 0.02
Ethanol	0.64 ± 0.02
1-Propanol	0.76 ± 0.04
1-Butanol	0.86 ± 0.05
1-Pentanol	0.89 ± 0.07
1-Hexanol	1.10 ± 0.14

Chapter 4

The influence of the alkyl chain length of ionic liquid [C_nMIm]BF_4 to physicochemical properties of the pocket formed in the IL and water confined in the pocket.

4.1 Introduction

In the previous chapter, the movement and interaction of water in the pocket and the size of the pocket in the same IL were discussed. This IL has nano-heterogeneous structure [Triolo et al. 2007]. The structure of imidazolium-based ILs is mainly composed of the nonpolar domain formed by alkyl chains and the polar domain formed by anions and imidazolium rings. It is reported that as the alkyl chain length increases, the alkyl chains tend to aggregate and the nonpolar domain becomes thicker [Lopes et al. 2006]. There is a possibility that the properties of the pocket may be changed by changing the alkyl chain length of ILs. Therefore, the purpose of this chapter is to investigate how the alkyl chain length of the IL affects the properties of pockets and the water in it by using systems in which water is mixed with an IL having various alkyl chain length.

4.2 Material and Method

4.2.1 Samples

Five ILs with different alkyl chain length were purchased from the Kanto Chemical Co., Inc. and used as-received without further purification: 1-ethyl-3-methylimidazolium tetrafluoroborate ($[C_2MIM]BF_4$), 1-butyl-3-methylimidazolium tetrafluoroborate, ($[C_4MIM]BF_4$), 1-hexyl-3-methylimidazolium tetrafluoroborate, ($[C_6MIM]BF_4$), 1-methyl-3-octylimidazolium tetrafluoroborate, ($[C_8MIM]BF_4$), and 1-decyl-3-methylimidazolium tetrafluoroborate, ($[C_{10}MIM]BF_4$) which are summarized in Table 4.1. The ultrapure water used in experimental work was supplied by a Synergy UV system (Millipore Inc.). The molar percentage, *x*, shows the water in mixtures with ILs. The details of the experiments performed are described in 3.2.2-3.2.4.

4.3 Result and Discussion

4.3.1 Solubility of water in $[C_nMIm]BF_4$

Water can be dissolved in $[C_2MIm]BF_4$ and $[C_4MIm]BF_4$ over the entire concentration range at 298 K; however, $[C_6MIm]BF_4$, $[C_8MIm]BF_4$ and $[C_{10}MIm]BF_4$ with water have a concentration range in which phase separation occurs at 298 K [Maia et al. 2012]. The explicit solubilities of water in $[C_6MIm]BF_4$, $[C_8MIm]BF_4$ and $[C_{10}MIm]BF_4$ at 298 K have not been specifically investigated. Therefore, the saturated solubility of water in $[C_6MIm]BF_4$, $[C_8MIm]BF_4$ and $[C_{10}MIm]BF_4$ was determined from ^{1}H NMR spectral measurements. Excess water was added to $[C_6MIm]BF_4$, $[C_8MIm]BF_4$ and $[C_{10}MIm]BF_4$ respectively until phase separation was visually confirmed, and after that, it was left for 24 h or more. The IL-rich saturated solutions was then sampled and ^{1}H-NMR spectra were measured. Representative ^{1}H-NMR spectra of $[C_nMIm]BF_4$/water systems at 50 mol% and pure $[C_4MIm]BF_4$ are shown in Figure 4.1.

The saturated solubility was determined from the ratio of the peak area intensity of the water to $[C_6MIm]BF_4$, $[C_8MIm]BF_4$ or $[C_{10}MIm]BF_4$ (74.6 mol%, 71.2 mol%, 72.5 mol%). Therefore, measurements of the chemical shift and the self-diffusion coefficient were performed below the saturation concentration for water.

4.3.2 Concentration dependence of density in $[C_nMIm][BF_4]$/water

In order to investigate the pocket volume change on IL/water systems caused by the difference of the alkyl chain length of the IL, the density of $[C_nMIm]BF_4$/water systems were compared. The dependence of the density on the water concentration in the $[C_nMIm]BF_4$/water systems at 298 K is shown in Figure 4.2 and Table 3.3, 4.2. In over trend, all the density of $[C_nMIm]BF_4$/water systems decreased with increasing alkyl chain length of the IL and showed the same concentration dependence. In particular, up to 75 mol%, density decrease loosely with increasing concentration whereas over 75 mol% decrease drastically with increasing concentration in $[C_2MIm]BF_4$ and $[C_4MIm]BF_4$ systems.

Subsequently, volume expansivity was calculated by using Eq. (3.2) in order to investigate solution volume change with various alkyl chain length of the IL. The dependence of the volume expansivity on the water concentration in the $[C_nMIm]BF_4$/water systems is shown in Figure 4.3 and Table 3.4, 4.3. As a result, volume expansivity of $[C_nMIm]BF_4$/water systems decreased with increasing alkyl chain length of the IL and that of $[C_{10}MIm]BF_4$/water system was less than 1 % at 50 mol%, suggesting that the water enters into the pocket at low water concentration. From this result, it is possible that the pocket size increase with increasing alkyl chain length of the IL. This findings is in good agreement with free-hole volume increasing with increasing molecular weight of an IL [Yu et al. 2012].

4.3.3 Concentration dependence of chemical shift in $[C_nMIm][BF_4]$/water

In order to investigate the properties of water in the pocket in ILs with various hydrophobicity, water was mixed with ILs having various alkyl chain length $[C_nMIm]BF_4$ (n=2, 4, 6, 8, 10). The dependence of the ^1H chemical shift of the cation on the water concentration in the $[C_nMIm]BF_4$/water mixtures at 298 K is shown in Figure 4.4-4.9 and Table 4.4-4.7. In over trend, all the ^1H chemical shift of cation showed the same concentration dependence in $[C_nMIM]BF_4$/water systems. At less than 75 mol%, there is no significant differences in chemical shift were observed. This result indicated that there is almost no change in the interactions that the cations undergo. In other words, the addition of water hardly affect the structure of the IL in a static view. Over 75 mol% of water, downfield shifts were also observed with an increase of the water concentration in $[C_2MIm]BF_4$/water and $[C_4MIm]BF_4$/water systems.

Figure 4.10 shows the ^{19}F chemical shift of the anion for the $[C_nMIM]BF_4$/water systems at 298 K. At less than 75 mol%, there is no significant differences in chemical shift were observed as well as cation data. In terms of both cations and anions, this suggested that the structure of the IL does not change significantly, even if water are added to the IL. In addition, over 75 mol% of water, the chemical shifts of the$[C_2MIM]BF_4$ system clearly moved downfield. On the other hand, there is no significant change over 75 mol% in $[C_4MIM]BF_4$/water system, meaning that the magnetic field environment felt by BF_4 is similar in pure $[C_4MIM]BF_4$ and water.

Figure 4.11 also showed the concentration dependence of the ^{1}H chemical shift for the hydroxyl groups of water. All the hydroxyl groups of the water in [C_nMIm]BF_4/water system showed almost the same concentration dependence over the entire concentration range. This suggests that the water may exist in almost the same environment. Furthermore, the downfield shift when a monomer becomes a polymer by hydrogen bonding has been reported [Eblinger et al. 1996, Aidas et al. 2006, Yamaguchi et al.]. The ^{1}H NMR chemical shift of hydroxyl groups is an average of the chemical shift values of water aggregations. Based on the ^{1}H chemical shift values of monomer, dimer, trimer, tetramer and pentamer of water calculated from the density functional theory (DFT) [Aidas et al. 2006], the average number of water aggregation in bulk water and [C_nMIM]BF_4/water were calculated from the chemical shift assuming that all water exists as a monomer at water concentration extrapolated to 0 mol%. In particular, the chemical shift difference ($\Delta\delta$) of the bulk water and monomer was calculated, and the chemical shift difference of the water cluster was calculated from the experimental value assuming that it was proportional to the literature value [Aidas et al. 2006] as shown in Figure 4.12 and Table 4.8. Firstly, the aggregation number in bulk water was calculated using a polynomial approximation function Eq. (4.1) as shown in Figure 4.13.

$$y = -0.0591x^3 + 0.5400x^2 - 0.3590x + 0.4681 \quad (R^2 = 0.995) \qquad (4.1)$$

where y is number of water aggregation, x is ^{1}H chemical shift. From this equation, the average water aggregation number of pure water was 4.65, and each difference between the chemical shift of monomer and each water aggregation were calculated as shown in Table 4.8. From the chemical shift

ratio of each water aggregation to bulk water (δ_n/δ_{bulk}) and the chemical shift at water concentration extrapolated 0 mol%, the chemical shifts of each water aggregation in $[C_nMIm]BF_4$ were calculated using Eq. (4.2), as shown in Figure 4.13.

$$\delta_{\text{water in IL}} = \delta_n/\delta_{bulk} \times (\delta_{bulk} - \delta_{\text{monomer in IL}}) + \delta_{\text{monomer in IL}} \quad (4.2)$$

where $\delta_{\text{water in IL}}$ is the chemical shift of aggregation number n, δ_n is the chemical shift of water aggregation number n, δ_{bulk} is the chemical shift of bulk water, $\delta_{\text{monomer in IL}}$ is the chemical shift of water in $[C_nMIm]BF_4$ at extrapolated 0 mol%. In order to calculate concentration dependence of water aggregation number, the relationship between the chemical shifts of each water aggregation and aggregation number was fitted using polynomial approximation function Eq. (4.3-7) each $[C_nMIm]BF_4$/water system.

In $[C_2MIm]BF_4$/water system

$$y = -0.2431x^3 + 2.6205x^2 - 7.4847x + 7.0481 \quad (R^2 = 0.995) \quad (4.3)$$

In $[C_4MIm]BF_4$/water system

$$y = -0.2814x^3 + 3.0825x^2 - 9.2259x + 9.0015 \quad (R^2 = 0.995) \quad (4.4)$$

In $[C_6MIm]BF_4$/water system

$$y = -0.2817x^3 + 3.0868x^2 - 9.2422x + 9.0202 \quad (R^2 = 0.995) \quad (4.5)$$

In $[C_8MIm]BF_4$/water system

$$y = -0.2658x^3 + 2.8940x^2 - 8.5119x + 8.1921 \quad (R^2 = 0.995) \quad (4.6)$$

In $[C_{10}MIm]BF_4$/water system

$$y = -0.2871x^3 + 3.1518x^2 - 9.4898x + 9.3033 \quad (R^2 = 0.995) \quad (4.7)$$

From these equation, concentration dependence of water aggregation number in $[C_nMIm]BF_4$ were calculated, as shown in Figure 4.14 and Table 4.9. The average number of water aggregation showed almost the same concentration dependence regardless of alkyl chain length of the IL. At less than 50 mol%, most of water exist as monomers or dimers. This results are in good agreement with $[C_4MIm]BF_4$/water system obtained by Raman measurements reported by Yoshimura et al. 2019b.

4.3.4 Concentration dependence of self-diffusion coefficient in $[C_nMIm][BF_4]$/water

In order to investigate how water in the IL having various alkyl chain length move, the self-diffusion coefficient for $[C_nMIm]BF_4$/water systems were measured. The self-diffusion coefficient (*D*) of protons at the 2H, 4H, 5H, alkyl root, alkyl tail, methyl, positions in the $[C_nMIm]$ cation was determined from ^{1}H-NMR measurements. There was no significant difference in the *D*s at all protons of the cation when compared at the same concentration. Therefore, their average value was taken as the *D*s of the cation. The *D* of the anions was measured using ^{19}F-NMR. The concentration dependence of the *D*s of the cations, anions and water of the $[C_nMIm]BF_4$/water systems at 298 K is shown in Figure 4.15-17 and Table 3.12, 4.10.

As an overall trend, the *D*s of anions, cations and water decreased with increasing the alkyl chain length of the IL. This result is expected to result from an increase in the cation molecule size and a stronger hydrophobic interaction between the alkyl chains. The *D*s of anions, cations and water in all the systems increased gradually for water concentrations up to 75 mol%. However, the *D*s of water then increased rapidly as the water concentration was increased to over 75 mol% in $[C_2MIm]BF_4$/water and $[C_4MIm]BF_4$/water. Therefore, it is considered that the nano-heterogeneous structure is maintained up to 75 mol% from a dynamic viewpoint as well as $[C_4MIm]BF_4$/water system.

To compare the movement of the IL and the water in more detail, we calculated the mean distance travelled (*L*) per 1 second by using Eq (3.3) at water concentration extrapolated to 0 mol%,

as shown in Figure 4.18 and Table 4.11. As a result, and the *L*s of anions, cations and water tends to decrease with increasing alkyl chain length of the IL and that of water are much larger than those of the bulk constituents of the ILs. $[C_nMIm]BF_4$/water systems didn't show limiting effect as well as $[C_4MIm]BF_4$/alcohol systems, suggesting that the water move fast between the pockets.

In order to deepen our understanding of this finding, we plotted the *L* ratio of the water to that of the anion or cation (L_{water}/L_{anion} or L_{water}/L_{cation}), as shown in Figure 4.19. Interestingly, the *L* ratios tend to increase with increasing alkyl chain length, meaning that the relative movement of water molecules within ILs tended to increase as the alkyl chains were lengthened. Considering Stokes Einstein equation (Eq. 3.4), the *L* for water is higher than that for the anion and cation may simply reflect the molecular radii difference. Therefore, we checked the relationship between the *D* ratio and *r* ratio at water concentration extrapolated to 0 mol% shown in Figure 4.20 (information on molecular size shown in Table 4.12 [Tokuda et al. 2005, Yoshimura et al. 2019a]). As a result, the *D* ratio was clearly larger than the *r* ratio for all alkyl chains and the *D* ratio clearly increased with increasing alkyl chain length compared to the *r* ratio, meaning that *D* ratio isn't simply proportional to the *r* ratio. Thus, the differences of the *D* between the water and the anions or the cations don't simply reflects the molecular size difference between water and anion or cation.

From the result of the IL structure maintaining up to 75 mol% from dynamic and static views, water move in pure IL structure at low water concentration. Therefore, it is expected that local interaction between the water and the IL does not directly reflect the bulk solution viscosity. For this

reason, the relationship between viscosity, which is a macroscopic property, and self-diffusion coefficient, which is a microscopic property, is discussed in next section.

4.3.5 Relationship between self-diffusion coefficient and viscosity in $[C_nMIm][BF_4]$/water

According to Eq. (3.5), the slope on $\log(D)$ vs. $\log\left(\frac{1}{\eta}\right)$ is simply reflected the relationship between the macroscopic viscosity and self-diffusion coefficient. From this equation, the relationship between the D and η were investigated in $[C_nMIm]BF_4$/water systems at less than 50 mol% as shown in in Figure 4.21-23 (viscosity value summarized in Table 3.15, 4.13). As a result, most of the slope of anions and cations calculated using least squares method showed 0.8-1.0 respectively, meaning that the movements of cation and anion are proportional to bulk solution movement. On the other hand, most of the slope of water had around 0.3 and were clearly lower than that of anion and cation, suggesting that the movements of the water doesn't reflect the movement of bulk solution. In other words, they moves independently of the movement of the bulk solution in $[C_nMIm]BF_4$/water systems to some extent.

The following dynamic model could be obtained for the water in the IL with various alkyl chain length as shown in Figure 4.24. The structure of the pure IL hardly change from the view of the dynamic (self-diffusion coefficient) and static (chemical shift) properties, even though water was added up to 75 mol%. The pocket size in the IL structure may increase with increasing alkyl chain length of the IL from the density data. As the alkyl chain length of the IL increases, the decrease in movement of the IL forming the pockets caused the decrease in movement of water. However, the relative movement of water within the IL tended to increase as the alkyl chains of the IL were lengthened. Because of fixing the volume of polar site (BF_4 and imidazolium ring), if the water exists

only in polar region of the IL, *D* ratio should depends on *r* ratio. But *D* ratio increase clearly more than *r* ratio. Thus, it is expected that the movement of the water is influenced by non polar site (alkyl chain). It suggests that the surface of the pocket existing in the IL contains both a nonpolar and polar site, and the ratio of polar surface to nonpolar surface decreases as the alkyl chain length of the IL increases. Consequently, the electrostatic interactions between the surface of the pocket and the water molecules decrease and the water molecules in the pocket move more independent of the IL. Moreover, from macroscopic (viscosity) and microscopic (self-diffusion coefficient) dynamic views, the movement of water in the IL isn't restricted in the pocket and move between the pockets.

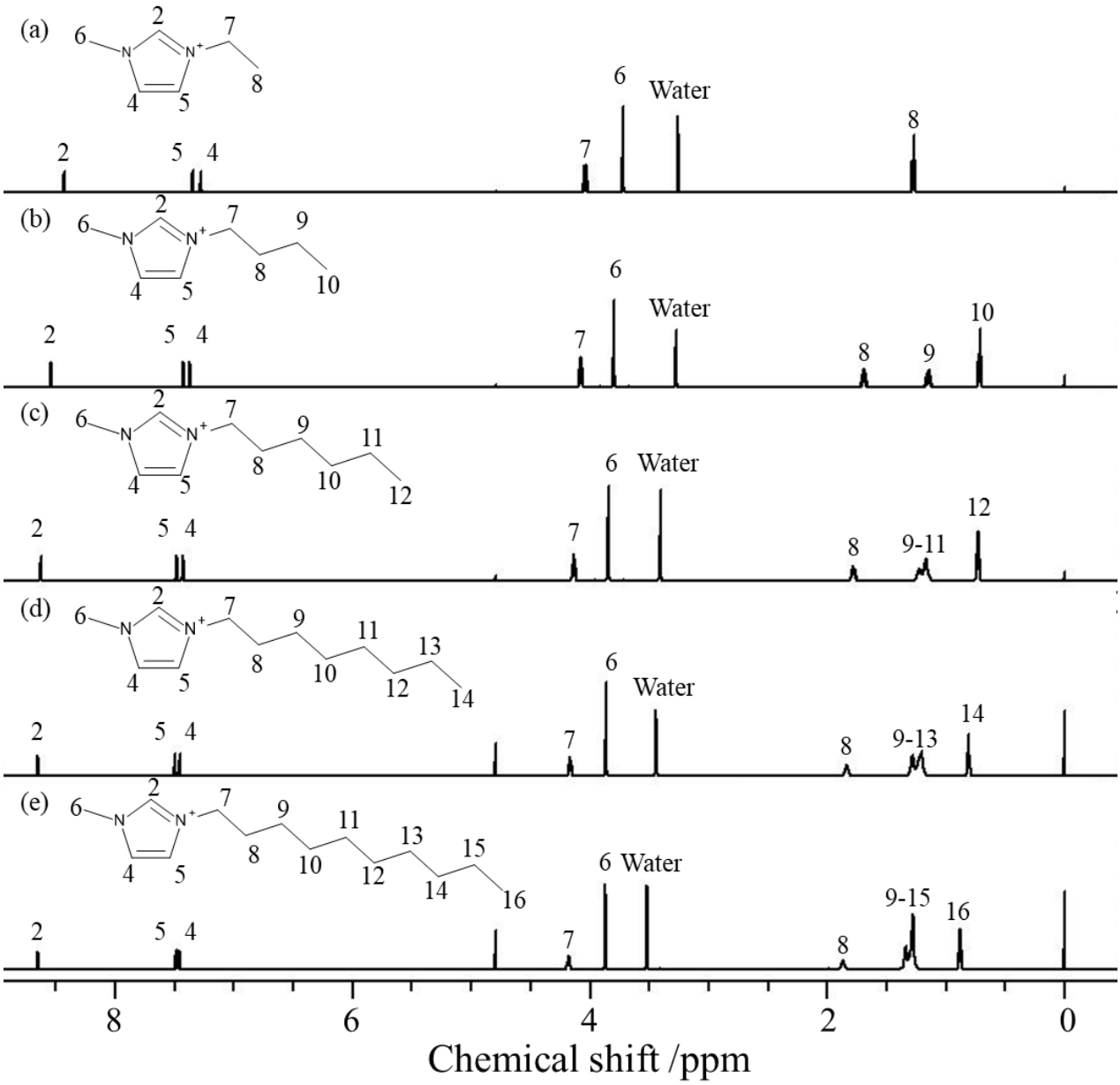

Figure 4.1 ^{1}H NMR spectra of ILs at ca. 50 mol% at 298 K: (a) $[C_2MIM][BF_4]$, (b) $[C_4MIM][BF_4]$, (c) $[C_6MIM][BF_4]$, (d) $[C_8MIM][BF_4]$, (e) $[C_{10}MIM][BF_4]$. The peak around 4.8 ppm is H_2O in an internal standard solution.

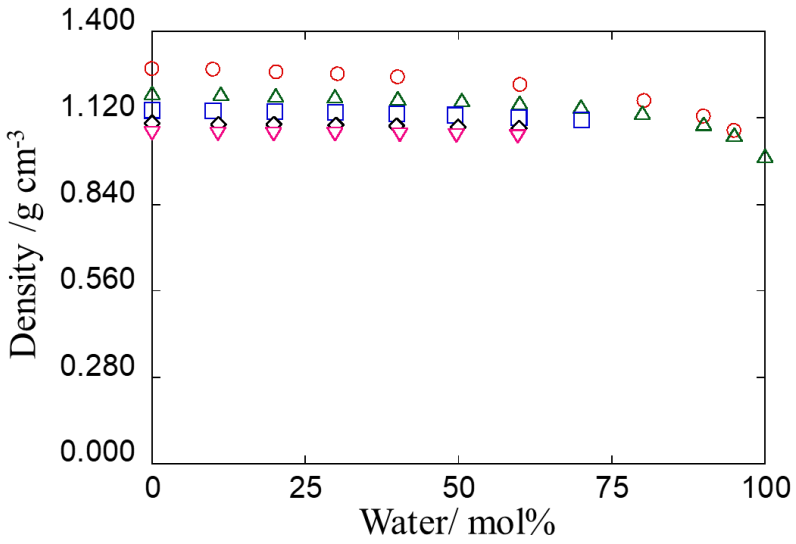

Figure 4.2 Density of $[C_nMIm]BF_4$/water systems at various concentrations of alcohol or water at 298 K. Legend: (○),$[C_2MIm]BF_4$; (△), $[C_4MIm]BF_4$; (□) $[C_6MIm]BF_4$; (◇) $[C_8MIm]BF_4$; (▽) $[C_{10}MIm]BF_4$.

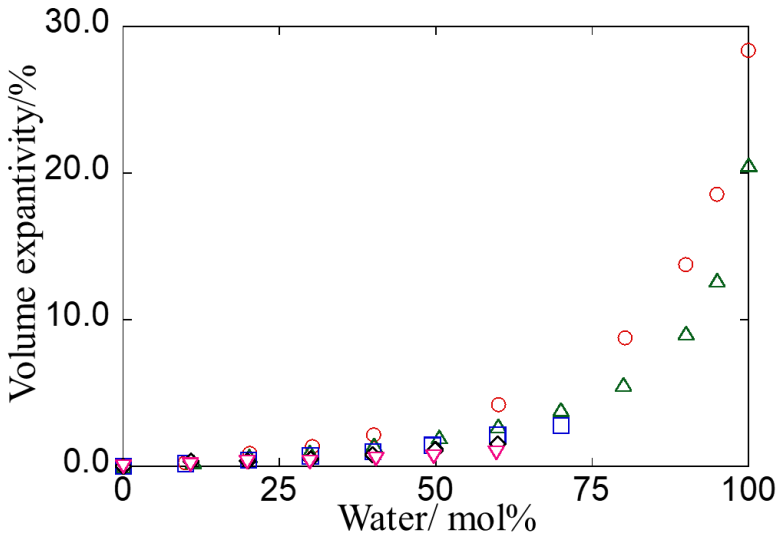

Figure 4.3 Volume expantivities of $[C_nMIm]BF_4$/water systems at various concentrations at 298 K. Legend: (○),$[C_2MIm]BF_4$; (△), $[C_4MIm]BF_4$; (□) $[C_6MIm]BF_4$; (◇) $[C_8MIm]BF_4$; (▽) $[C_{10}MIm]BF_4$.

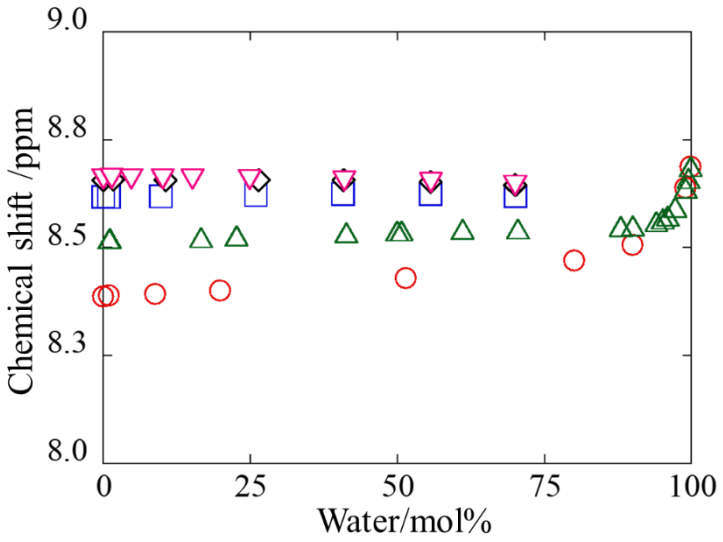

Figure 4.4 ^{1}H chemical shift for 2H of [C_nMIm] cation at various concentrations of water at 298 K: Legend: (○),[C_2MIM]BF_4; (△), [C_4MIM]BF_4; (□) [C_6MIM]BF_4; (◇) [C_8MIM]BF_4; (▽) [C_{10}MIM]BF_4.

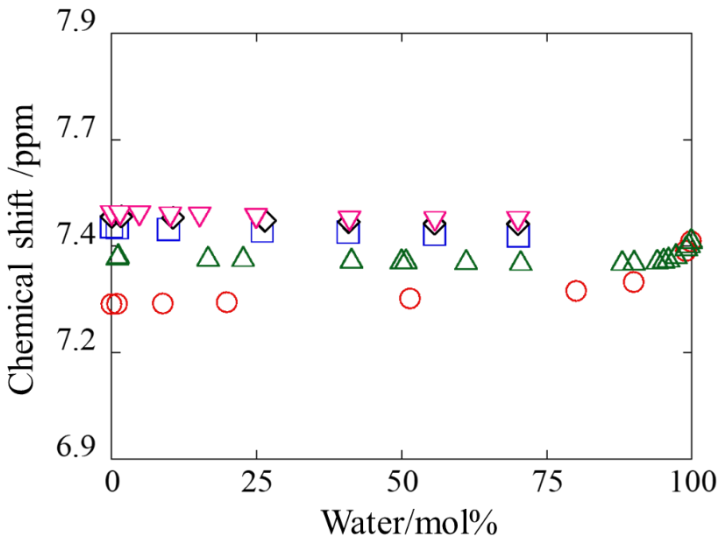

Figure 4.5 ^{1}H chemical shift for 4H of [C_nMIm] cation at various concentrations of water at 298 K: Legend: (○),[C_2MIm]BF_4; (△), [C_4MIm]BF_4; (□) [C_6MIm]BF_4; (◇) [C_8MIm]BF_4; (▽) [C_{10}MIm]BF_4.

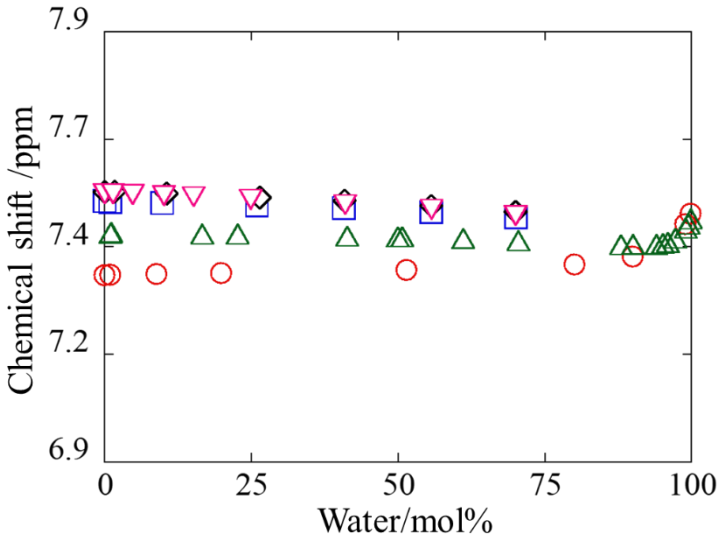

Figure 4.6 ^{1}H chemical shift for 5H of [C_nMIm] cation at various concentrations of water at 298 K: Legend: (○),[C_2MIm]BF_4; (△), [C_4MIm]BF_4; (□) [C_6MIm]BF_4; (◇) [C_8MIm]BF_4; (▽) [C_{10}MIm]BF_4.

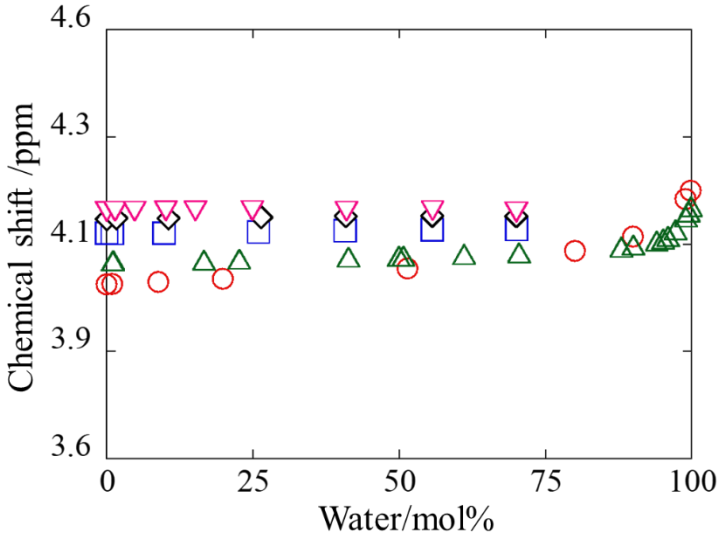

Figure 4.7 ^{1}H chemical shift for alkyl root of [C_nMIm] cation at various concentrations of water at 298 K: Legend: (○),[C_2MIm]BF_4; (△), [C_4MIm]BF_4; (□) [C_6MIm]BF_4; (◇) [C_8MIm]BF_4; (▽) [C_{10}MIm]BF_4.

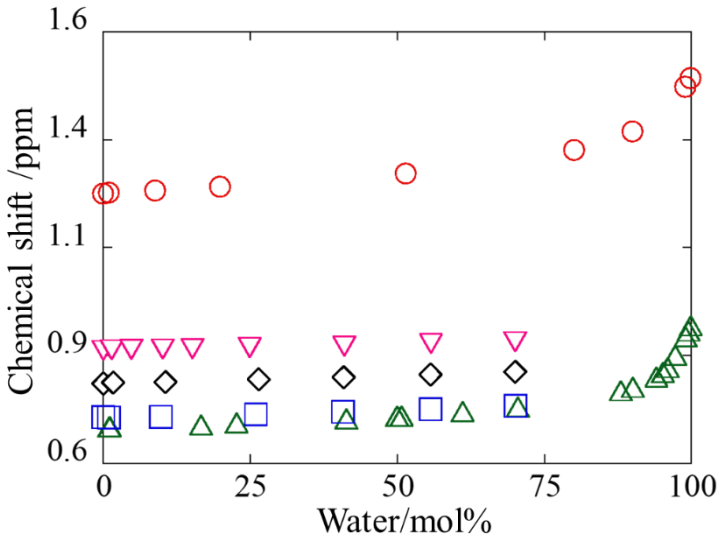

Figure 4.8 ^{1}H chemical shift for alkyl tail of [C_nMIm] cation at various concentrations of water at 298 K: Legend: (○),[C_2MIm]BF_4; (△), [C_4MIm]BF_4; (□) [C_6MIm]BF_4; (◇) [C_8MIm]BF_4; (▽) [C_{10}MIm]BF_4.

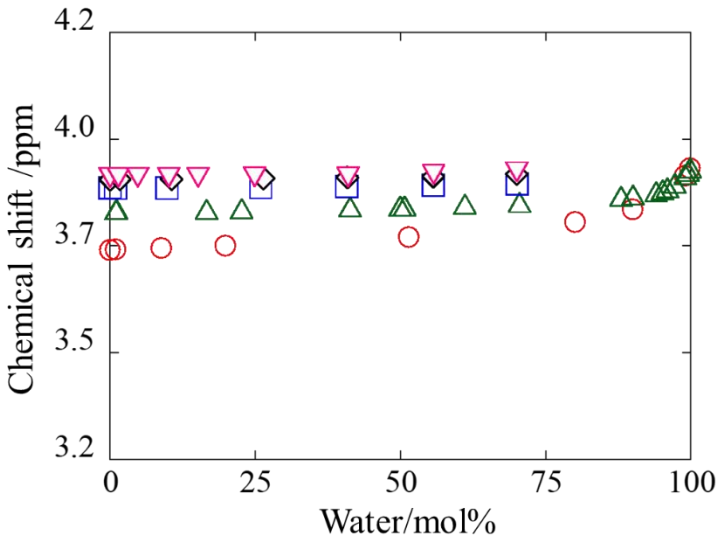

Figure 4.9 ^{1}H chemical shift for methyl group of [C_nMIm] cation at various concentrations of water at 298 K: Legend: (○),[C_2MIm]BF_4; (△), [C_4MIm]BF_4; (□) [C_6MIm]BF_4; (◇) [C_8MIm]BF_4; (▽) [C_{10}MIm]BF_4.

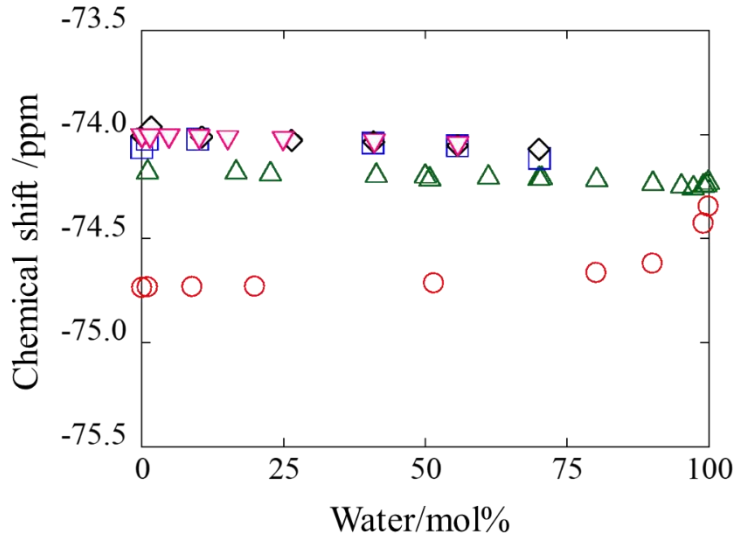

Figure 4.10 ^{19}F chemical shift for BF_4 anion at various concentrations of water at 298 K: Legend: (○),[C_2MIm]BF_4; (△), [C_4MIm]BF_4; (□) [C_6MIm]BF_4; (◇) [C_8MIm]BF_4; (▽) [C_{10}MIm]BF_4.

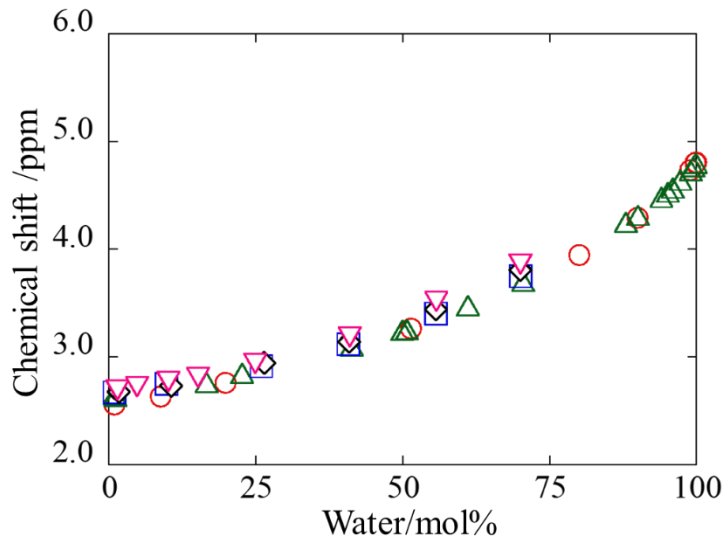

Figure 4.11 ^{1}H chemical shift for hydroxyl group of water at various concentrations of water at 298 K: Legend: (○),[C_2MIm]BF_4; (△), [C_4MIm]BF_4; (□) [C_6MIm]BF_4; (◇) [C_8MIm]BF_4; (▽) [C_{10}MIm]BF_4.

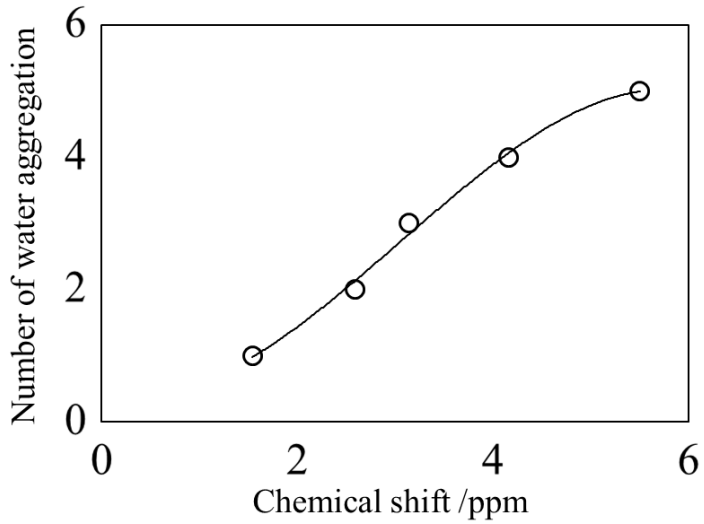

Figure 4.12 Relationship between number of water aggregation and chemical shift using literature value [Aidas et al. 2006].

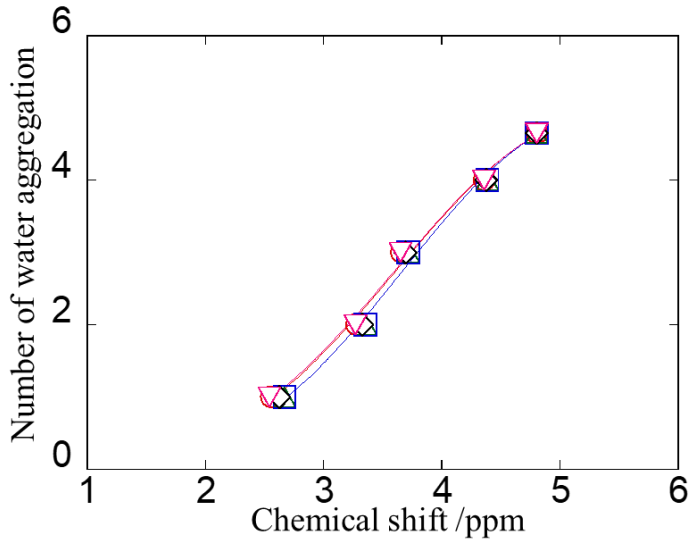

Figure 4.13 Relationship between number of water aggregation and chemical shift in $[C_nMIm]BF_4$/water systems. Legend: (○),$[C_2MIm]BF_4$; (△), $[C_4MIm]BF_4$; (□) $[C_6MIm]BF_4$; (◇) $[C_8MIm]BF_4$; (▽) $[C_{10}MIm]BF_4$.

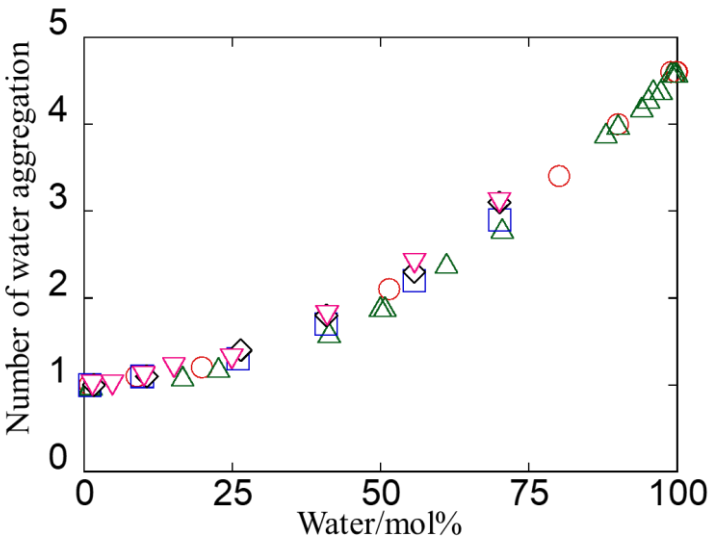

Figure 4.14 Concentration dependence of water aggregation in $[C_nMIm]BF_4$/water systems. Legend: (○),$[C_2MIm]BF_4$; (△), $[C_4MIm]BF_4$; (▫) $[C_6MIm]BF_4$; (◇) $[C_8MIm]BF_4$; (▽) $[C_{10}MIm]BF_4$.

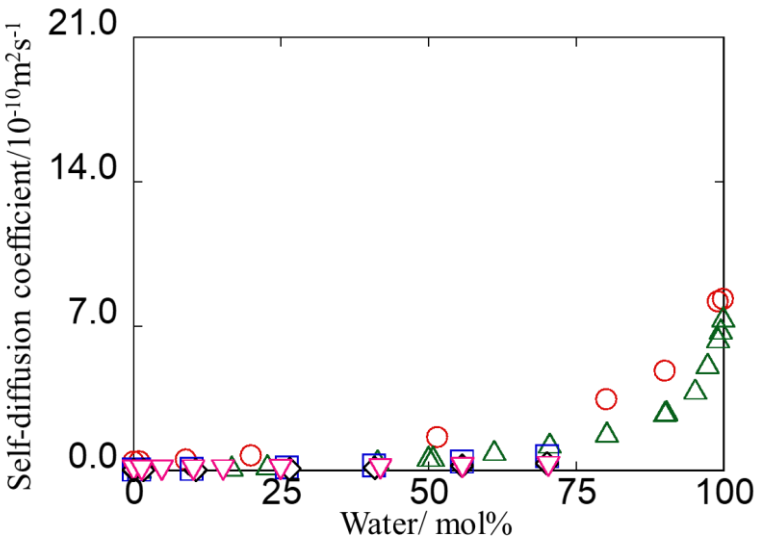

Figure 4.15 Self-diffusion coefficients of [C_4MIm] at various concentrations of water at 298 K. Legend: (○),[C_2MIm]BF_4; (△), [C_4MIm]BF_4; (□) [C_6MIm]BF_4; (◇) [C_8MIm]BF_4; (▽) [C_{10}MIm]BF_4.

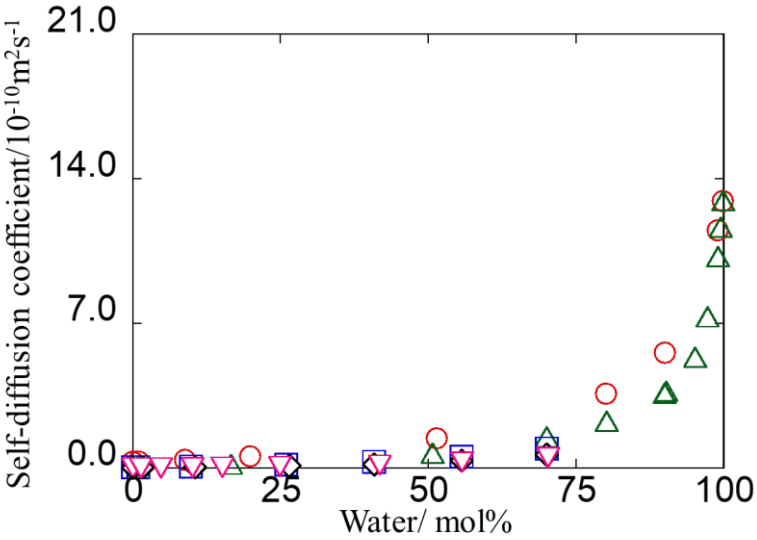

Figure 4.16 Self-diffusion coefficients of BF_4 at various concentrations of water at 298 K. Legend: (○),[C_2MIm]BF_4; (△), [C_4MIm]BF_4; (□) [C_6MIm]BF_4; (◇) [C_8MIm]BF_4; (▽) [C_{10}MIm]BF_4.

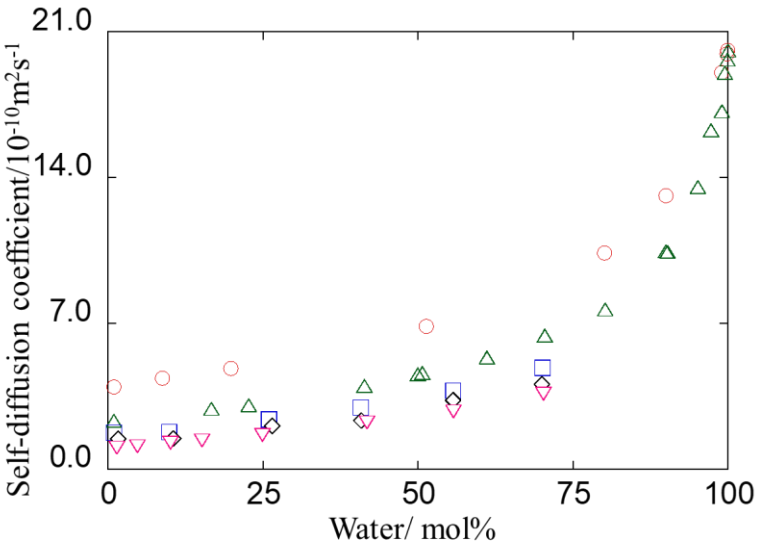

Figure 4.17 Self-diffusion coefficients of water at various concentrations of water at 298 K. Legend: (○),[C_2MIm]BF_4; (△), [C_4MIm]BF_4; (□) [C_6MIm]BF_4; (◇) [C_8MIm]BF_4; (▽) [C_{10}MIm]BF_4.

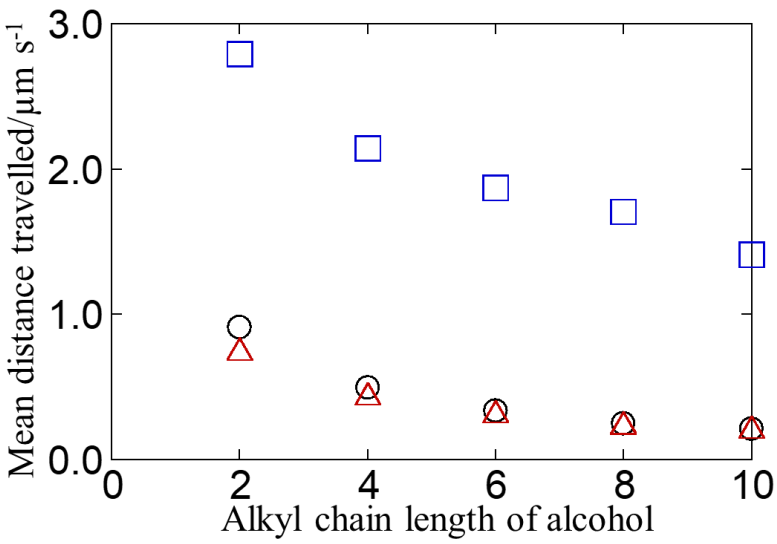

Figure 4.18 Mean distance travelled of cations, anions andwater and alcohol in $[C_nMIm]BF_4$/water and $[C_4MIm]BF_4$/alcohol systems at alcohol or water concentration extrapolated to 0 mol% at 298 K. Legend: anion (△), cation (○) and water (□).

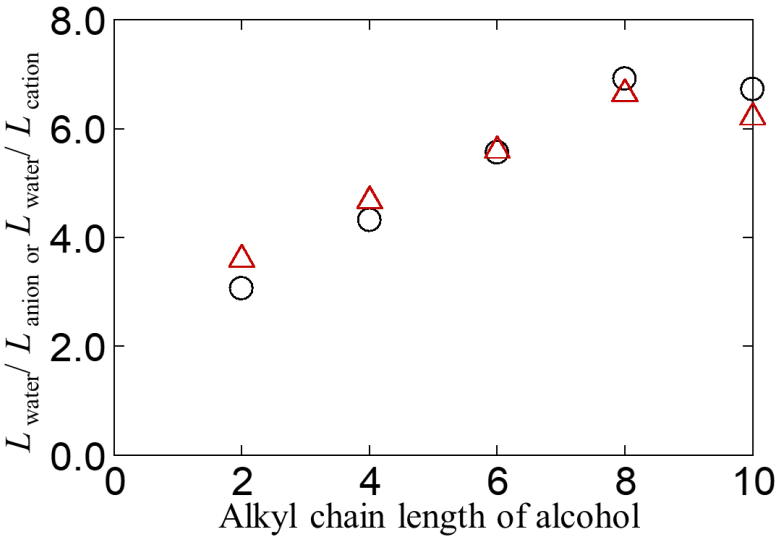

Figure 4.19 Mean distance travelled ratio of water to IL in $[C_nMIm]BF_4$/water systems at or water concentration extrapolated to 0 mol% at 298 K. Legend: L_{water}/L_{anion} (△), L_{water}/L_{cation} (○).

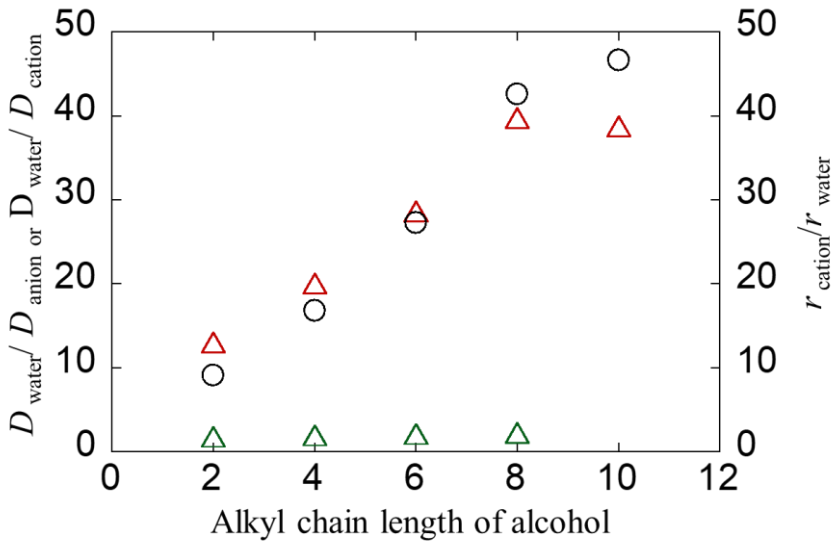

Figure 4.20 Alkyl chain length dependence of D_{water}/D_{anion} or D_{water}/D_{cation} at water concentration extrapolated to 0 mol% and r_{anion}/r_{water} or r_{cation}/r_{water} in the pure IL at 298 K [Tokuda et al. 2005]. Legend: D_{water}/D_{anion} (△), D_{water}/D_{cation} (○) and r_{cation}/r_{water} (△).

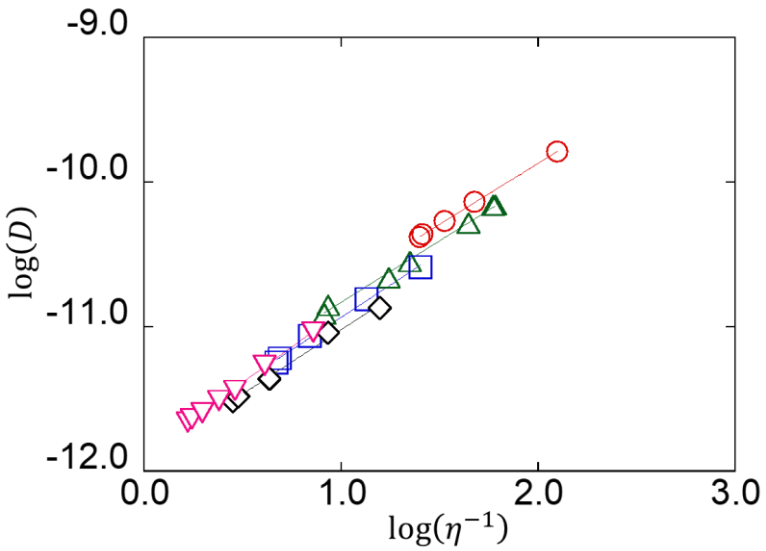

Figure 4.21 Relationships between logarithm reciprocal of viscosity and logarithm self-diffusion coefficient of [C_nMIm] at less than 50 mol% at 298 K. The viscosity was calculated using a polynomial approximation function. Legend: (○),[C_2MIm]BF_4; (△), [C_4MIm]BF_4; (□) [C_6MIm]BF_4; (◇) [C_8MIm]BF_4; (▽) [C_{10}MIm]BF_4.

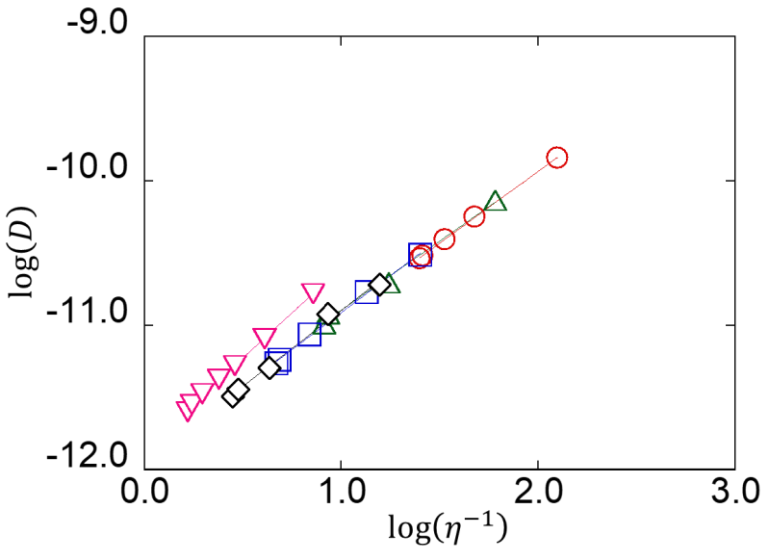

Figure 4.22 Relationships between logarithm reciprocal of viscosity and logarithm self-diffusion coefficient of BF_4 at less than 50 mol% at 298 K. The viscosity was calculated using a polynomial approximation function. Legend: (○),[C_2MIm]BF_4; (△), [C_4MIm]BF_4; (□) [C_6MIm]BF_4; (◇) [C_8MIm]BF_4; (▽) [C_{10}MIm]BF_4.

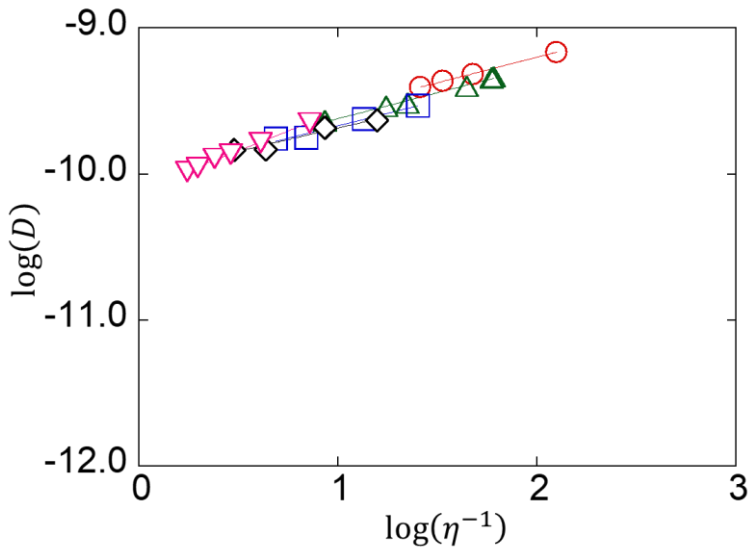

Figure 4.23 Relationships between logarithm reciprocal of viscosity and logarithm self-diffusion coefficient of water at less than 50 mol% at 298 K. The viscosity was calculated using a polynomial approximation function. Legend: (○),[C_2MIm]BF_4; (△), [C_4MIm]BF_4; (□) [C_6MIm]BF_4; (◇) [C_8MIm]BF_4; (▽) [C_{10}MIm]BF_4.

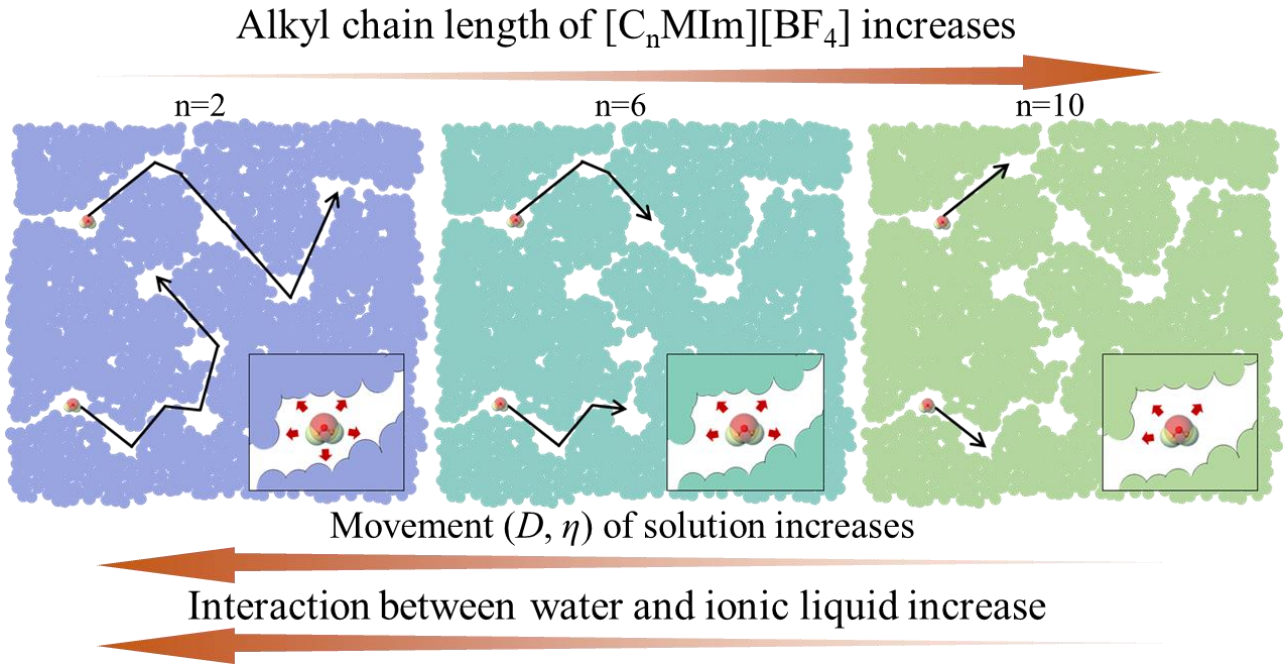

Figure 4.24 Dynamic model of a pocket in $[C_nMIm]BF_4$/water systems with the least amount of water. Black arrows show the mean distance travelled, red arrows shows electrostatic interactions.

Table 4.1 Samples information

ionic liquid	abbreviation	mass fraction purity	supplier
1-ethyl-3-methylimidazolium tetrafluoroborate	$[C_2MIm]BF_4$	>0.95	Kanto Chemical Co., Inc
1-butyl-3-methylimidazolium tetrafluoroborate	$[C_4MIm]BF_4$	>0.95	Kanto Chemical Co., Inc
1-hexyl-3-methylimidazolium tetrafluoroborate	$[C_6MIm]BF_4$	>0.99	Kanto Chemical Co., Inc
1-methyl-3-octylimidazolium tetrafluoroborate	$[C_8MIm]BF_4$	>0.99	Kanto Chemical Co., Inc
1-decyl-3-methylimidazolium tetrafluoroborate	$[C_{10}MIm]BF_4$	>0.98	Kanto Chemical Co., Inc

Table 4.2 Concentration dependence of density in $[C_nMIM]BF_4$/water systems at 298 K.

$[C_2MIm]BF_4$		$[C_6MIm]BF_4$		$[C_8MIm]BF_4$		$[C_{10}MIm]BF_4$	
x/mol%	ρ/gcm^{-3}	x/mol%	ρ/gcm^{-3}	x/mol%	ρ/gcm^{-3}	x/mol%	ρ/gcm^{-3}
0	1.27980	0	1.14555	0	1.10330	0	1.07129
9.98	1.27680	9.96	1.14339	10.85	1.09962	10.74	1.07006
20.29	1.26867	20.039	1.14066	19.86	1.09938	19.85	1.06824
30.30	1.26295	29.96	1.13749	29.99	1.09760	29.86	1.06793
40.09	1.25304	39.89	1.13416	39.92	1.09470	40.41	1.06584
60.05	1.22829	49.42	1.12935	49.91	1.09088	49.64	1.06425
80.30	1.17686	59.86	1.12136	59.88	1.08668	59.65	1.06135
90.03	1.12520	70.022	1.11439				
95.00	1.07957						

Table 4.3 Concentration dependence of expansivity in $[C_nMIM]BF_4$/water systems at 298 K.

$[C_2MIm]BF_4$		$[C_6MIm]BF_4$		$[C_8MIm]BF_4$		$[C_{10}MIm]BF_4$	
x/mol%	$\Delta V/\%$	x/mol%	$\Delta V/\%$	x/mol%	$\Delta V/\%$	x/mol%	$\Delta V/\%$
0	0	0	0	0	0	0	0
9.98	0.23	9.96	0.19	10.85	0.33	10.74	0.11
20.29	0.88	20.04	0.43	19.86	0.36	19.85	0.29
30.30	1.33	29.96	0.71	29.99	0.52	29.86	0.31
40.09	2.14	39.89	1.00	39.92	0.79	40.41	0.51
60.05	4.19	49.42	1.43	49.91	1.14	49.64	0.66
80.30	8.75	59.86	2.16	59.88	1.53	59.65	0.94
90.03	13.74	70.02	2.80				
95.00	18.55						
100	28.36						

Table 4.4 Concentration dependence of chemical shift in $[C_2MIm]BF_4$/water system at 298 K.

	Chemical Shift /ppm							
x/mol%	2H	4H	5H	7H	tail	6H	F	OH
0	8.387	7.263	7.334	4.005	1.225	-74.735	-74.735	
1.03	8.388	7.264	7.335	4.007	1.227	-74.732	-74.732	2.554
8.86	8.392	7.265	7.336	4.011	1.232	-74.731	-74.731	2.630
19.89	8.400	7.268	7.339	4.018	1.240	-74.728	-74.728	2.757
51.46	8.429	7.276	7.346	4.042	1.271	-74.713	-74.713	3.259
80.13	8.470	7.294	7.358	4.084	1.326	-74.663	-74.663	3.942
90.07	8.506	7.316	7.377	4.117	1.369	-74.618	-74.618	4.291
99.00	8.638	7.388	7.453	4.204	1.472	-74.425	-74.425	4.732
99.90	8.687	7.410	7.477	4.224	1.492	-74.345	-74.345	4.799
100								4.804

Tail is the protons of alkyl chain tail, F is ^{19}F of anion, OH is hydroxyl group of water.

Table 4.5 Concentration dependence of chemical shift in $[C_6MIm]BF_4$/water system at 298 K.

	Chemical Shift /ppm							
x/mol%	2H	4H	5H	root	tail	methyl	F	OH
0	8.619	7.445	7.506	4.126	0.707	3.836	-74.062	
0.96	8.618	7.444	7.505	4.125	0.706	3.835	-74.021	2.675
9.84	8.619	7.441	7.502	4.126	0.709	3.836	-74.022	2.750
25.94	8.622	7.436	7.497	4.129	0.714	3.838		2.915
40.78	8.625	7.433	7.491	4.131	0.719	3.840	-74.040	3.121
55.64	8.625	7.428	7.481	4.134	0.726	3.843	-74.052	3.404
70.07	8.620	7.424	7.469	4.135	0.733	3.846	-74.113	3.752

Tail is the protons of alkyl chain tail, F is ^{19}F of anion, OH is hydroxyl group of water.

Table 4.6 Concentration dependence of chemical shift in $[C_8MIm]BF_4$/water system at 298 K.

	Chemical Shift /ppm							
x/mol%	2H	4H	5H	root	tail	methyl	F	OH
0	8.656	7.469	7.528	4.158	0.786	3.856	-74.006	
1.65	8.658	7.470	7.528	4.160	0.788	3.857	-73.963	2.678
10.58	8.657	7.467	7.525	4.161	0.789	3.857	-74.010	2.736
26.45	8.656	7.460	7.515	4.163	0.795	3.858	-74.026	2.949
40.87	8.657	7.457	7.508	4.165	0.800	3.860	-74.035	3.142
55.65	8.653	7.454	7.495	4.166	0.806	3.863	-74.052	3.443
69.99	8.646	7.452	7.481	4.165	0.813	3.868	-74.070	3.809

Tail is the protons of alkyl chain tail, F is ^{19}F of anion, OH is hydroxyl group of water.

Table 4.7 Concentration dependence of chemical shift in $[C_{10}MIm]BF_4$/water system at 298 K.

	Chemical Shift /ppm							
x/mol%	2H	4H	5H	root	tail	methyl	F	OH
0	8.660	7.473	7.524	4.176	0.863	3.860	3.860	
1.43	8.660	7.473	7.524	4.177	0.864	3.861	3.861	2.693
4.77	8.660	7.471	7.522	4.177	0.864	3.861	3.861	2.725
10.10	8.659	7.470	7.519	4.178	0.865	3.861	3.861	2.772
15.17	8.659	7.468	7.517	4.178	0.866	3.861	3.861	2.813
24.91	8.658	7.465	7.511	4.178	0.869	3.862	3.862	2.939
41.00	8.654	7.459	7.499	4.177	0.872	3.863	3.863	3.189
55.70	8.652	7.459	7.487	4.178	0.879	3.869	3.869	3.517
70.00	8.644	7.459	7.474	4.176	0.883	3.874	3.874	3.864

Tail is the protons of alkyl chain tail, F is ^{19}F of anion, OH is hydroxyl group of water.

Table 4.8 Relationship between number of water aggregation and water chemical shift [Aidas et al. 2006].

	Number of water aggregation					
	1	2	3	4	4.653	5
δ/ppm	1.54	2.59	3.14	4.16	4.804	5.50
δ_{bulk}-$\delta_{monomer}$/ppm		1.05	1.6	2.62	3.264	
δ_n/δ_{bulk}		0.3217	0.4902	0.8027	1	
$\delta_{monomer\ in\ [C_2MIm]BF_4}$	2.560	3.282	3.660	4.361	4.804	
$\delta_{monomer\ in\ [C_4MIm]BF_4}$	2.667	3.354	3.714	4.382	4.804	
$\delta_{monomer\ in\ [C_6MIm]BF_4}$	2.668	3.355	3.715	4.382	4.804	
$\delta_{monomer\ in\ [C_8MIm]BF_4}$	2.626	3.327	3.694	4.374	4.804	
$\delta_{monomer\ in\ [C_{10}MIm]BF_4}$	2.540	3.268	3.650	4.357	4.804	

Table 4.9 Concentration dependence of water aggregation in $[C_nMIm]BF_4$/water systems

$[C_2MIm]BF_4$		$[C_4MIm]BF_4$		$[C_6MIm]BF_4$		$[C_8MIm]BF_4$		$[C_{10}MIm]BF_4$	
x/mol%	N_{water}	x/mol%	N_{water}	x/mol%	N_{water}	x/mol%	N_{water}	x/mol%	N_{water}
0		0.97	1.0	0		0		0	
1.03	1.0	1.14	1.0	0.96	1.0	1.65	1.0	1.43	1.0
8.86	1.1	16.65	1.1	9.84	1.1	10.58	1.1	4.77	1.0
19.89	1.2	22.70	1.2	25.94	1.3	26.45	1.4	10.10	1.1
51.45	2.1	41.33	1.6	40.78	1.7	40.87	1.8	15.17	1.2
80.13	3.4	49.99	1.9	55.64	2.2	55.65	2.3	24.91	1.3
90.07	4.0	50.71	1.9	70.07	2.9	69.99	3.1	41.00	1.8
99.00	4.6	61.10	2.4					55.70	2.4
99.90	4.6	70.48	2.8					70.00	3.1
100	4.6	88.00	3.9						
		90.02	4.0						
		94.04	4.2						
		95.11	4.3						
		96.00	4.4						
		97.27	4.4						
		98.99	4.6						
		99.50	4.6						
		99.90	4.6						

N_{water} is average number of water aggregation.

Table 4.10 Self-diffusion coefficients of the anions, cations and water in $[C_nMIm]BF_4$/water systems at 298 K.

$[C_2MIm]BF_4$				$[C_6MIm]BF_4$			
	$D/10^{-10}m^2s^{-1}$				$D/10^{-10}m^2s^{-1}$		
x/mol%	$[C_2MIm]$	BF_4	water	x/mol%	$[C_6MIm]$	BF_4	water
0	0.415	0.290		0.000	0.057	0.055	
1.0	0.433	0.303	3.930	0.957	0.061	0.058	1.754
8.9	0.537	0.393	4.349	9.840	0.087	0.087	1.780
19.9	0.727	0.563	4.828	25.940	0.155	0.169	2.385
51.5	1.624	1.446	6.850	40.775	0.258	0.308	2.957
80.1	3.457	3.593	10.370	55.641	0.435	0.563	3.773
90.1	4.830	5.572	13.130	70.068	0.694	0.971	4.874
99.0	8.203	11.505	19.040				
99.9	8.314	12.905	19.930				
100			20.100				
$[C_8MIm]BF_4$				$[C_{10}MIm]BF_4$			
	$D/10^{-10}m^2s^{-1}$				$D/10^{-10}m^2s^{-1}$		
x/mol%	$[C_8MIm]$	BF_4	water	x/mol%	$[C_{10}MIm]$	BF_4	water
0	0.030	0.032		0.000	0.022	0.025	
1.6	0.033	0.036	1.458	1.399	0.023	0.028	1.043
10.5	0.044	0.051	1.480	4.770	0.026	0.034	1.113
26.5	0.091	0.119	2.081	10.100	0.031	0.043	1.280
40.9	0.135	0.191	2.339	15.170	0.036	0.053	1.374
55.7	0.236	0.381	3.313	24.910	0.054	0.081	1.652
70.0	0.361	0.663	4.076	41.790	0.092	0.166	2.247
				55.700	0.148	0.314	2.771
				70.240	0.209	0.535	3.626

Table 4.11 Mean distance travelled of [C_nMIm], BF_4 and water at water concentration extrapolated to 0 mol% at 298 K.

		L/μms^{-1}
	[C_2MIm]	0.91
[C_2MIm]BF_4	BF_4	0.76
	Water	2.79
	[C_4MIm]	0.50
[C_4MIm]BF_4	BF_4	0.45
	Water	2.14
	[C_6MIm]	0.34
[C_6MIm]BF_4	BF_4	0.33
	Water	1.87
	[C_8MIm]	0.25
[C_8MIm]BF_4	BF_4	0.25
	Water	1.71
	[C_{10}MIm]	0.21
[C_{10}MIm]BF_4	BF_4	0.22
	Water	1.41

Table 4.12 Molecular radii of [C_nMIm] and water [Tokuda et al. 2005].

	r/Å
Water	1.6
[C_2MIm]	3.03
[C_4MIm]	3.30
[C_6MIm]	3.53
[C_8MIm]	3.73

Table 4.13 Concentration dependence of viscosity in $[C_nMIm]BF_4$/ water systems at 298 K.

$[C_2MIm]BF_4$		$[C_6MIm]BF_4$		$[C_8MIm]BF_4$		$[C_{10}MIm]BF_4$	
x/mol%	η/mPas	x/mol%	η/mPas	x/mol%	η/mPas	x/mol%	η/mPas
0	39.93	0	212.13	0	353.48	0	600.21
9.98	28.20	9.96	146.06	10.85	236.45	10.74	415.86
20.29	20.81	20.04	93.81	19.86	147.36	19.85	285.52
30.30	15.68	29.96	60.92	29.99	99.31	29.86	202.26
40.09	11.01	39.89	41.70	39.92	67.14	40.41	147.30
60.05	5.98	49.42	28.78	49.91	50.33	49.64	114.63
80.30	2.84	59.86	19.26	59.88	35.15	59.65	81.97
90.03	1.88	70.02	13.19				
95.00	1.27						

Chapter 5

General conclusion

In this study, the properties of the pocket and the water in an IL/water system were elucidated. In Chapter 2, how the macroscopic physicochemical property of IL/water systems depend on the type of IL was investigated based on refractive index. As a result, the IL concentration dependence of the normalized deviation between ideal and experimental refractive index for all studied ILs were completely overlapped. These results suggest that by normalization their respective IL characters are not necessarily reflected in the refractive indices of many IL-water mixtures, although IL-water mixtures have the unique structural properties, suggesting that the properties of IL/water system doesn't depend on IL species in a macroscopic view.

In Chapter 3, the pocket size was estimated by mixing water or alcohol with various alkyl chain length into an IL, respectively. The physicochemical properties of IL/water and IL/alcohol systems were also investigated based on chemical shift, self-diffusion coefficient, density and viscosity. As a result, the volume expansivity of $[C_4MIm]BF_4$/alcohol and $[C_4MIm]BF_4$/water systems were less than 4 % up to 20 mol%. Therefore, adding water or alcohols into $[C_4MIm]BF_4$ didn't increase solution volume significantly, indicating that the water and alcohols enter into the pocket at less than 20 mol%. Furthermore the structure of the pure IL hardly change from the view of the dynamic (self-diffusion coefficient) and static (chemical shift) properties, even though water to 1-hexanol was added up to 20 mol%. From the result of density, the pocket size in the IL structure is

at least more than 1-hexanol size (100 $Å^3$). Interestingly, the result of relationship between macroscopic (viscosity) and microscopic (self-diffusion coefficient) properties suggests that the movement of water and small alcohols in the IL isn't restricted in the pocket and move between the pockets whereas that of large alcohols are restricted in the pocket compared water and small alcohols.

In Chapter 4, the influence of the alkyl chain length of the IL to the properties of pockets and the water in it were investigated based on chemical shift, self-diffusion coefficient, density and viscosity. As a result, volume expansivity of $[C_nMIm]BF_4$/water systems decreased with increasing alkyl chain length of the IL and that of $[C_6MIm]BF_4$/water system was less than 1.5 % at 50 mol%, meaning that the pocket size may increase with increasing alkyl chain length of the IL. Moreover, the structure of the pure IL hardly change from the view of the dynamic (self-diffusion coefficient) and static (chemical shift) properties, even though water was added up to 75 mol%. In the structure, the pocket size may increase with increasing alkyl chain length of the IL from the density data. Furthermore since self-diffusion coefficient ratio of water to IL clearly increase more than molecular radius ratio suggests that the surface of the pocket existing in the IL contains both a nonpolar and polar site, and the ratio of polar surface to nonpolar surface decreases as the alkyl chain length of the IL increases. Moreover, from macroscopic (viscosity) and microscopic (self-diffusion coefficient) dynamic views, the movement of water in the IL isn't restricted in the pocket and move between the pockets. Considering the contents of chapter 2 and 4, it reveals that the result of the properties of IL/water system doesn't depend on IL species in a macroscopic view whereas that of depends on IL

(alkyl chain length) especially in a dynamic microscopic view to some extent.

References

Abe H., Takekiyo T., Shigemi M., Yoshimura Y., Tsuge S., Hanasaki T., Ohishi K., Takata S., Suzuki J. (2015) Size-tunable Confined Water in a Room Temperature Ionic Liquid. JPS Conf. Proc. 8: 033001.

Aidas K., Marsalka A., Kimtys L., Urba V., Balevicius V. (2016) MAGNETIC SHIELDING PROPERTIES OFWATER IN VARIOUS MOLECULAR AND MOLECULAR-IONIC STRUCTURES. Lithuanian Journal of Physics 46:169-175.

Aki S.N.V.K., Mellein B.R., Saurer E.M., Brennecke J.F. (2004) High-Pressure Phase Behavior of Carbon Dioxide with Imidazolium-Based Ionic Liquids. J. Phys. Chem. B, 108:20355-20365.

Anouti M., Vigeant A., Jacquemin J., Brigouleix C., Lemordant D. (2010) Volumetric properties, viscosity and refractive index of the protic ionic liquid, pyrrolidinium octanoate, in molecular solvents. J. Chem. Thermodyn. 42:834–845.

Anthony J.L., Anderson J.L., Maginn E.J., Brennecke J.F. (2005) Anion effects on gas solubility in ionic liquids. J. Phys. Chem. B 109:6366-6374.

Arimoto S., Sugimura M., Kageyama H., Torimoto T., Kuwabata S. (2008) Development of new techniques for scanning electron microscope observation using ionic liquid. Electrochimica Acta 53:6228–6234.

Bernardes C.E.S., Piedade M.E.M., Lopes J.N.C. (2011) The Structure of Aqueous Solutions of a Hydrophilic Ionic Liquid: The Full Concentration Range of 1-Ethyl-3-methylimidazolium

Ethylsulfate and Water. J. Phys. Chem. B 115:2067–2074.

Blanchard L.A., Gu Z., Brennecke J.F. (2001) High-Pressure Phase Behavior of Ionic Liquid/CO_2 Systems. J. Phys. Chem. B 105:2437-2444.

Cadena C., Anthony J.L., Shah J.K., Morrow T. I., Brennecke J.F., Maginn E.J. (2004) Why Is CO_2 So Soluble in Imidazolium-Based Ionic Liquids? J. Am. Chem. Soc. 126:5300-5308.

Chiehming C., Kou-Lung J, C., Chang-Yih C. (1998) A new apparatus for the determination of P–*x*–*y* diagrams and Henry's constants in high pressure alcohols with critical carbon dioxide. J. Supercrit. Fluids, 12:223-237.

Crosthwaite J.M., Aki S.N.V.K., Maginn E.J., Brennecke J.F. (2004) Liquid Phase Behavior of Imidazolium-Based Ionic Liquids with Alcohols. J. Phys. Chem. B, 208:5113–5119.

Crosthwaite J.M., Aki S.N.V.K., Maginn E.J., Brennecke J.F. (2005) Liquid phase behavior of imidazolium-based ionic liquids with alcohols: effect of hydrogen bonding and non-polar interactions. Fluid Phase Equilib. 228–229:303-309.

Eblinger F., Schneider H. (1996) Self-Association of Water and Water−Solute Associations in Chloroform Studied by NMR Shift Titrations† J. Phys. Chem. 100:5533-5537.

Einstein A. (1956) Investigations on the theory of Brownian movement. Dover, New York.

Feng S., Voth G.A. (2010) Molecular dynamics simulations of imidazolium-based ionic liquid/water mixtures: Alkyl side chain length and anion effects. Fluid Phase Equilib. 294 (2010) 148–156.

Gao J., Wagner N.J. (2016) Water Nanocluster Formation in the Ionic Liquid 1-Butyl-3-methylimidazolium Tetrafluoroborate ([C_4mim][BF_4])–D_2O Mixtures. Langmuir 32:5078–5084.

González E.J., Domínguez Á., Macedo E.A. (2012) Physical and Excess Properties of Eight Binary Mixtures Containing Water and Ionic Liquids. J. Chem. Eng. Data 57:2165–2176.

Huang X., Margulis C.J., Li Y., Berne B.J. (2005) Why Is the Partial Molar Volume of CO_2 So Small When Dissolved in a Room Temperature Ionic Liquid? Structure and Dynamics of CO_2 Dissolved in [$Bmim^+$] [PF_6^-]. J. Am. Chem. Soc. 127:17842–17851.

Iglesias-Otero M.A., Troncoso J., Carballo E., Romanı L. (2008) Density and refractive index in mixtures of ionic liquids and organic solvents: Correlations and predictions. J. Chem. Thermodyn. 40:949–956.

Jiang W., Wang Y., Voth G.A. (2007) Molecular Dynamics Simulation of Nanostructural Organization in Ionic Liquid/Water Mixtures† J. Phys. Chem. B 111:4812–4818.

Kaneko K., Yoshimura Y., Shimizu A. (2018a) Water concentration dependence of the refractive index of various ionic liquid-water mixtures. J. Mol. Liq. 250:283-286.

Kaneko K., Saihara K., Masuda Y., Yoshimura Y., Shimizu A. (2018b) Dynamic properties of water molecules in ionic liquid/water mixture with various alkyl chain length. J. Mol. Liq. 264:337-342.

Kaneko K., Mori T., Hattori S., Takekiyo T., Masuda Y., Yoshimura Y., Shimizu A. (2019) Dynamic

and static properties of mixtures of 1-butyl-3-methylimidazolium tetrafluoroborate and alcohols with various alkyl chain lengths. J. Mol. Liq. 111718, In press.

Kashin A.S., Galkin K.I., Khokhlova E.A., Ananikov V.P. (2016) Direct Observation of Self-Organized Water-Containing Structures in the Liquid Phase and Their Influence on 5-(Hydroxymethyl)furfural Formation in Ionic Liquids. Angew. Chem. Int. Ed. 55:2161–2166.

Kordikowski A., Schenk A.P., Van Nielen R.M., Peters C. J. (1995) Volume expansions and vapor-liquid equilibria of binary mixtures of a variety of polar solvents and certain near-critical solvents. J. Supercrit. Fluids, 8:205-216.

Lopes J.N.C., Gomes M.F.C., Pàdua A.A.H. (2006) Nonpolar, Polar, and Associating Solutes in Ionic Liquids. J. Phys. Chem. B 110:3330–3335.

Maia F.M., Rodríguez O., Macedo E.A. (2012) Relative hydrophobicity of equilibrium phases in biphasic systems (ionic liquid + water). J. Chem. Thermodyn. 48:221–228.

Makio T, Sakurai M., Kanakubo M. (2013) Solubilities of Gases in Ionic Liquids and its Applications to Separation Processes. J. Vac. Soc. Jpn. 56:88-96.

Mokhtarani B., Mojtahedi M.M., Mortaheb H.R., Mafi M., Yazdani F., Sadeghian F. (2008) Densities, Refractive Indices, and Viscosities of the Ionic Liquids 1-Methyl-3-octylimidazolium Tetrafluoroborate and 1-Methyl-3-butylimidazolium Perchlorate and Their Binary Mixtures with Ethanol at Several Temperatures. J.Chem. Eng. Data 53:677–682.

Rollet A.L., Porion P., Vaultier M., Billard I., Deschamps M., Bessada C., Jouvensal L. (2007)

Anomalous Diffusion of Water in [BMIM][TFSI] Room-Temperature Ionic Liquid. J. Phys. Chem. B 111:11888–11891.

Saha S., Hamaguchi H. (2006) Effect of Water on the Molecular Structure and Arrangement of Nitrile-Functionalized Ionic Liquids. J. Phys. Chem. B 110:2777–2781.

Seki S., Tsuzuki S., Hayamizu K., Umebayashi Y., Serizawa N., Takei K., Miyashiro H. (2012) Comprehensive Refractive Index Property for Room-Temperature Ionic Liquids. J. Chem. Eng. Data 57:2211–2216.

Sieffert N., Wipff G. (2006) The [BMI][Tf2N] Ionic Liquid/Water Binary System: A Molecular Dynamics Study of Phase Separation and of the Liquid−Liquid Interface. J. Phys. Chem. B 110:13076–13085.

Soriano A.N., Doma Jr. B.T., Li M. (2009) Measurements of the density and refractive index for 1-n-butyl-3-methylimidazolium-based ionic liquids. J. Chem. Thermodyn. 41:301–307.

Stejskal E.O. (1965) Use of Spin Echoes in a Pulsed Magnetic‐Field Gradient to Study Anisotropic, Restricted Diffusion and Flow. J. Chem. Phys. 43:3597–3603.

Sugimori Y., Miyata T., Hashiguchi H., Okunishi E., Mizoguchi T. (2019) Atomic-scale investigation of the heterogeneous structure and ionic distribution in an ionic liquid using scanning transmission electron microscopy RSC Adv. 9:10520-10527.

Swatloski R.P., Spear S.K., Holbrey J.D., Rogers R.D. (2002) Dissolution of Cellose with Ionic Liquids. J. Am. Chem. Soc. 124:4974-4975.

Tariq M., Forte P.A.S., Gomes M.F.C., Lopes J.N.C., Rebelo L.P.N. (2009) Densities and Refractive Indices of Imidazolium and Phosphonium based Ionic Liquids: Effect of Temperature, Alkyl Chain Length and Anion. J. Chem. Thermodyn. 41:790–798.

Tokuda H., Hayamizu K., Ishii K., Susan M.A.B.H., Watanabe m. (2005) Physicochemical properties and structures of room temperature ionic liquids. 2. Variation of alkyl chain length in imidazolium cation. J. Phys. Chem. B 109:6103-6110.

Triolo A., Russina O., Bleif H.J., Cola E.D. (2007) Nanoscale Segregation in Room Temperature Ionic Liquids† J. Phys. Chem. B 111:4641–4644.

Vercher E., Llopis F.J., Gonza'lez-Alfaro V., Miguel P.J., Martínez-Andreu A. (2011) Refractive Indices and Deviations in Refractive Indices of Trifluoromethanesulfonate-Based Ionic Liquids in Water J. Chem. Eng. Data 56:4499–4504.

Welton T. (1999) Room-Temperature Ionic Liquids. Solvents for Synthesis and Catalysis Chem. Rev. 99:2071–2084.

Wilkes J.S., Zaworotko M.J. (1992) Air and water stable 1-ethyl-3-methylimidazolium based ionic liquids, J. Chem. Soc., Chem. Commun. 965-967.

Wilkes J.S. (2002) A short history of ionic liquids—from molten salts to neoteric solvents Green Chem. 4:73-80.

Yamaguchi Y., Yasutake N., Nagaoka M. (2001) Theoretical prediction of proton chemical shift in supercritical water using gas-phase approximation. Chem. Phys. Lett. 340:129-136.

Yoshimura Y., Mori T., Kaneko K., Hattori S., Takekiyo T., Masuda Y., Shimizu A. (2019a) Raman investigation on the local structure of alcohols in 1-butyl-3-methylimidazolium tetrafluoroborate J. Mol. Liq. 293:111508.

Yoshimura Y., Mori T., Kaneko K., Nogami K., Takekiyo T., Masuda Y., Shimizu A. (2019b) Confirmation of local water structure confined in ionic liquids using H/D exchange. J. Mol. Liq. 286:110874.

Yu Y., Beichel W., Dlubek G., Krause-Rehberg R., Paluch M., Pionteck J., Pfefferkorn D., Bulut S., Friedrich C., Pogodina N., Krossing I. (2012) Free volume and phase transitions of 1-butyl-3-methylimidazolium based ionic liquids from positron lifetime spectroscopy. Phys. Chem. Chem. Phys. 14:6856–6868.